2017-12-01

Comparative Oncogenomics Identifies Novel Regulators and Clinical Relevance of Neural Crest Identities in Melanoma

Arvind M. Venkatesan
University of Massachusetts Medical School

COMPARATIVE ONCOGENOMICS IDENTIFIES NOVEL REGULATORS AND CLINICAL RELEVANCE OF NEURAL CREST IDENTITIES IN MELANOMA

A Dissertation Presented

By

Arvind Murali Venkatesan

Submitted to the faculty of the
University of Massachusetts Medical School, Worcester
in partial fulfillment of the of the requirements for the degree of

DOCTORATE OF PHILOSOPHY

December 1, 2017

Interdisciplinary Graduate Program

COMPARATIVE ONCOGENOMICS IDENTIFIES NOVEL REGULATORS AND CLINICAL RELEVANCE OF NEURAL CREST IDENTITIES IN MELANOMA

A Dissertation Presented
By

Arvind Murali Venkatesan

This work was undertaken in the Graduate School of Biomedical Sciences

Interdisciplinary Graduate Program

Under the mentorship of

Craig. J. Ceol, Ph.D., Thesis Advisor

The signatures of the Dissertation Defense Committee signify completion and approval as to style and content of the Dissertation

Michael Green, Ph.D., Member of Committee

Nathan Lawson, Ph.D., Member of Committee

Stephen Jones, Ph.D., Member of Committee

David Fisher, Ph.D., External Member of Committee

The signature of the Chair of the Committee signifies that the written dissertation meets the requirements of the Dissertation Committee.

Eric Baehrecke, Ph.D., Chair of Committee

The signature of the Dean of the Graduate School of Biomedical Sciences signifies that the student has met all graduation requirements of the school.

Anthony Carruthers, Ph.D.,
Dean of the Graduate School of Biomedical Sciences

December 1, 2017

ACKNOWLEDGEMENTS

John C Crosby said ‘Mentoring is a brain to pick, an ear to listen, and a push in the right direction.’ This phrase perfectly fits my thesis advisor Craig Ceol. Craig has been extremely supportive and encouraging during times of success and failure. I have learnt several important lessons from him in the past few years, and that has already helped in my professional and personal life. The most important lesson he imparted was to strive for perfection. I thank him for believing in me and providing me opportunities to explore my scientific curiosity. I hope to receive critical feedback from him throughout my career.

I also wish to thank all the members of the Ceol lab. Rajesh, Ana, James, Alec, Revati, Tyler and Missy were good peers to work with. I want to specially thank Rajesh Vyas for being my friend, philosopher and guide. The daily coffee sessions that included long conversations about science and philosophy was great fun.

I consider myself very lucky to have had the best mentors as a part of my TRAC. Eric, Michael, Nathan and Steve have always provided insightful feedback about my research. I was also lucky to have worked in the labs of Eric and Michael. Special thanks to my TRAC chair, Eric Baehrecke for his constant support and counsel. I am also grateful to Dr. David Fisher who accepted to be my external examiner in midst of his busy schedule. I

I wish to thank the admin and support staff from UMass Medical School, without whom none of my work would have been possible. I specially want to thank Mary Ellen Lane for the support when needed. I will always cherish the TA sessions with her. I also wish to specially thank Stratton Annette and Mindy Donovan for all their support and for the fun conversations.

From a personal standpoint, I wish to thank all my close friends. Aditya V, Rohit, Sudesh, Niranj, Priya, Sonal, Divya, Padma, Aditya B, Bunny, Mayuri, Ankita and many others. They became my family away from home. I will always cherish the great memories I had with all of them.

Finally, I wish to thank the pillars of my life, my family. Although physically they stayed thousands of miles apart, my parents Murali and Lakshmi, and my sister, Sukanya accompanied me in this long journey. The daily conversations with them gave me the strength and tenacity to successfully complete my PhD. I was also lucky to get married to Rohini during this time, whose love helped me finish my PhD research and move on to the next chapter of life.

ABSTRACT

Cancers often resurrect embryonic molecular programs to promote disease progression. In melanomas, which are tumors of the neural crest (NC) lineage, a molecular signature of the embryonic NC is often reactivated. These NC factors have been implicated in promoting pro-tumorigenic features like proliferation, migration and therapy resistance. However, the molecular mechanisms that establish and maintain NC identities in melanomas are largely unknown. Additionally, whether the presence of a NC identity has any clinical relevance for patient melanomas is also unclear. Here, using comparative genomic approaches, I have a) identified a novel role for GDF6-activated BMP signaling in reawakening a NC identity in melanomas, and b) identified a NC signature as a clinical predictor of melanoma progression.

Like the genomes of many solid cancers, melanoma genomes have widespread copy number variations (CNV) harboring thousands of genes. To identify disease-promoting drivers amongst such huge numbers of genes, I used a comparative oncogenomics approach with zebrafish and human melanomas. This approach led to the identification of a recurrently amplified oncogene, *GDF6,* that acts via BMP signaling to invoke NC identities in melanomas. In maintaining this identity, GDF6 represses the melanocyte differentiation gene MITF and the proapoptotic factor SOX9, allowing melanoma cells to remain undifferentiated and survive. Functional analysis in zebrafish embryos indicated a role of GDF6 in

blocking melanocyte differentiation, suggesting that the developmental function of GDF6 is reiterated in melanomas. In clinical assessments, a major fraction of patient melanomas expressed high GDF6, and its expression correlated with poor patient survival. These studies provide novel insights into regulation of NC identities in melanomas and offer GDF6 and components of BMP pathway as targets for therapeutic intervention.

In additional studies, I wanted to test whether a broader NC identity in melanomas had any clinical relevance. In these studies, I performed transcriptome analysis of zebrafish melanomas and derived a 15-gene NC signature. This NC gene signature positively correlated with the expression of SOX10, a known NC marker in human melanomas. Patients whose melanomas expressed this signature showed poor overall survival. These findings identify an important predictive signature in human melanomas and also illuminate the clinical importance of NC identity in this disease.

TABLE OF CONTENTS

List of tables

List of figures

Chapter I

Chapter II

List of Symbols, Abbreviation or Nomenclature

aCGH	array Comparative Genomic Hybridization
AP-2α	Activating Protein -2 alpha
ATCC	American Type Culture Collection
ALK	Activin-Like Kinase
BMP	Bone Morphogenic Protein
BMPR	Bone Morphogenic Protein Receptor
CAS9	CRISPR associated protein 9
CCND1	Cyclin D1
CDKN	Cyclin-dependent Kinase
ChIP	Chromatin Immunoprecipitation
CNV	Copy Number Variation
CSC	Cancer Stem Cell
CTLA4	Cytotoxic T-Lymphocyte Associated Antigen 4
DAPI	4',6-diamidino-2-phenylindole
DIDO1	Death-Inducer Obliterator 1
DMEM	Dulbecco's Modified Eagle's Medium
DMH1	Dorsomorphin Homolog 1
DNA	Deoxyribonucleic Acid
EDTA	Ethylene Diamine Tetraacetic Acid
EGFP	Enhanced Green Fluorescent Protein

EMT	Epithelial Mesenchyme Transition
ES	Enrichment Score
FACS	Flow-Activated Cell Sorting
FBS	Fetal Bovine Serum
FOXD3	Forkhead Box D3
FWER	Family-wise Error Rate
GAPDH	Glyceraldehyde 3-phosphate dehydrogenase
GDF	Growth Differentiation Factor
GSEA	Gene Set Enrichment Analysis
H&E	Hematoxylin and Eosin
ID	Inhibitor of Differentiation
IHC	Immunohistochemistry
JNK	Jun Nuclear Kinase
MAPK	mitogen-activated protein kinase
MEK	MAPK ERK kinase
MITF	Microphthalmia-Associated Transcription Factor
mTOR	Mammalian Target of Rapamycin
MYC	Avian myelocytomatosis virus oncogene cellular homolog
NC	Neural Crest
NES	Normalized Enrichment Score
NOD/SCID	Non-obese diabetic / Severe combined immunodeficiency

NS	Not Significant
ORF	Open Reading Frame
P13K	Phosphatidylinositide 3-kinase
PAX3	Paired Box Protein 3
PD1	Programmed Cell Death Protein 1
PRKACA	Protein Kinase CAMP-Activated Catalytic Subunit Alpha
PTEN	Phosphatase and tensin homolog
qRT-PCR	Quantitative Real Time Polymerase Chain Reaction
R-SMAD	Receptor- Suppressor of Mothers Against Decapentaplegic
RLU	Relative Luciferase Units
RNAi	Ribonucleic Acid Interference
RNAseq	RNA deep sequencing
RPMI	Rosemary Park Memorial Institute
SDS	Sodium Dodecyl Sulfate
s.e.m	Standard Error Mean
shRNA	Short Hairpin Ribonucleic acid
SKCM	Skin Cutaneous Melanoma
SMAD	Suppressor of Mothers Against Decapentaplegic
SOX	Sex Determining Region Y-Box 9
TALEN	Transcription activator-like effector nuclease
TCGA	The Cancer Genome Atlas
TERT	Telomerase reverse transcriptase

TF	Transcription Factor
TFAP	Transcription factor Activator Protein-2 alpha
TGF-β	Transforming Growth Factor beta
TRP1	Tyrosinase-Related Protein 1
TUNEL	Terminal deoxynucleotidyl transferase (TdT) dUTP Nick-End Labeling
UV	Ultraviolet
ZEB1	Zinc finger E-box-binding homeobox 1

Preface

First chapter: Arvind Venkatesan and Craig Ceol conceived the project, designed and analyzed the experiments, and wrote the manuscript. Arvind Venkatesan, Alec Gramman and Craig Ceol performed the zebrafish experiments. Arvind Venkatesan and Rajesh Vyas designed, performed and analyzed the cell culture experiments and with Sanchita Bhatnagar performed the mouse xenotransplant experiments. Arvind Venkatesan and Simon Xi designed the zebrafish aCGH arrays. Sagar Chhangawala and Yariv Houvras provided zebrafish bioinformatics support. Arvind Venkatesan, Sharvari Gujja and Yvonne Edwards performed bioinformatics analyses of RNAseq data from A375 cells. Sharvari Gujja and Yvonne Edwards analyzed human melanocyte and TCGA melanoma transcriptome data. Karen Dresser and April Deng conducted IHCs on human melanoma samples and the tissue microarray. Arvind Venkatesan, Craig Ceol and April Deng analyzed and scored individual melanoma samples and Camila Gomes and Christine Lian provided, analyzed and scored the tissue microarray. The Journal of Clinical Investigation has accepted this manuscript.

Second Chapter: Arvind Venkatesan and Craig Ceol conceived the project, performed the analysis. The manuscript containing this project is under preparation.

CHAPTER I

INTRODUCTION

Melanoma

Overview

Melanoma is the most fatal skin cancer, with a growing incidence. It originates from melanocytes, which are melanin-producing cells present in the basal layer of skin epidermis. Melanin provides color to the skin and hair (Lin and Fisher, 2007) and absorbs ultraviolet (UV) rays from the sun, thereby protecting other cells in the deep skin layers from UV-induced DNA photodamage. In 2012, 232,000 cases of melanoma, resulting in 55,000 deaths, were reported worldwide. In the United States, approximately 9,000 people die due to melanoma annually (Guy, 2015). In the last four decades, the frequency of melanomas has increased by 15-fold (Weinstock, 2001).

The progression of melanoma can be simply defined as a stepwise process (Figure 1.1)(Miller and Mihm, 2006). On exposure to mutagens such as UV rays, normal melanocytes undergo uncontrolled proliferation to form benign lesions called moles or nevi. Mutation-laden melanocytes can also transform into malignant melanomas, either through nevus formation or independently. In the early stages, melanoma growth is confined to the epidermis. As the disease progresses, melanomas invade through the basement membrane into the dermis and the underlying subcutaneous tissues. Eventually, the cancer cells metastasize to lymph nodes and other distant sites of the body. When diagnosed

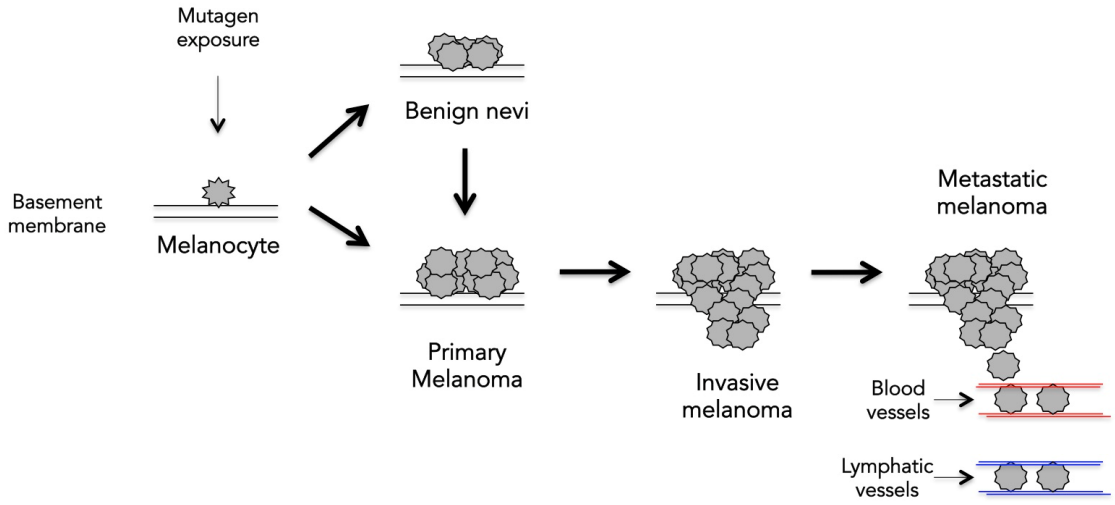

Figure 1.1: Progression of melanoma
When melanocytes are exposed to mutagens, they form either benign nevi or malignant melanomas. Melanomas initially proliferate within the basal layer of the skin. Upon further disease progression, melanoma cells firstly invade into the basement membrane and the underlying subcutaneous tissue and eventually they metastasize to distant sites using blood and lymphatic vessels.

at early stages, patients with melanoma have more than 90% chance of survival; however, advanced-stage melanoma patients with distant metastasis have low chances of survival (Eggermont et al., 2016; Noone et al., 2017).

Melanoma therapeutics have greatly advanced in the past few years. Until a decade ago, chemotherapy was the only mode for treating patients with advanced-stage melanomas; however, these patients had poor survival rates because their melanomas were highly resistant to chemotherapeutic treatment. Several recent functional genomic studies have yielded targeted and immune therapies for melanoma treatment (Bollag et al., 2010; Hodi et al., 2010), with excellent clinical benefits. The survival rate of patients with advanced-stage melanomas has increased from 18% to approximately 40% (Eggermont et al., 2016; Noone et al., 2017). Although significant progress has been made in melanoma therapy, a considerable number of patients either do not respond or show resistance to current therapies. Hence, most efforts in melanoma research are currently focused on improving current treatment modes, testing combinatorial therapeutic approaches, targeting drug resistance mechanisms, and identifying new therapeutic targets.

Genomic Changes in Melanomas

Comprehensive screening of the melanoma genome through whole-genome and exome sequencing has demonstrated extensive genetic alterations and helped identify novel cancer genes (Akbani, 2015; Berger et al., 2012; Hodis

et al., 2012; Krauthammer et al., 2012). Oncogenomic studies on several human cancers have identified melanomas as one of the most highly mutated cancers (Lawrence et al., 2013); several types of genetic alterations, including base substitution mutation, copy number variation (CNV), and translocation, have been identified. A metastatic melanoma genome harbors approximately 33,000 base substitutions (Pleasance et al., 2010). A majority of these base substitutions are C>T/G>A transitions, a mutational spectrum caused by UV light exposure. Among this large pool of mutations, researchers have used computational and functional tools to distinguish disease-promoting driver gene mutations from randomly altered passenger gene changes that do not affect disease progression. These studies have led to the identification of recurrent mutations in BRAF, NRAS, PTEN, CDKN1A, and P53 mutations in melanoma and have (1) identified novel oncogenes and tumor suppressor genes; (2) revealed the role of the mitogen-activated protein kinase (MAPK), mTOR, p53, and other pathways in melanoma progression; and (3) enabled targeted therapy approaches for melanoma by using small molecular inhibitors, such as vemurafenib (mutant BRAFV600E inhibitor) and dabrafenib (MEK inhibitor).

The melanoma genome also harbors numerous CNVs. Approximately 10% of the melanoma genome, comprising approximately 2,000 genes, undergoes recurrent CNV (Beroukhim et al., 2010; Lin et al., 2008). Among these genes, only a few have been predicted to be disease-promoting drivers. In the regions of focal CNVs, consisting of few altered genes, several driver genes have

been identified; for instance, the presence of MITF, CCND1, BRAF, CDKN2A, and PTEN in the focal CNV regions of the melanoma genomes has enabled the identification and validation of their roles in melanomagenesis (Ghosh and Chin, 2009; Lin et al., 2008; Shi et al., 2012; Vizkeleti et al., 2012). However, melanomas also harbor broad CNVs including the amplification or deletion of an entire chromosome or an arm of a chromosome (Lin et al., 2008). In these cases, numerous genes within these intervals confound the identification of the driver genes (Figure 1.2). Thus, the identification of these drivers may aid in understanding the biology of melanomas further and provide new therapeutic targets.

Roles of Developmental Mechanisms in Melanoma Progression

In addition to identifying new cancer genes, genomic studies have reported changes in the cellular identity of tumor cells to a more precursor-like state (Mack et al., 2016; Wong et al., 2015). Melanomas are derivatives of the neural crest (NC) lineage because they invoke NC identities (Maguire et al., 2015; Shakhova, 2014). NC cells are multipotent embryonic cells that transform to neurons, glia, cartilage, and melanocytes. These cells can self-renew and migrate, thus enabling them to generate distinct cell types and populate different regions of the embryo. A complex network of signaling pathways orchestrates these processes in these cells. The differentiated cell types (e.g., melanocytes) subsequently turn off these pathways because they lack the need to self-renew

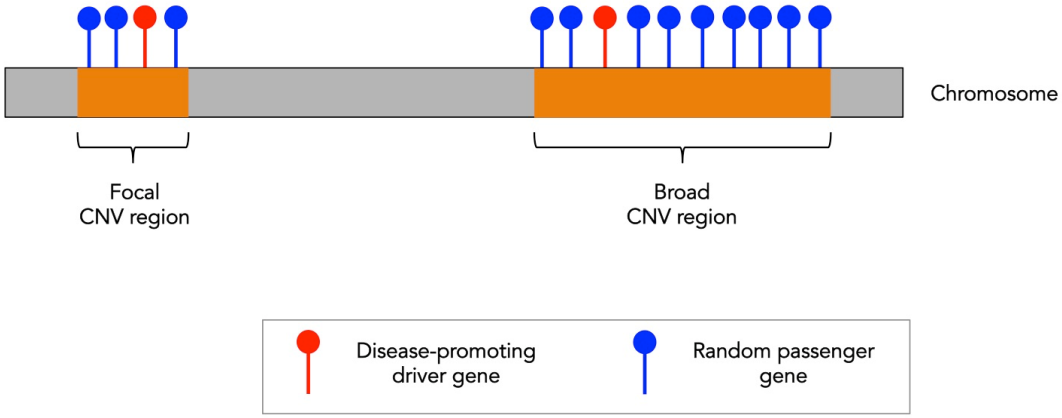

Figure 1.2: Driver and passenger genes in regions of CNV
Melanoma genomes harbor focal and broad regions of recurrent CNVs. In focal CNV regions, driver genes are found amongst a small number of passenger genes as compared to broad CNV regions, which harbor driver genes amongst a large number of passenger genes.

or migrate. However, some of these developmental pathways are reactivated in NC lineage-derived tumors, such as melanomas (Maguire et al., 2015). This activation confers protumorigenic properties, such as self-renewal, proliferation, and migration properties, to the tumor cells.

Several factors expressed in NC cells are dysregulated in melanomas, and these factors contribute to melanoma progression in multiple ways. Early studies from the Weinberg lab reported a role of the NC factor Slug in promoting EMT to enable melanoma metastasis (Gupta et al., 2005). Subsequently, several embryonic factors regulating EMT, such as SNAIL and TWIST, were reported to be associated with melanoma metastasis (Caramel et al., 2013). Notably, a reason that melanomas are believed to be so metastatic is the inherent nature of the NC-derived cells to migrate. Studies from the Sommer lab also indicated a role of the NC factors SOX10 and SOX9 in regulating tumor cell survival (Shakhova et al., 2015; Shakhova et al., 2012). Other NC factors such as BRN3a and PAX3 also promote cell survival; loss of these factors caused apoptotic cell death in melanoma cells (Eccles et al., 2013; Hohenauer et al., 2013). Thus, considering this wide variety of roles of NC factors, developmental signaling is a crucial part of melanoma progression.

Melanoma cells are highly plastic in nature; this plasticity is potentially regulated by the developmental program regulating melanocyte differentiation. Recent studies have indicated that melanoma cells undergo a process called “phenotype switching,” wherein tumor cells shuttle between a proliferation-

promoting differentiated state and an invasiveness-promoting dedifferentiated state (Bailey et al., 2012; Knappe et al., 2016). Furthermore, the expression and activity of the master regulator of melanocyte development MITF potentially regulates melanoma cell plasticity (Vachtenheim and Ondrusova, 2015). Although MITF is recurrently amplified and was originally identified as a melanoma oncogene (Garraway et al., 2005), subsequent studies have indicated a more complex role of MITF in melanoma. MITF potentially follows a rheostat model, wherein different levels of MITF activity can have distinct effects on melanoma cells: (1) a very high MITF level leads to terminal differentiation followed by cell cycle exit and cell death, (2) a high MITF level promotes proliferation, (3) a low MITF level promotes invasion and inhibits proliferation, and (4) a very low MITF level results in senescence (Goding, 2011; Golan et al., 2015; Riesenberg et al., 2015). MITF is strongly regulated by microenvironmental and intrinsic signals at transcriptional, translational, and posttranslational levels (Dar et al., 2016; Feige et al., 2011; Hartman et al., 2015; Lauss et al., 2015; Shah et al., 2010; Zhao et al., 2011). These regulation levels enable MITF levels to remain highly dynamic within melanomas, which majorly contributes toward tumor cell differentiation and plasticity in melanomas.

Although the aforementioned studies indicated the importance of developmental programs in melanoma progression, these fundamental mechanisms have not been understood completely. First, the stage in which the developmental programs are turned on in melanomas remains unclear. Although

several studies have indicated the role of NC identities in advanced melanomas, a recent study using a zebrafish model indicated their earlier role in melanoma initiation (Kaufman et al., 2016); furthermore, several NC factors appear to be essential for tumor cell survival and therefore could be essential for early transformation. Second, whether the expression of different NC factors is regulated independently or a global change in the identity of these melanoma cells regulates the expression of these NC factors remains unclear. Although melanomas have a global NC identity, the factors regulating this identity remain unknown. Finally, no study has correlated NC identities to the clinical characteristics of patients with melanoma.

Bone Morphogenic Protein Signaling Pathway

Overview

Bone morphogenic proteins (BMPs) belong to the transforming growth factor β (TGF-β) superfamily and were originally identified as factors that induce bone formation (Urist, 1965). Subsequent studies indicated a broad range of roles of BMP signaling in regulating processes, such as differentiation, proliferation, angiogenesis, and apoptosis (Hemmati-Brivanlou and Thomsen, 1995; Kobayashi et al., 2005; Mitchell et al., 2010; Stewart et al., 2010; Zou and Niswander, 1996), during development and in mature adult tissues. Dysregulation of this pathway is involved in genesis and progression of several disorders, including cancer.

BMP signaling involves ligand–receptor binding at the cell surface followed by the activation of the SMAD transcriptional cascade to regulate gene expression (Figure 1.3). BMP ligands are synthesized as large inactive precursor proteins. These contain two cleavage sites, R-X-K-R and R-X-X-R, which are cleaved by furin and procollagen C-proteinases, respectively, to yield mature BMP monomers (Cui et al., 2001). These monomers form homodimers or heterodimers with other BMP monomers through a cysteine disulfide bond to produce biologically active BMP ligands. These ligands are secreted outside the cell, where they bind to and activate the BMP receptor complex. In the absence of the ligand, two type I and two type II BMP receptors are present as independent homodimers on the cell surface (Rosenzweig et al., 1995). The presence of the ligand signals the receptors to assemble into a tetraheteromeric complex. Following the complex formation, the constitutively active type II receptor phosphorylates and activates the kinase domain of the type I receptor. The type I BMP receptor then phosphorylates the receptor SMADs (SMAD1, SMAD5, and SMAD8), enabling their release from the membrane. This phosphorylated SMAD1/5/8 complex then binds to SMAD4 and translocates to the nucleus to promote or repress expression of downstream genes. In addition to the aforementioned canonical pathway, BMPs can also independently regulate noncanonical pathways, such as the MAPK, phopshoinositide 3-kinase, and c-Jun amino-terminal kinase pathways (Derynck and Zhang, 2003).

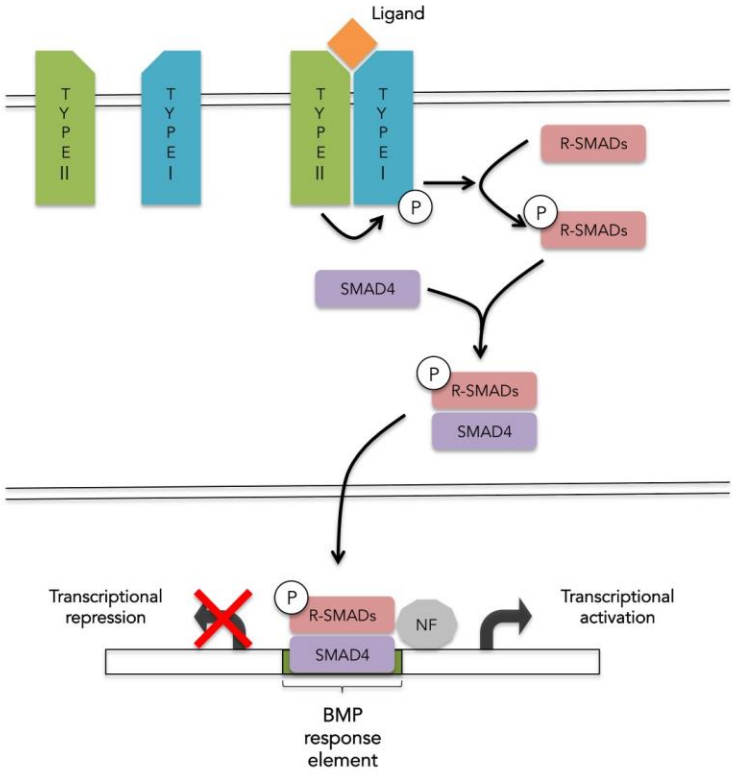

Figure 1.3: BMP signaling pathway
Upon binding of the BMP ligand, the type II BMP receptor forms a complex with the type I BMP receptor, phosphorylates and actvates its kinase domain. The type I BMP receptor then phosphorylates and activates SMAD1/5/8 (Receptor SMADs or R-SMADs). Activated R-SMADs bind SMAD4 and translocate to the nucleus. Within the nucleus, these SMADs bind other nuclear factors and regulate transcipritional activation or repression of genes.

BMP signaling is regulated at multiple levels, thus aiding this pathway in regulating a broad spectrum of biological activities. First, the large number of BMP ligands and receptors provides the first layer of pathway regulation. Approximately 20 BMP ligands, 4 type I BMP receptors, and 3 type II BMP receptors have been identified in mammals. Different homodimeric or heterodimeric BMP ligand complexes have varying affinities toward different BMP receptor complexes. Although some of these complexes act redundantly, distinct spatial and temporal expression of their ligands and receptors facilitates pathway regulation in a physiological setting. Second, the factors that negatively regulate this pathway provide a secondary layer of regulation. BMP pathway antagonists, such as chordin, noggin, and follistatin, are secreted, factors which bind to BMP ligands and block their binding to BMP receptors, thereby negatively regulating BMP signaling (Groppe et al., 2002; Harrington et al., 2006; Zhang et al., 2008). The BMP pathway is also intrinsically regulated as a part of a negative feedback loop by inhibitory SMADs (SMAD6 and SMAD7), which act by competing with SMAD1 to bind to BMP receptors (Hanyu et al., 2001; Ishida et al., 2000). Finally, the specificity of BMP pathway targets, achieved at a transcriptional level, provides an additional level of regulation. Depending on cofactor expression, the SMAD1/5/8 transcriptional complex can positively or negatively regulate the expression of different sets of genes in different cell types (Morikawa et al., 2013).

Genome-wide mapping studies using phosphoSMAD1/5/8 antibodies and ChIPseq or promoter arrays have identified several BMP target genes. These studies have been performed on different cell types, such as endothelial, embryonic fibroblast, pulmonary arterial smooth muscle, hair follicle stem, and embryonic stem cells (Genander et al., 2014; Kaneda et al., 2011; Morikawa et al., 2011), and have revealed the following: (1) The SMAD1 binding motif is somewhat unique in different tissues. (2) Although genes such as ID1, ID2, ID3, and SMAD6 are canonical BMP targets found in all cell types, cell type-specific BMP target genes are also present, potentially because context-dependent cofactor-binding. (3) BMP-SMAD1 can transcriptionally activate or repress gene expression.

BMP Signaling in Cancer (Including Melanoma)

Although BMP signaling has been implicated in many cancers, understanding its precise role in tumorigenesis has been difficult because of the complexity of the pathway and its functional diversity. This has also hindered the use of BMP pathway modulators for therapeutic purposes. However, several recent studies have identified specific roles of the BMP pathway in tumorigenesis (Table 1.1). These studies have indicated a bidirectional role of BMP signaling in tumorigenesis. BMP signaling activity can either promote or inhibit tumorigenesis: depending on the ligand–receptor complex combination, cancer type, and

Cancer	BMP pathway components	Role	Function of BMP pathway	Reference
Colorectal cancer	*BMPRII, SMAD4, BMP2*	Tumor suppressive	Anti-proliferation	(Hardwick et al., 2004; Kodach et al., 2008)
Colorectal cancer	BMP4, BMP7 (SMAD4-independent role)	Tumor promoting	Pro-invasion (Promotes EMT)	(Deng H, 2007; Grijelmo C, 2007)
Gastric carcinoma	BMP2, BMP4	Tumor suppressive	Anti-proliferation	(Shirai et al., 2011)
Prostrate cancer	BMP7	Tumor suppressive	Anti-proliferation	(Miyazaki et al., 2004)
Glioblastoma	BMP4, BMPR1B	Tumor suppressive	Promotes terminal differentiation of cancer stem cells (CSC)	(Lee et al., 2008; Piccirillo et al., 2006)
Heptacellular carcinoma	BMP4	Tumor suppressive/ Tumor promoting	Promotes terminal differentiation of CSCs at high levels Inhibits terminal differentiation of CSCs at low levels	(Zhang et al., 2012)
Pancreatic tumors, Melanoma	BMP9/ALK1	Tumor promoting	Promotes angiogenesis	(Cunha et al., 2010; Hu-Lowe et al., 2011)
Breast cancer	BMP2, BMP7, BMPR1B	Tumor promoting	Promotes metastasis	(Alarmo et al., 2008; Helms et al., 2005; Katsuno et al., 2008)
Breast cancer	BMP7, Noggin (BMP pathway antagonist)	Tumor suppressive	Inhibits metastasis	(Buijs et al., 2007; Tarragona et al., 2012)

Table 1.1: Bidirectional roles and diverse functions of BMP pathway during cancer progression

tumorigenesis stage, BMPs can regulate diverse biological functions to promote or inhibit tumorigenesis. Thus, the BMP pathway is pleiotropic in tumors.

The role of BMP signaling in melanomagenesis remains unclear. Cell line-based studies have reported distinct and somewhat contradicting roles of BMP factors in melanomagenesis. Studies from the Rothhammer lab have demonstrated that the BMP ligands BMP4 and BMP7 are overexpressed in melanomas (Rothhammer et al., 2005). BMP7 can either promote or inhibit cell migration in different melanoma cell lines (Hsu et al., 2008; Rothhammer et al., 2005). Independent studies have also found the role of a known BMP target, DIDO1, in promoting melanoma cell survival (Braig and Bosserhoff, 2013). Although these cell-based in vitro studies have implicated the role of BMP signaling in melanomas, cellular consequences caused by BMP signaling and the downstream targets of this pathway in melanomas is largely unknown. This is partly because genome-wide ChIP studies on phosphoSMAD1/5/8 in melanoma cells and studies on the role of BMP signaling in an in vivo model of melanoma are scant. Notably, no genome-wide mapping studies has reported phosphoSMAD1/5/8 in any cancer, thus indicating the need to further exploit the role of BMP signaling in tumorigenesis.

BMP Signaling in NC and During Melanocyte Development

BMP signaling has been implicated in several aspects of NC development. First, functional and genetic studies in avian, zebrafish, and Xenopus models

have reported critical roles of BMP signaling in (1) inducing NC (Liem et al., 1995; Marchant et al., 1998; Mayor et al., 1997; Nguyen et al., 1998; Ragland and Raible, 2004); (2) delaminating NC, by regulating EMT to enable cells to migrate and populate different parts of the embryo (Coles et al., 2004; Sela-Donenfeld and Kalcheim, 1999, 2000); (3) regulating cell death, to maintain appropriate tissue morphogenesis and patterning (Ellies et al., 2002; Graham et al., 1994; Marazzi et al., 1997); and (d) specifying NC fate (Reissmann et al., 1996; Shah et al., 1996).

The BMP and Wnt signaling pathways act antagonistically in NC during fate specification and differentiation of neurons and melanocytes. Studies in zebrafish and avian systems have indicated that NC fate specification occurs in a progressive manner, where multipotent NC cells are initially fate-restricted to generate neurons and later to generate melanocytes (Bronner-Fraser M, 1988; Raible and Eisen, 1994). BMP and Wnt signaling governs lineage segregation of neurons and melanocytes, respectively (Dorsky et al., 1998; Jin et al., 2001; Reissmann et al., 1996; Shah et al., 1996). BMP receptors and ligands are present in NC and adjacent tissues, respectively, during neuronal fate specification (McPherson et al., 2000; Schneider et al., 1999). Their expression is progressively downregulated; this downregulation spatially and temporally overlaps with Wnt-induced melanocyte fate specification (Jin et al., 2001). Concurrently, the induction of BMP signaling in cultured quail NC cells can promote neuronal differentiation at the expense of melanocytes (Jin et al., 2001).

Taken together, these studies have indicated that BMP signaling is important for neuronal fate specification; however, it can also inhibit Wnt signaling-induced melanocyte differentiation at least in vitro.

GDF6/BMP13

GDF6 (also called BMP13) is a BMP pathway ligand, with sequence similarity with other BMP ligands (Chang et al., 1994; Storm et al., 1994). GDF6 has 20%–30% amino acid homology with TGF-β and 40%–60% homology with other BMP ligands (Williams et al., 2008). The closest family members of GDF6 are GDF5 and GDF7, with 80%–90% amino acid homology with each other. Because of this high homology, these factors may act redundantly. Although several BMP ligands have orthologs in invertebrate species, such as Drosophila, GDF6 appears to be vertebrate-specific (Ducy and Karsenty, 2000).

Although the GDF6 structure requires further elucidation, cell-based studies have demonstrated that GDF6 can activate both canonical and noncanonical BMP signaling. Because of its sequence similarity with other BMP ligands, GDF6 potentially undergoes processing similar to that other BMP ligands do, to form a bioactive cytokine. In vitro, the bioactive GDF6 unit forms either a homodimer or a heterodimer with BMP2 and BMP4, when expressed in the same cell (Chang and Hemmati-Brivanlou, 1999); however, the in vivo mechanism of the dimer formation has not been reported thus far. Similar to most BMP ligands, GDF6 binds to BMPR2 and can activate BMPR1A (ALK3) in chondrocytes

(Wang et al., 2013b) and BMPR1B (ALK6) in pluripotent mesenchymal cells (Erlacher et al., 1998), followed by the activation of the canonical SMAD1/58 axis of BMP signaling (Hanel and Hensey, 2006; Pant et al., 2013; Wang et al., 2013b). GDF6-driven BMP receptor activation can also activate the noncanonical p38 MAPK pathway (Pant et al., 2013; Wang et al., 2013b) to enable a different set of functions. Because of the lack of genome-wide mapping studies on the aforementioned transcription factors, the transcriptional targets of GDF6-induced BMP signaling remain unknown.

The expression and function of GDF6 were primarily identified in the adult cartilaginous tissues; however, its expression was low or absent in other tissues, such as intestinal, muscular, and placental tissues (Chang et al., 1994). Nevertheless, subsequent studies identified GDF6 expression in several structural tissues, such as connective, tendon, and ligament tissues, during bone repair and healing (Chuen et al., 2004; Wong et al., 2005). Several in vitro studies on the role of GDF6 in adult tissues have indicated that it can induce the expression of structural extracellular matrix proteins, such as collagen and proteoglycan, during bone repair and healing (Li et al., 2003; Nochi et al., 2004; Yeh et al., 2004). Therefore, GDF6 most probably acts as a factor that provides structural support during tendon repair.

As mentioned, GDF6 expression was initially identified only in adult tissues; subsequently, the expression and roles of GDF6 homologs were also noted during embryogenesis. In zebrafish, during the earliest expression of

GDF6, its ortholog gdf6a or radar is expressed as a maternal protein (Goutel et al., 2000). At this stage, gdf6a/radar regulates dorsoventral patterning of the embryo: its loss leads to a dorsalized phenotype, whereas its overexpression results in a ventralized phenotype. In zebrafish, Xenopus, and mice, GDF6 orthologs have also been implicated in retinal development; their loss leads to increased cell death in the developing retina, thus reducing the eye size (Asai-Coakwell et al., 2009; Gosse and Baier, 2009; Hanel and Hensey, 2006; Pant et al., 2013). Consistent with this, the GDF6 locus of patients with coloboma, a disease that causes ocular abnormalities, carries a recurrent deletion (Asai-Coakwell et al., 2007; Gonzalez-Rodriguez et al., 2010). GDF6 also regulates the differentiation of mesenchymal progenitors during skeletal development (Clendenning and Mortlock, 2012). Mice with complete loss of gdf6 demonstrate incomplete skull joint development and bone fusion in the wrists and ankles, because of precocious differentiation (Asai-Coakwell et al., 2009; Settle et al., 2003). Mice with a loss-of-function mutation in gdf5 and gdf6 demonstrate more pronounced skeletal defects and do not progress to adulthood (Settle et al., 2003). Consistent with this, Klippel-Feil syndrome, a disorder associated with skeletal defects in humans, is frequently associated with GDF6 mutations (Tassabehji et al., 2008). Taken together, these findings indicate that GDF6 is pleiotropic with functions, including providing mechanical support to tissues, promoting cell survival, and regulating differentiation.

Zebrafish Model for Melanoma

Overview

Biological and biomedical research using small animal models, such as the zebrafish model, has revealed crucial results. The animal models represent miniature systems to study fundamental biological processes in a physiological context, thereby closing the gap between high-throughput in vitro cell-based systems and low-throughput mouse model systems. These models also have unique attributes, such as ex vivo development at rapid rates, high fecundity, and visual accessibility because of the transparency of embryos. These features have facilitated researchers in elucidating several developmental and disease-related processes.

The use of zebrafish to model cancers and study aspects of tumor biology has increased considerably. Among the several modeled cancers, substantial work has been focused on melanoma research, partly because these models have been exploited for studying NC and melanocyte development. Several genetically engineered melanoma models have been created in zebrafish. In 2005, Patton et al. created the first genetic model of melanoma in zebrafish. The authors coupled melanocyte-specific expression of human mutant BRAF (BRAFV600E) along with loss-of-function P53 to induce melanoma initiation. In subsequent studies, additional melanoma models were created by using other commonly altered melanoma genes, such as NRAS and HRAS (Dovey et al., 2009; Santoriello et al., 2010). Melanomas arising in these zebrafish models

grow outwards and therefore are easy to visualize, dissect, and analyze (Figure 1.4). Histological analysis of melanomas arising in zebrafish had pathological characteristics similar to human melanomas (Dovey et al., 2009; Patton et al., 2005; Santoriello et al., 2010).

Transgenic tools have also been created using zebrafish to study the effect of potential cancer genes on melanoma progression (Ceol et al., 2011) (Figure 1.5). This approach uses two key components: (1) Tg(Pmitfa:BRAFV600E);p53(lf);mitfa(lf) zebrafish, which lacks melanocytes because of a loss-of-function mutation in *mitfa*, and (2) the miniCoopR vector, which harbors both a wild-type copy of *mitfa* and an adjacent cassette into which a potential gene of interest could be recombined and expressed under the mitfa promoter. After the injection of a miniCoopR plasmid into Tg(Pmitfa:BRAFV600E);p53(lf):mitfa(lf) zebrafish embryos, wild-type *mitfa* enables reconstitution of melanocytes, which also express the recombined gene of interest. Because of the genetic background, reconstituted melanocytes also express the tumor-promoting BRAFV600E oncogene, become p53 mutant, and have the propensity to develop into melanomas. If the gene of interest has tumor-promoting properties, it may further accelerate the melanoma onset. Owing to the high fecundity of zebrafish, the aforementioned approach was originally used to screen large numbers of genes for their oncogenic role in melanoma progression (Iyengar et al., 2012). Subsequently, this approach was adapted with Crispr-

Figure 1.4: A zebrafish model of melanoma
Zebrafish with melanocyte-specific expression of *BRAFV600E* and loss of function *P53* develop externally visible melanomas.

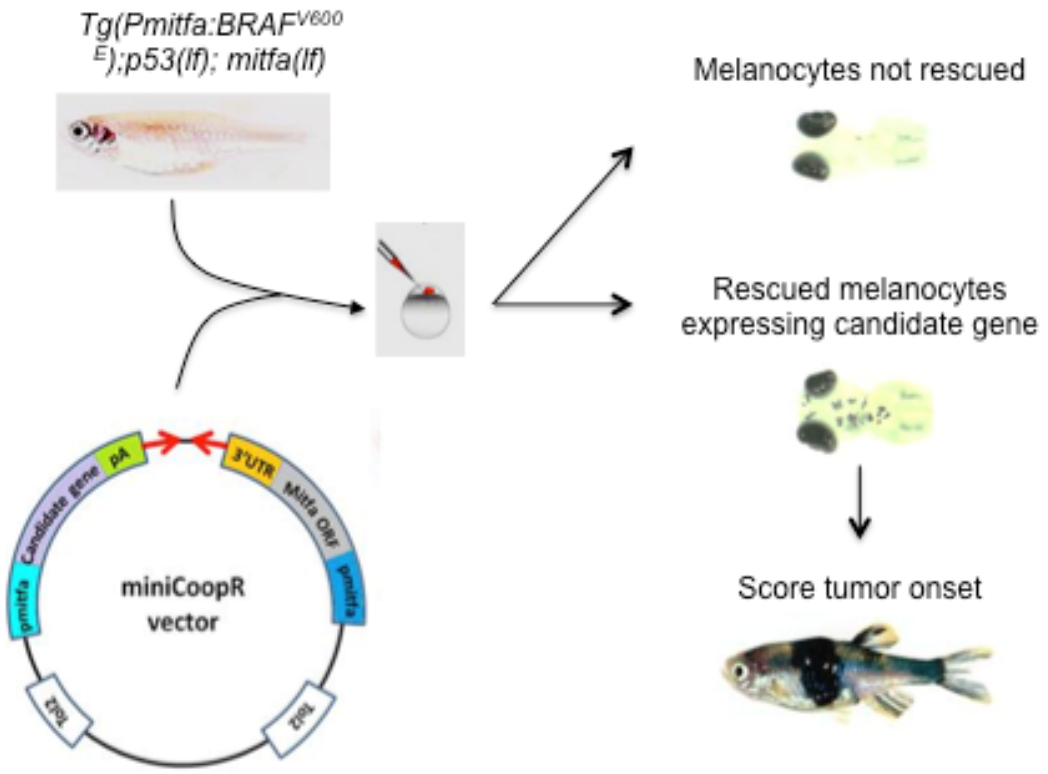

Figure 1.5: miniCoopR assay
Injection of the miniCoopR vector, which contains a mitfa ORF and a candidate gene of interest, into embryos of *mitfa* loss of function zebrafish that lack melanocytes causes a chimeric rescue of melanocytes, and these melanocytes also express the candidate gene. Zebrafish with rescued melanocytes are monitored into adulthood and scored for melanoma onset, and the potential of a gene to accelerate melanoma onset as compared to a control like *EGFP* is measured.

Cas9 targeting to knockout candidate tumor suppressors and test for accelerated tumor onset (Ablain et al., 2015).

Zebrafish Melanoma Genome

The zebrafish melanoma genome has been explored to determine the use of cross-species comparative oncogenomics for identifying commonly altered drivers. Yen et al. (2013) performed exome sequencing of BRAFV600E and NRASQ61K mutant zebrafish melanomas to define DNA base substitutions and recurrent CNVs. DNA base substitution analysis revealed a low mutational burden, unlike human melanomas. Furthermore, mutational analysis indicated a low number of recurrently mutated genes, suggesting that these mechanisms may not considerably contribute to tumor progression. However, zebrafish melanomas, similar to their human counterparts, displayed widespread CNVs. Moreover, the orthologs of human PRKACA and TERT—both of which are known melanoma drivers—were amplified in zebrafish melanomas. These studies suggest that zebrafish melanomas may be primarily driven by CNVs. The results of comparative genomic analysis with human and zebrafish melanomas for ascertaining common genes with CNVs may facilitate the identification of novel cancer drivers.

Examining Role of Developmental Mechanisms in Melanoma Using Zebrafish

Signaling mechanisms involved in melanocyte differentiation are often dysregulated in melanomas, and the zebrafish model has helped gain insight into these mechanisms. As described previously, the role of MITF in melanomas is complex; MITF promotes proliferation at high levels, whereas at low levels, it promotes invasion (Goding, 2011; Golan et al., 2015; Riesenberg et al., 2015). This multifaceted role of MITF has been studied in the zebrafish model during melanocyte development and in melanoma progression. Taylor and colleagues (2011) used a hypomorphic, conditional mitfa, an ortholog of human MITF, to show that low mitfa activity, which was not endogenous, enables the division of terminally differentiated melanocytes. Corroborating these results in the melanoma context, Lister and colleagues (2014) reported that low mitfa activity elevated the oncogenic potential of melanocytes in zebrafish. The authors coupled melanocyte-specific gain-of-function BRAFV600E expression with the hypomorphic mitfa allele and reported that low nonendogenous mitfa activity can initiate tumors and that complete loss of mitfa from an established melanoma leads to tumor regression; thus, MITF is a lineage-addiction oncogene, the expression of which is regulated at a moderate level in melanomas. In addition to MITF, SOX10 and SOX9 are transcription factors that form the core gene regulatory network, which orchestrates melanocyte differentiation (Greenhill et al., 2011). By using mathematical modeling and through experimental observations in zebrafish, Greenhill and colleagues (2011) reported that (1) SOX10 represses MITF-dependent activation of melanocyte lineage genes and

(2) SOX9 activates melanocyte lineage genes in a MITF-independent manner. Notably, in melanomas, SOX10 and SOX9 antagonistically crossregulate each other (Shakhova et al., 2015). SOX10 is essential for melanoma cell survival; SOX10 loss results in SOX9 upregulation, leading to cell cycle arrest and death. Taken together, these findings indicate that the gene regulatory network involved in melanocyte differentiation is critical for melanoma cell growth and survival.

The study of melanomas using zebrafish models has revealed newer roles of NC identities in the early stages of melanomagenesis. Kauffman and colleagues (2016) used zebrafish melanoma to probe NC identities; the authors noted that these identities are invoked in the early stages of tumorigenesis. The authors engineered transgenic zebrafish that expressed EGFP under the promoter of an NC-specific retroelement, crestin. In these fish, EGFP expression was specifically observed in the NC, and this expression was turned off in differentiated melanocytes. When the promoter was introduced in a tumor-prone zebrafish strain, these reporter fish revealed EGFP expression only in melanocytes, which ultimately developed into tumors. These data indicated a fate change toward a more NC state during tumor initiation. Forced activation of this state, by using melanocyte-specific overexpression of the NC sox10, accelerated melanoma onset. In fish and human melanoma cells, the authors reported epigenetic changes that activated several NC factors, indicating a genome-level change in melanomas toward an NC state.

RATIONALE AND OBJECTIVES

Melanomas have widespread CNVs; differentiating driver genes among linked passenger genes within a region of recurrent CNVs is difficult. Here we plan to address this issue of identifying drivers amongst passengers by taking advantage of synteny. Evolution of the genome has caused a great degree of genome reorganization between species. Species whose evolutionary distance is more have more extensive genome reorganization. Because humans and zebrafish have an evolutionary distance of approximately 400 million years, their genome organization is very distinct. While a driver is physically linked to a set of passengers within a CNV region of human melanomas, the ortholog of that driver will most likely be linked to a different set of passengers in zebrafish melanomas. Therefore, I predict that comparative copy number analysis to identify genes commonly amplified or deleted in melanoma of both species should be enriched for driver genes. By using this approach, I plan to identify novel melanoma genes, which recurrently undergo CNVs. Through this approach of comparative genomics, I identify a novel melanoma oncogene, GDF6 and study its functional and mechanistic role in melanoma progression as well as the clinical relevance of its expression in patients with melanoma.

Melanomas can invoke NC identities; however, no study has reported the clinical relevance of these identities in patients with melanoma. Here, I use transcriptome analysis in a zebrafish model of melanoma to identify the NC gene

signature. I further identify the clinical relevance of this signature in patients with melanoma.

CHAPTER II

Ligand-activated BMP signaling inhibits cell differentiation and death to promote melanoma

ABSTRACT

Oncogenomic studies have revealed copy number variations (CNVs) that alter genes involved in tumor progression, but identifying such genes has been difficult because they are often contained in large chromosomal intervals amongst several bystander genes. To address this problem and identify new oncogenes, we performed comparative oncogenomics of human and zebrafish melanomas and found the BMP ligand *GDF6. GDF6*-induced BMP signaling maintains a trunk neural crest gene signature in melanomas. In maintaining this signature, *GDF6* represses the melanocyte differentiation gene *MITF* and the proapoptotic factor *SOX9,* allowing melanoma cells to remain undifferentiated and survive. *GDF6* is specifically expressed in melanomas and not melanocytes, and its expression level in melanomas inversely correlates with patient survival. Our study uncovers a fundamental role for *GDF6* and BMP signaling in governing an embryonic cell gene signature to promote melanoma progression and provides new opportunities for targeted therapy of GDF6-positive cancers.

Introduction

The identification of new cancer-promoting genes has yielded mechanistic insights into tumor progression and led to the development of several targeted therapies. In cutaneous melanoma, the finding of common *BRAF* mutations highlighted the importance of ERK pathway activation in tumor initiation and maintenance. These studies also triggered the design of vemurafenib and other MAPK pathway inhibitors, which were the first drugs to extend survival of patients with advanced disease (Bollag et al., 2010; Chapman et al., 2011; Davies et al., 2002; Larkin et al., 2014). Immunotherapies, such as the CTLA4 inhibitor Ipilimumab and the PD1 inhibitors Nivolumab and Pembrolizumab (Atkins and Larkin, 2016; Leach et al., 1996), have also had a major impact on melanoma therapy as they have dramatically improved the long-term survival rates of advanced-stage patients (Eggermont et al., 2016; Robert et al., 2015b). Despite this progress, many patients do not respond to certain therapies whereas others suffer from drug toxicity, therapy resistance or disease relapse (Robert et al., 2015a; Su et al., 2012; Weber et al., 2012), underscoring a need to identify additional targets for therapeutic intervention.

Along with identifying BRAF and other recurrently mutated cancer genes, sequencing strategies have also defined genomic intervals subject to recurrent copy number variation (CNVs). However, cancer-promoting genes in CNVs have been difficult to identify because: 1) they are often not affected by point mutations and 2) are typically present in large CNVs alongside several bystander genes

that have no effect on tumor progression. Analysis of CNVs has the potential to uncover several new cancer-promoting genes in solid tumors such as melanoma, in which a large percentage of the genome is subject to recurrent CNV (Hodis et al., 2012).

Oncogenomic studies have also revealed expression profiles that reflect broad changes in cellular identity that distinguish cancer cells from normal tissue (Roy and Hebrok, 2015). In many cancers, tumor cells adopt cellular and molecular identities that overlap with their lineally-related embryonic cells. Adopting these identities can endow tumor cells with properties, such as the ability to proliferate or migrate, not found in their differentiated counterparts (Daley, 2008; Hendrix et al., 2007; Maguire et al., 2015). Reawakening of neural crest character in nascent melanomas, as exemplified by expression of neural crest specification factors *SNAI2 (SLUG)* and *BRN3A (POU4F1)* has been shown to enable pro-tumorigenic properties like migration and survival, respectively (Gupta et al., 2005; Hohenauer et al., 2013). Subsequent studies have noted additional gene expression and functional relationships between melanoma and neural crest cells (Shakhova, 2014; White et al., 2011). Whereas similarities between tumor and embryonic cells in melanomas and other cancers have been recognized, the factors that establish and maintain an embryonic identity in tumor cells are poorly understood. Specifically, it is not clear whether embryonic genes are regulated separately to reconstitute an embryonic identity or whether a programmatic change that simultaneously regulates many genes is

involved. In addition, the consequences of abrogating embryonic identity in melanoma and other cancers have not been thoroughly investigated.

In this study we report the identification of the *GDF6* oncogene, a BMP factor that is recurrently amplified and specifically expressed in melanomas. *GDF6*, which is expressed in the embryonic neural crest, regulates a trunk neural crest gene signature in melanomas. Loss of *GDF6* results in differentiation and death of melanoma cells, indicating that *GDF6* and the BMP signaling pathway are required for tumor maintenance and are thus potentially important targets in melanoma therapy.

Results

Comparative oncogenomics and expression analyses identify *GDF6* dysregulation in melanoma

We hypothesized that a cross-species comparative approach with zebrafish would aid in identification of cancer genes in regions of broad CNVs. Humans and zebrafish are diverged by 420 million years (Postlethwait et al., 1999), and the genomic reorganization that has occurred over time is predicted to frequently place orthologous driver genes next to different neighboring genes in each species. Consequently, orthologous driver genes would be altered in both species, but changes to neighboring passenger genes would be limited to a single species. To test this hypothesis, we sought to compare genes that are recurrently amplified in human melanomas, roughly 10% of the genome (Beroukhim et al., 2010), to genes recurrently amplified in zebrafish melanomas. Using melanomas that arose autochthonously in a *Tg(mitfa:BRAFV600E); p53(lf)* zebrafish strain (Patton et al., 2005), we performed array comparative genomic hybridization (aCGH) to generate CNV profiles (Figure 2.1). The *Tg(mitfa:BRAFV600E); p53(lf)* strain combines a transgene that drives expression of human *BRAFV600E* in the melanocyte lineage with a *p53* loss-of-function mutation, and every animal of this genotype ultimately develops one or more melanomas. aCGH values were analyzed with the JISTIC algorithm (Sanchez-Garcia et al., 2010) to define recurrently varied intervals, which largely overlapped with intervals obtained in an independent study of zebrafish

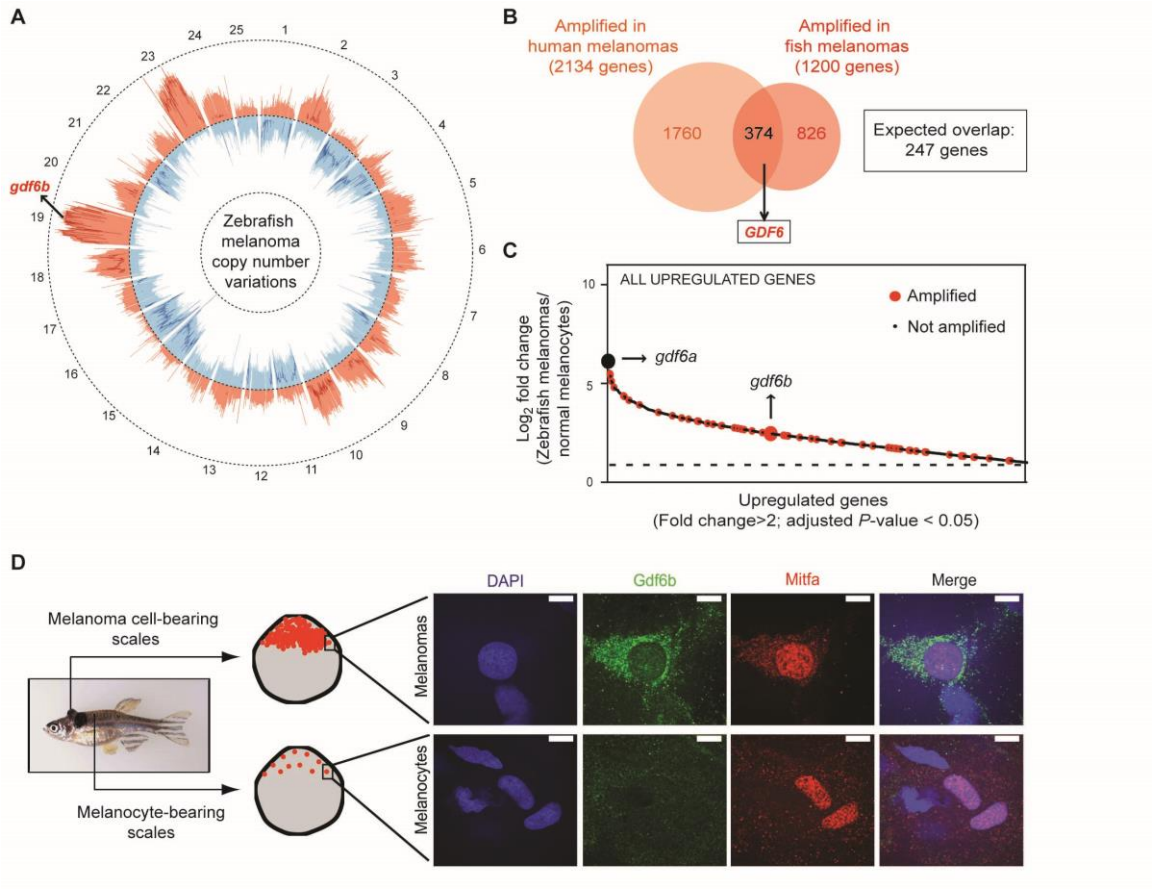

Figure 2.1: *GDF6* is recurrently amplified and specifically expressed in melanomas

(**A**) Circos plot displaying gene copy number gains and losses of zebrafish melanomas across 25 chromosomes. JISTIC G-scores are displayed as pale red shading (amplifications (min=0; max=1550)) and blue shading (deletions (min=0; max=2150)). –log10-transformed JISTIC Q-values with a cut-off of 0.6 (corresponding to an untransformed Q-value of 0.25) are displayed as bold red lines (amplifications (min=0; max=11)) and bold blue (deletions (min=0; max=11)). Dotted circles represent –log10-transformed Q-value of 0 (center) and 11 (outer: amplification; inner: deletion). (**B**) Venn diagram of orthologous genes significantly amplified in human and zebrafish melanomas from a total of 10380 human-zebrafish gene pairs (hypergeometric test, *P*-value: $2.0e^{-15}$) (**C**) Genes significantly upregulated in zebrafish melanomas as compared to melanocytes (microarray dataset) are plotted in order of their fold change. Only genes with fold change > 2 and adjusted *p*-value <0.05 are plotted. Recurrently amplified genes with amplified human orthologs are indicated (red). *gdf6b* (big red dot) and *gdf6a* (big black dot) are indicated. Dashed horizontal line represents a fold change of

2. (**D**) Immunostaining of *Tg(mitfa:BRAF(V600E));p53(lf)* zebrafish scales bearing melanoma cells (top) or normal melanocytes (bottom). DAPI (blue), Gdf6b (green), Mitfa (red), and a merged image of all channels are shown. Mitfa antibody specificity is shown in Figure 2.3. Scale bar, 10 µm.

melanomas (Yen et al., 2013). Recurrently amplified genes from JISTIC intervals were compared to their human orthologs. The degree of overlap between orthologs amplified in both species (374 genes) is greater than would be expected by chance (247 genes) (Figure 2.1), suggesting that amplification of similar driver genes mechanistically underlies tumor formation in both species. As further indication of mechanistic conservation, known melanoma drivers were recurrently amplified in both species, including *TERT*, *MYC* and *SETDB1* (Ceol et al., 2011; Kraehn et al., 2001; Pirker et al., 2003).

Expression analyses were used to further winnow the list of candidates. Since copy-number-amplified driver genes predominantly act by upregulation of wild-type transcripts, we obtained transcriptional profiles of zebrafish melanomas and normal melanocytes. Briefly, unpigmented EGFP-positive melanocytes and melanoma cells were sorted from scales and tumors, respectively, of *Tg(mitfa:BRAFV600E); p53(lf); Tg(mitfa:EGFP); alb(lf)* fish. RNA was prepared from each cell population and subjected to both microarray analysis and massively parallel RNA sequencing (RNAseq). Genes recurrently amplified and transcriptionally upregulated in both species (120 genes; fold change >2, adjusted *P*-value < 0.05) included the BMP factor *GDF6* (a.k.a. *BMP13*) and its zebrafish ortholog *gdf6b* (Figure 2.1, B and C and Figure 2.2, A-C). To determine if Gdf6b protein was similarly enriched in melanomas, we generated an antibody that specifically recognizes Gdf6b (Figure 2.3). Whereas Gdf6b protein was readily detected in tumor cells from *Tg(mitfa:BRAFV600E);p53(lf)* fish, we did not

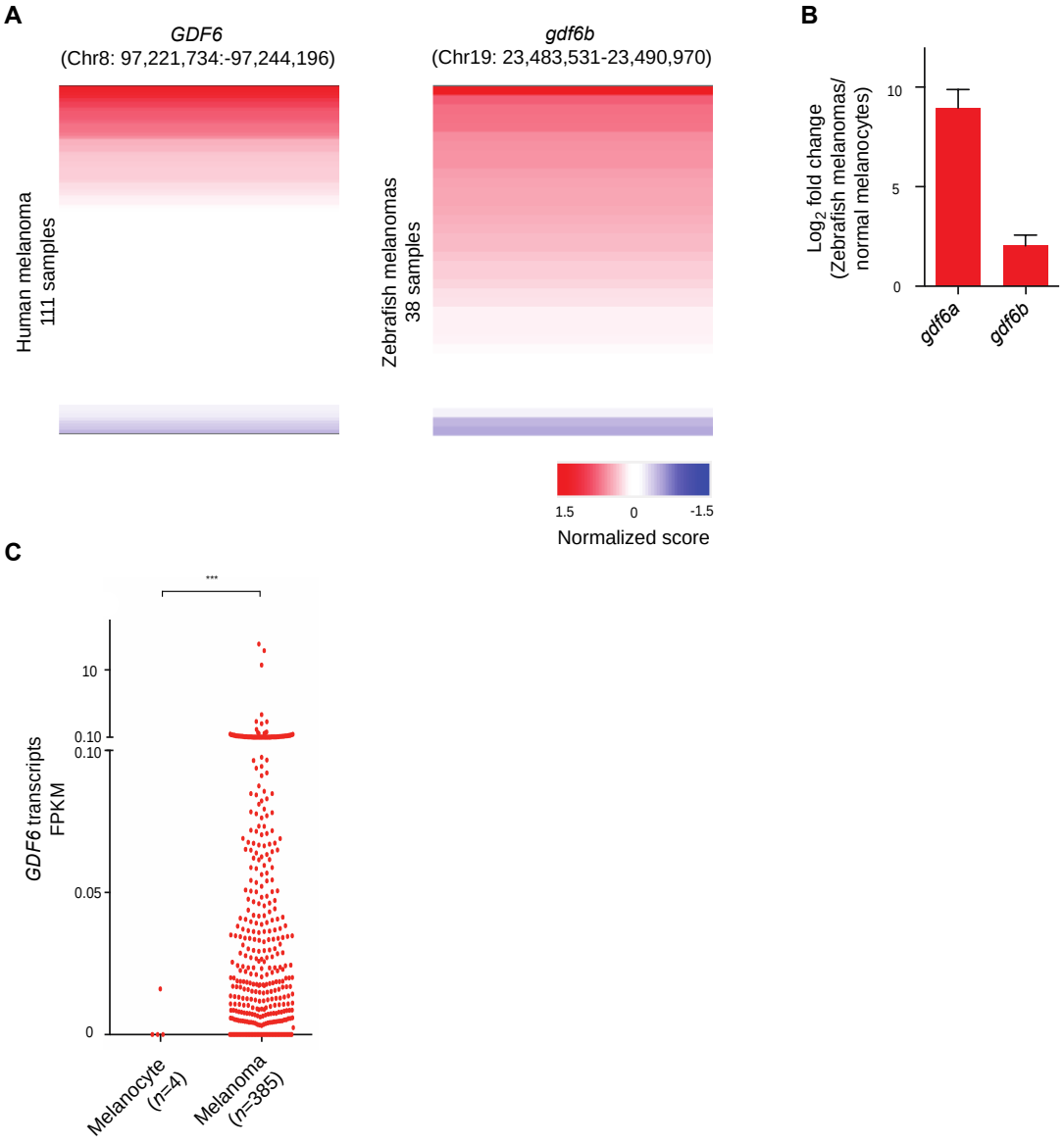

Figure 2.2: *GDF6* orthologs are amplified and upregulated in human and zebrafish melanomas

(**A**) Heat map showing the human *GDF6* locus across 111 human melanomas (left) and the zebrafish *gdf6b* locus across 38 zebrafish melanomas (right). Red indicates amplification, blue indicates deletion. (**B**) Log2-transformed fold change of *gdf6a* and *gdf6b* expression in zebrafish melanomas as compared to melanocytes as determined by qRT-PCR. (**C**) *GDF6* transcript FPKM values from normal human melanocytes and melanomas. Two-tailed Welch's *t*-test ***P<0.001.

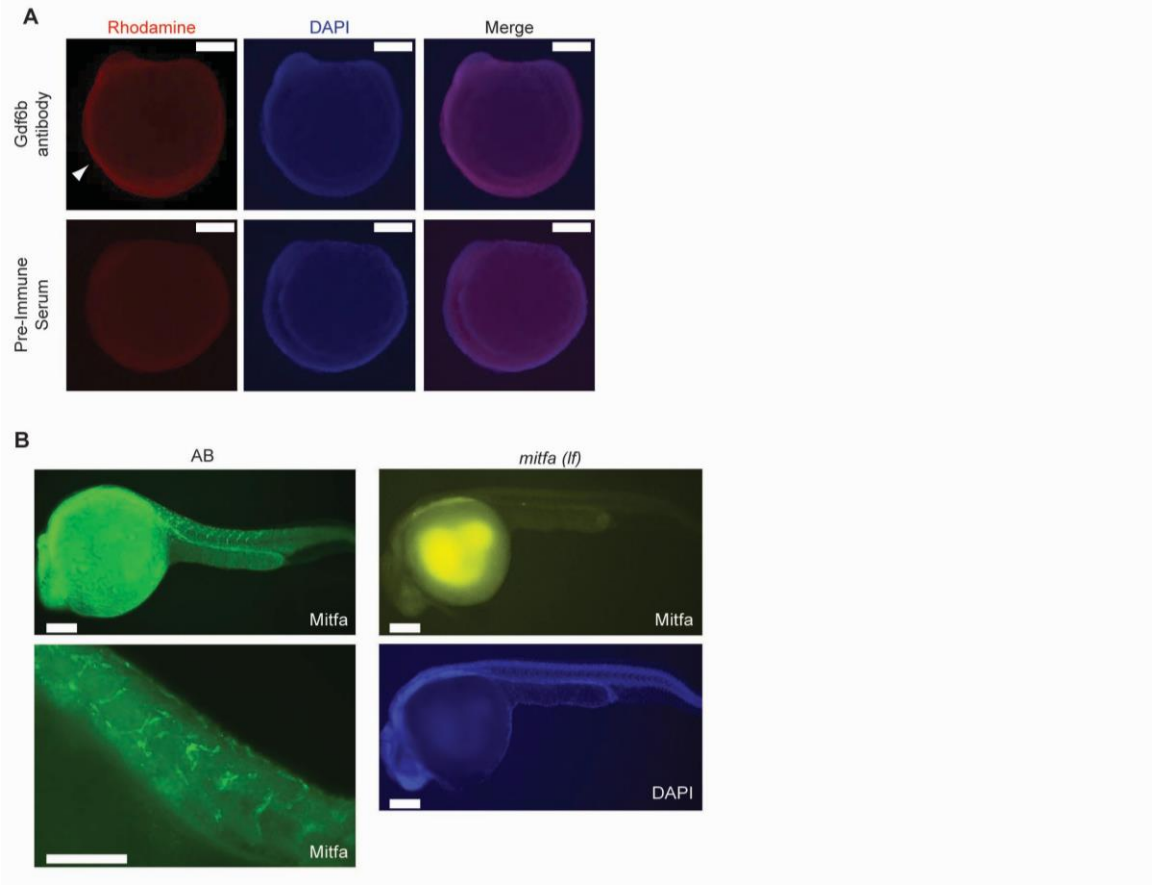

Figure 2.3: Specificity of zebrafish Gdf6b and Mitfa antibodies
(**A**) Immunostaining with Gdf6b antibody (top) and pre-immune serum (bottom) in 4-somite stage AB embryos. Expression of Gdf6b is seen in the neural plate (arrow head) as described previously (Bruneau and Rosa, 1997). Scale bars, 100 µM. (**B**) Left, immunostaining with Mitfa antibody in wild-type AB zebrafish embryos. Right, immunostaining with Mitfa antibody in *mitfa(lf)* zebrafish embryos. Mitfa (top), DAPI (bottom). Scale bars, 100 µM.

detect Gdf6b in normal melanocytes from these same animals (Figure 2.1D). Human genes often have two zebrafish orthologs because of a partial genome duplication in the teleost lineage. The second zebrafish ortholog of human *GDF6*, *gdf6a*, was not recurrently amplified but was among the most transcriptionally upregulated genes in melanomas as compared to melanocytes (Figure 2.1C and Figure 2.2B). Together, these data highlight the recurrent amplification and tumor-specific expression of *GDF6* genes in human and zebrafish melanomas.

GDF6 orthologs were particularly interesting because their expression pattern in zebrafish embryos suggested they may regulate melanocyte development. Zebrafish orthologs of *GDF6* are expressed during neurulation and development of the neural crest, the embryonic tissue that gives rise to melanocytes (Bruneau and Rosa, 1997; Reichert et al., 2013; Rissi et al., 1995). Using in situ hybridization we confirmed expression of *gdf6a* and *gdf6b* in the neural tube and the neural crest, respectively. Later in development, we found that their expression was absent from differentiating embryonic melanocytes (Figure 2.4). Factors involved in neurulation and neural crest signaling have been previously implicated in promoting melanoma progression (Gupta et al., 2005; Kaufman et al., 2016; Maguire et al., 2015), and we were intrigued by the notion that a developmental role for *GDF6* genes could be reiterated to promote melanomagenesis.

GDF6 modulation alters melanoma onset in zebrafish

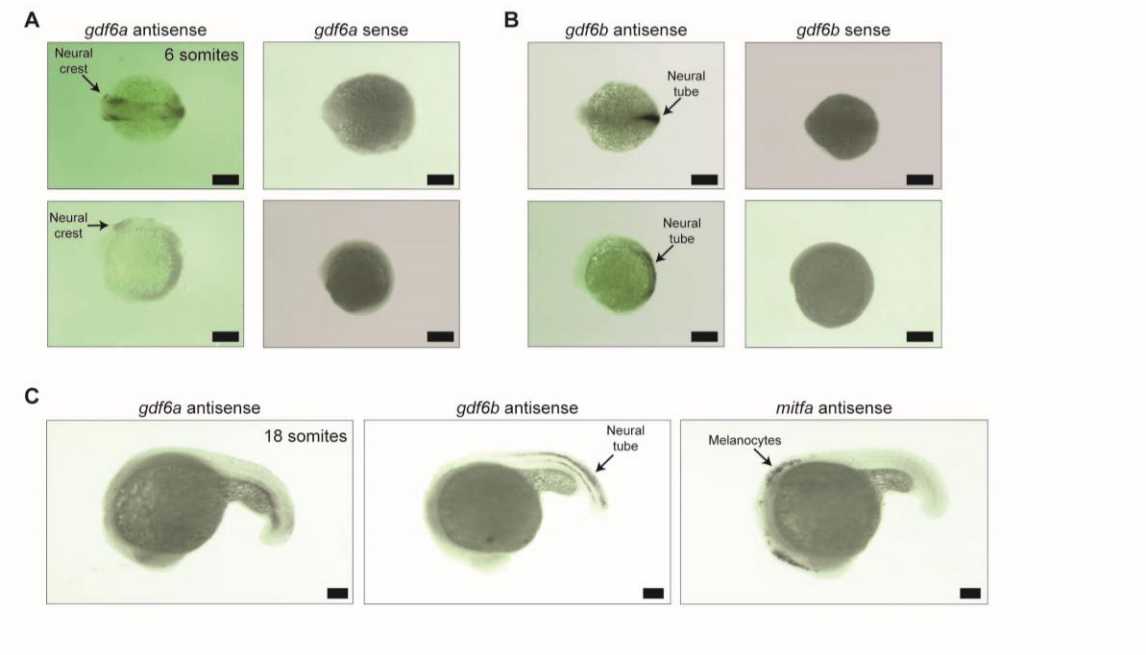

Figure 2.4: Expression of zebrafish *GDF6* orthologs during embryonic development

(**A**) *In situ* hybridization with *gdf6a* antisense probe showing expression of *gdf6a* in the neural crest at the 6-somite stage. A *gdf6a* sense probe was used as a negative control. Top, dorsal view. Bottom, lateral view. Scale bar, 100 µM (**B)** *In situ* hybridization with *gdf6b* antisense probe showing expression of *gdf6b* in the neural tube at the 6-somite stage. A *gdf6b* sense probe was used as a negative control. Top, dorsal view. Bottom, lateral view. Scale bar, 100 µM (**C**) *In situ* hybridization with *gdf6a* and *gdf6b* probes showing their lack of expression at the 18-somite stage. *In situ* hybridization of *mitfa* shows melanocyte specification at this stage. No *gdf6a* or *gdf6b* staining was found in developing melanocytes. Scale bar, 100 µM.

To assess whether *GDF6* genes could promote melanoma, we first examined how their elevated expression affected tumor onset in zebrafish. We expressed *gdf6a* and *gdf6b* in the melanocyte lineage of *Tg(mitfa:BRAFV600E); p53(lf); mitfa(lf)* zebrafish using the miniCoopR system, as previously described (Ceol et al., 2011). The *mitfa(lf)* mutation prevents melanocyte development and melanoma formation in *Tg(mitfa:BRAFV600E); p53(lf)* fish. When single-cell embryos from the *Tg(mitfa:BRAFV600E); p53(lf); mitfa(lf)* strain were injected with miniCoopR-*EGFP,* 21% of these animals later developed chimeric rescue of melanocytes. However, in embryos injected with miniCoopR-*gdf6a* or miniCoopR-*gdf6b,* only 0.6% and 7% of injected animals had melanocyte rescue, respectively (Figure 2.5A). This lack of melanocyte rescue was not observed in control embryos that were injected with miniCoopR vectors that had premature stop codons engineered into the *gdf6* genes (Figure 2.5A). In addition to the low percentages of miniCoopR-*gdf6a* or miniCoopR-*gdf6b*-injected embryos that showed melanocyte rescue, the embryos that were rescued had significantly lower numbers of melanocytes (Figure 2.5B). Because of this poor rescue we were only able to perform melanomagenesis assays with miniCoopR-*gdf6a*-injected animals. When allowed to develop to adulthood, fish with melanocyte-driven *gdf6b* expression had accelerated melanoma onset (median onset = 13 weeks) as compared to *EGFP*-expressing controls (median onset = 17 weeks) (Figure 2.6A). Accelerated onset was dependent on *BRAFV600E* and loss of

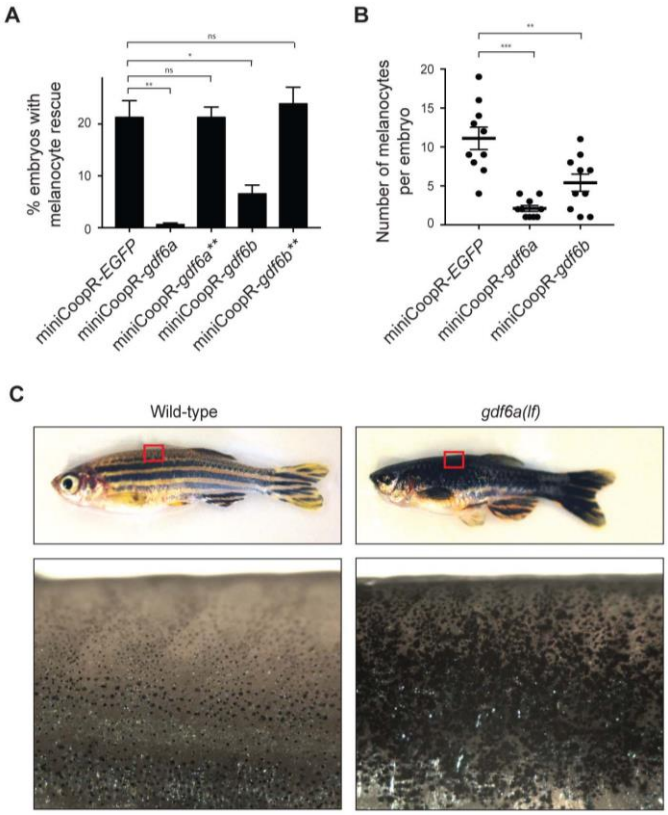

Figure 2.5: Effects of zebrafish *GDF6* orthologs on melanocyte numbers
(A) Quantification of the fraction of zebrafish embryos with melanocyte rescue following injection of indicated miniCoopR constructs in *Tg(mitfa:BRAFV600E);p53(lf);mitfa(lf)* zebrafish. *gdf6a*** and *gdf6b*** are forms of *gdf6a* and *gdf6b* with premature stop codons, respectively. Error bars indicate s.e.m.: *n*=3 independent experiments. **(B)** Quantification of the number of melanocytes per rescued embryo. Error bars indicate s.e.m.: *n*=10 embryos. (**C**) Representative images of *Tg(mitfa:BRAFV600E);p53(lf);gdf6a(lf)/+* and *Tg(mitfa:BRAFV600E);p53(lf);gdf6a(lf)* zebrafish**.** Boxed region from the top panel is shown in the bottom panel. Two-tailed Student's *t*-test, **P*< 0.05, ***P*< 0.01, ****P*< 0.001, ns, not significant.

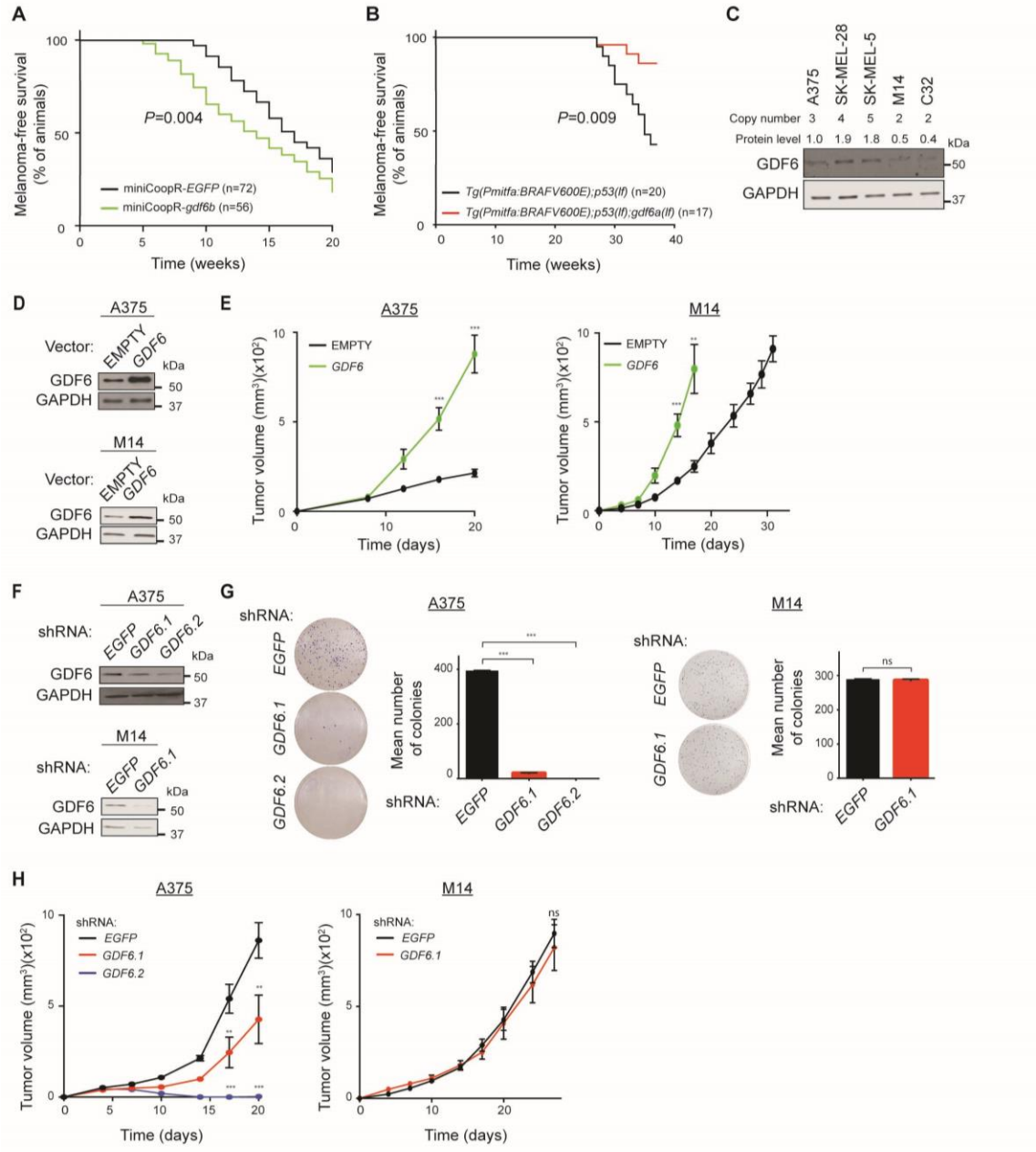

Figure 2.6: *GDF6* modulation alters melanoma growth
(**A**) Melanoma-free survival curves for *Tg(mitfa:BRAFV600E);p53(lf);mitfa(lf)* zebrafish injected with miniCoopR-*gdf6b* or miniCoopR-*EGFP*. Statistical analysis was performed with a Wilcoxon rank sum test. (**B**) Melanoma-free survival curves for *Tg(mitfa:BRAFV600E);p53(lf)* and *Tg(mitfa:BRAFV600E);p53(lf);gdf6a(lf)* zebrafish. Statistical analysis was performed with a Wilcoxon rank sum test. (**C**) Immunoblot showing expression

and quantification of GDF6 protein levels (relative to GDF6 protein in A375 melanoma cells) in melanoma cell lines. Loading control used was GAPDH. Copy number values of the GDF6 locus in the different melanoma cell lines obtained from the COSMIC database are shown. (**D**) Immunoblots showing expression of GDF6 and GAPDH in A375 melanoma cells (top) and M14 melanoma cells (bottom) overexpressing *GDF6*. (**E**) Left, tumor formation in mice injected with A375 cells ($1x10^6$ cells injected per mouse) overexpressing *GDF6* or empty vector control. Error bars indicate s.e.m.; *n*=3. Right, tumor formation in mice injected with M14 cells ($1x10^6$ cells injected per mouse) overexpressing *GDF6* or empty vector control. Error bars indicate s.e.m.; *n*=3. (**F**) Top, immunoblots showing expression of GDF6 in A375 melanoma cells expressing an shRNA targeting *EGFP* or two independent *GDF6*-targeted shRNAs. Bottom, immunoblots showing expression of GDF6 in M14 melanoma cells expressing an shRNA targeting *EGFP* or the *GDF6*-targeted shRNA *GDF6.1*. (**G**) Left, colony formation assay with A375 cells expressing an shRNA targeting *EGFP* or two independent *GDF6*-targeted shRNAs. Error bars indicate s.e.m.; *n*=3. Right, colony formation assay with M14 cells expressing an shRNA targeting *EGFP* or the *GDF6*-targeted shRNA *GDF6.1*. Error bars indicate s.e.m.; *n*=3. (**H**) Left, tumor formation in mice injected with A375 cells ($1x10^7$ cells injected per mouse) expressing an shRNA targeting *EGFP* or two independent *GDF6*-targeted shRNAs. Right, tumor formation in mice injected with M14 cells ($1x10^7$ cells injected per mouse) expressing an shRNA targeting *EGFP* or the *GDF6*-targeted shRNA *GDF6.1*. Error bars indicate s.e.m.; *n*=3. Two-tailed Student's *t*-test, ***P*< 0.01, ****P*< 0.001, ns, not significant. For figure panels 1E and 1H, two-tailed Student's *t*-test was performed by comparing tumor volumes of two groups at a given time point.

p53, as expression of *gdf6b* in *Tg(mitfa:BRAFV600E)* transgene (n=33) or *p53(lf)* (n=24) backgrounds alone did not produce tumors.

We next assayed the consequences of *GDF6* loss in vivo using a zebrafish melanoma model. Since *gdf6a* loss-of-function animals were previously established (Gosse and Baier, 2009), we used these mutants to test the role of *GDF6* loss in melanoma onset. We bred a *gdf6a* loss-of-function mutation into tumor-prone *Tg(mitfa:BRAFV600E); p53(lf)* zebrafish and found that the resulting *Tg(mitfa:BRAFV600E); p53(lf); gdf6a(lf)* mutant animals had substantially delayed melanoma onset as compared to control siblings (Figure 2.6B). Together these results indicate that *GDF6* ortholog activity is important for melanoma initiation: overexpression of *gdf6b* caused accelerated tumor onset, whereas loss of *gdf6a* caused a delay in disease onset.

We also found that *gdf6a*-mutant zebrafish had a profoundly altered pigmentation pattern. An increase in melanocytes in the flank of *gdf6a*-mutant homozygotes was observed, whereas wild-type siblings had normal pigmentation (Figure 2.5C). In combination with our findings above that increased expression of *GDF6* orthologs caused a reduction in the number of embryonic melanocytes, we speculate that these genes have a role in inhibiting melanocyte development.

GDF6 modulation affects tumorigenicity of human melanoma cells

We next wanted to test if *GDF6* modulation altered the growth of human melanoma cells. We first identified cell lines with *GDF6* amplification (A375, SK-

MEL-28 and SK-MEL-5) and others without amplification (M14, C32)(Forbes et al., 2017). Those with amplification had higher levels of GDF6 protein as compared to the non-amplified lines (Figure 2.6C). We overexpressed GDF6 in A375, SK-MEL-28 and M14 melanoma cells (Figure 2.6D and Figure 2.7A), followed by transplantation into immunocompromised mice. In each case elevation of GDF6 expression elevated tumor-forming potential as compared to empty vector controls (Figure 2.6E and Figure S2.7, B and C). GDF6 overexpression also caused an increase in colony-forming potential of A375 cells, indicating that it can also enhance tumorigenic capacity in vitro (Figure 2.7D). These data indicate that increased GDF6, regardless of its endogenous levels, can promote tumorigenicity of melanoma cells.

To determine the effects of *GDF6* loss, we knocked down endogenous *GDF6* in melanoma cells with amplifications and normal copy number of the *GDF6* locus. Knockdown in amplified A375, SK-MEL-28 and SK-MEL-5 cells led to a growth disadvantage in vitro, as measured by anchorage-dependent colony formation (Figure 2.6, F and G, and Figure 2.7, E and F). In xenografts of A375 and SK-MEL-28 cells with *GDF6* knockdown we observed a substantial reduction in tumorigenic potential as compared to control cells with *EGFP* knockdown (Figure 2.6H and Figure 2.7G). However, knockdown of *GDF6* in non-amplified M14 and C32 cells caused little change in anchorage-dependent colony formation (Figure 2.6, F and G, and Figure 2.7, E and F). In addition, in xenografts there was no change in the tumor-forming potential of M14 cells with

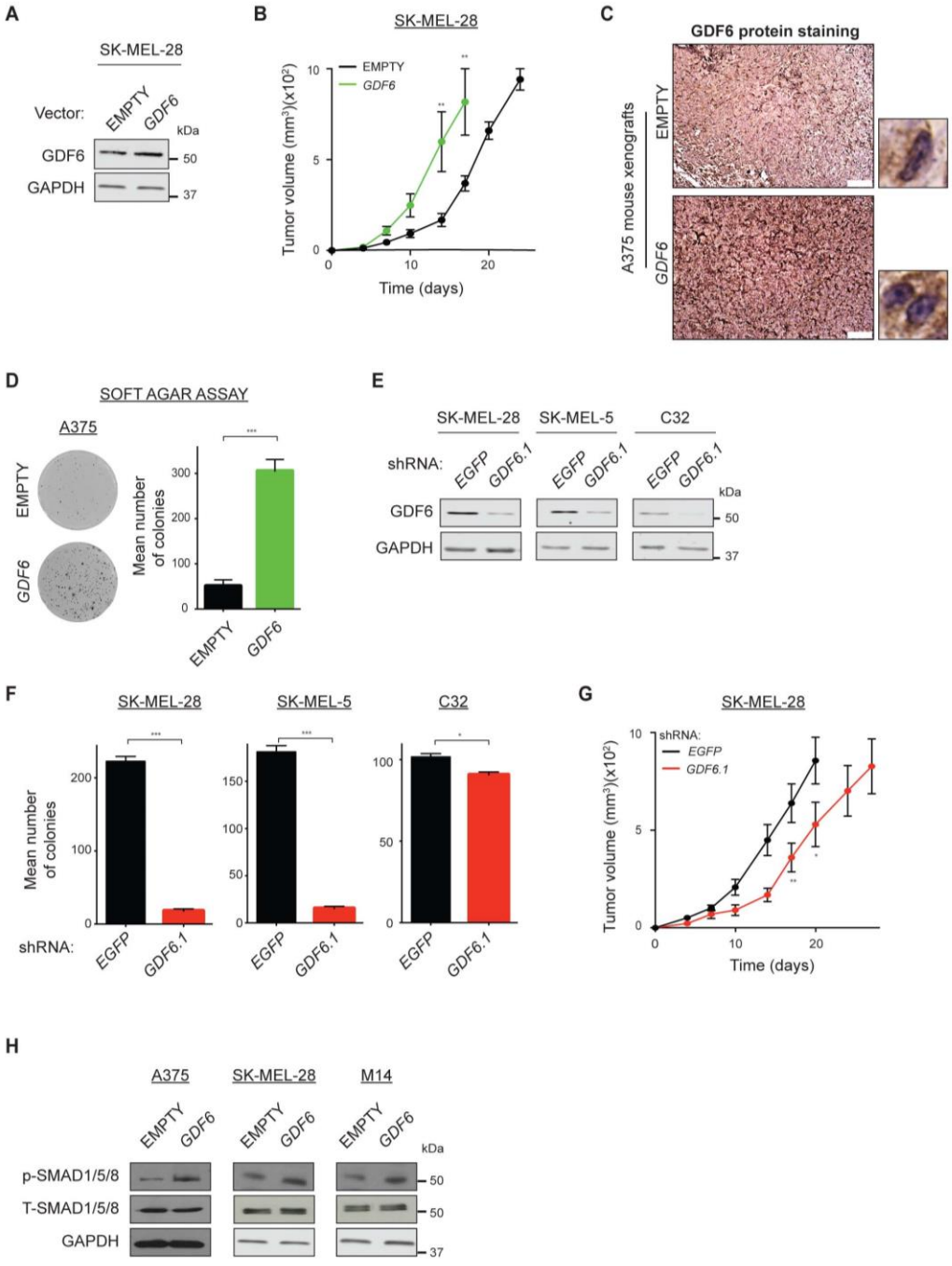

Figure 2.7: *GDF6* modulation alters the tumorigenicity of human melanoma cells

(**A**) Immunoblots of GDF6 and GAPDH from SK-MEL-28 melanoma cells overexpressing *GDF6*. (**B**) Tumor formation in mice injected with SK-MEL-28 cells (1x10^6 cells injected per mouse) overexpressing *GDF6* or empty vector control. Error bars indicate s.e.m.; *n*=3. (**C**) GDF6 staining of mouse xenografts

with A375 melanoma cells overexpressing *GDF6* as compared to empty vector control. Scale bars, 50 μm. Single cells are shown on the right. (**D**) Soft agar assay with A375 melanoma cells overexpressing *GDF6*. Error bars indicate s.e.m.; *n*=3. (**E**) Immunoblots of GDF6 and GAPDH in melanoma cells (labeled at top) expressing *shEGFP* or *shGDF6.1*. (**G**) Colony formation assay with melanoma cells (indicated above) expressing *shEGFP* or *shGDF6.1*. Error bars indicate s.e.m.; *n*=3. (**H**) Tumor formation in mice injected with SK-MEL-28 cells ($1x10^7$ cells injected per mouse) expressing an shRNA targeting *EGFP* or the *GDF6*-targeted shRNA, *GDF6.1*. Error bars indicate s.e.m.; *n*=3. (**I**) Immunoblots of phospho-SMAD1/5/8, total SMAD1/5/8 and GAPDH in melanoma cell lines (indicated above) overexpressing *GDF6* or empty vector control. Two-tailed Student's *t*-test, **P*< 0.05, ***P*< 0.01, ****P*< 0.001. For figure panels S5B and S5G, two-tailed Student's *t*-test was performed by comparing tumor volumes of two groups at a given time point.

GDF6 knockdown as compared to control M14 cells with *EGFP* knockdown (Figure 2.6H). Therefore, whereas all cells examined displayed increased tumorigenic potential upon *GDF6* overexpression, only cells with amplification and higher levels of GDF6 protein were sensitive to *GDF6* knockdown. These results suggest that *GDF6* does not serve a housekeeping function, but that cells with *GDF6* amplification and high expression have become dependent on it for their tumorigenic potential.

BMP signaling is active in melanomas and is driven by *GDF6* ligand

Encoding BMP ligands, *GDF6* genes are predicted to act through *SMAD1/5/8* transcription factors. For this reason we investigated whether SMAD-dependent signaling was activated in melanomas. Using an antibody that specifically recognizes phosphorylated SMAD1/5/8 proteins to monitor BMP pathway activity, we found robust phospho-SMAD1/5/8 nuclear staining in zebrafish melanomas (Figure 2.8A). Furthermore, transcriptome analyses indicated upregulation in zebrafish melanomas of genes that support BMP signaling, including the *BMPR1A* and *BMPR2* receptor subunits, through which GDF6 is known to act (Wang et al., 2013b)(Figure 2.8B). *gdf6a* and *gdf6b* were the only BMP ligands upregulated in zebrafish melanomas leading us to hypothesize that BMP signaling in melanomas is largely dependent on *GDF6* (Figure 2.8C). To address this hypothesis we modulated *GDF6* activity in human melanoma cells. *GDF6* knockdown caused a profound reduction in phospho-

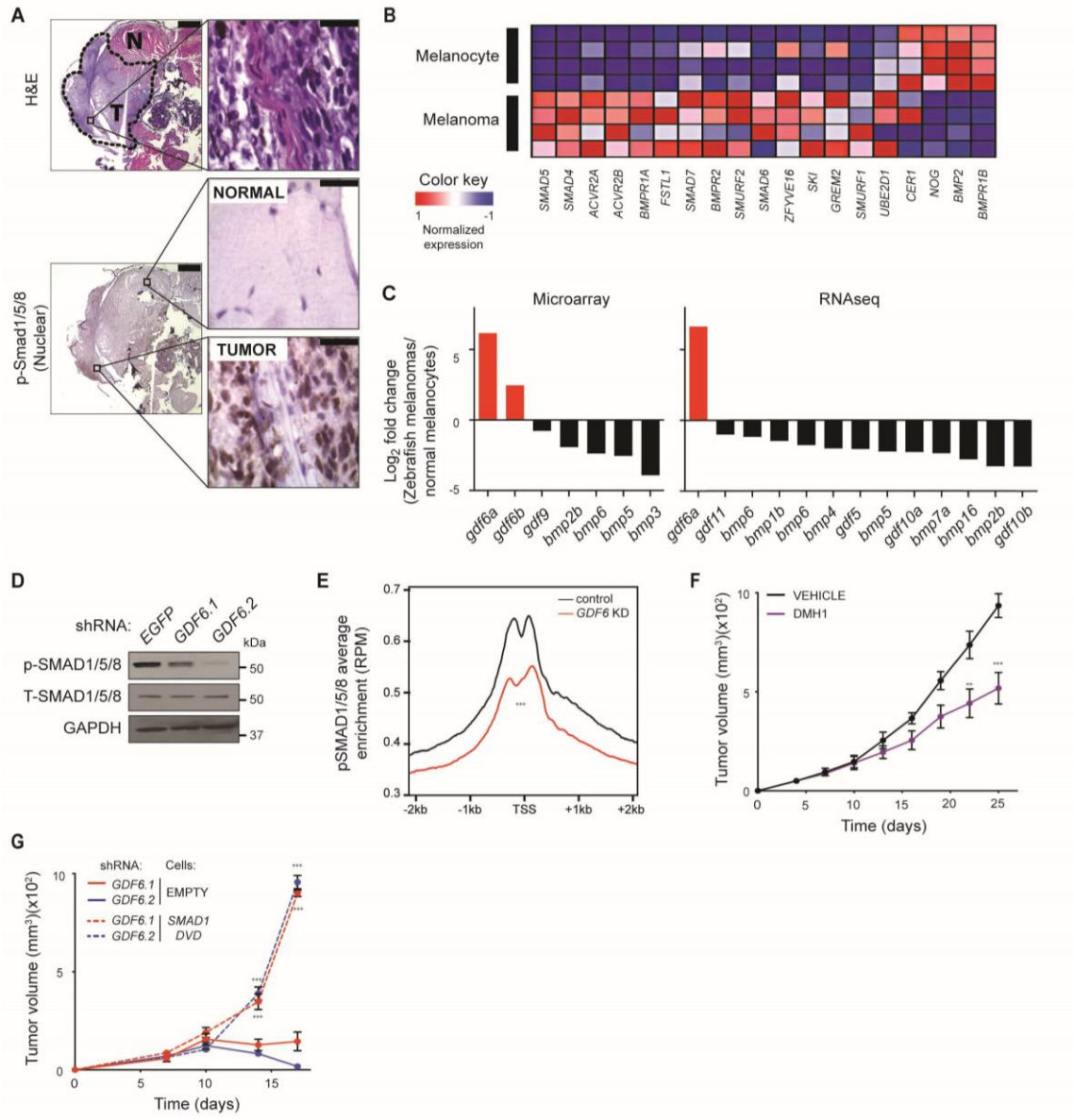

Figure 2.8*: GDF6*-dependent BMP activity in melanomas
(**A**) Transverse sections of a *Tg(mitfa:BRAFV600E);p53(lf)* zebrafish bearing an invasive melanoma in the dorsal musculature. Top, hematoxylin and eosin staining. Bottom, phospho-SMAD1/5/8 staining. Left, scale bar, 500 µm. Right, scale bar, 50 µm. For phospho-SMAD1/5/8 staining, normal muscle (top) and a tumor region (bottom) are shown. Note that normal scale tissue (running vertically through middle of image) in the tumor region is phospho-SMAD1/5/8 negative. T, tumor. N, normal. (**B**) Heat map of gene expression of BMP pathway genes (Reactome gene set R-HSA-201451.3) in zebrafish melanomas as

compared to melanocytes. Human orthologs of zebrafish genes are displayed. (**C**) Log2-transformed fold change of gene expression in zebrafish melanomas as compared to melanocytes (y-axis). Expression of BMP ligands in microarray analysis (left) and RNAseq analysis (right). Only BMP ligands with a significant dysregulation (adjusted *p*-value<0.05) are shown. (**D**) Immunoblots of phospho-SMAD1/5/8 and total SMAD1/5/8 in A375 melanoma cells expressing an shRNA targeting *EGFP* or two independent *GDF6*-targeted shRNAs. (**E**) Aggregation plot of phospho-SMAD1/5/8 ChIPseq enrichment at annotated transcriptional start sites (TSSs) in A375 melanoma cells expressing an shRNA targeting *EGFP* or the *GDF6*-targeted shRNA, *GDF6.1*. ****P* < 2.2e-16 by two-sample Kolmogorov-Smirnov test after summing TSS-proximal reads (-2kb to 2kb) for each gene (*n*=49,344 TSSs). (**F**) Tumor formation in mice injected with A375 cells ($1x10^6$ cells injected per mouse) treated with vehicle control or 25 mg/kg DMH1 every other day. Error bars indicate s.e.m.; *n*=8. (**G**) Tumor formation in mice injected with A375-empty or A375-*SMAD1DVD* cells expressing two independent *GDF6*-targeted shRNAs. Each mouse was injected with $1x10^7$ cells. Error bars indicate s.e.m.; *n*=3. Two-tailed Student's *t*-test, ***P*< 0.01, ****P*< 0.001.

SMAD1/5/8 levels (Figure 2.8D), whereas *GDF6* overexpression led to an increase in phospho-SMAD1/5/8 (Figure 2.7H). Phospho-SMAD1/5/8 proteins translocate to the nucleus where they, in complexes with SMAD4 and/or other regulatory proteins, bind DNA and modulate transcription of target genes. To determine if *GDF6* regulates SMAD1/5/8 DNA-binding activity, we performed chromatin immunoprecipitation and massively parallel sequencing (ChIPseq) of phospho-SMAD1/5/8 in control and *GDF6* knockdown A375 melanoma cells. Binding of phospho-SMAD1/5/8 to promoter regions of target genes was markedly reduced upon *GDF6* knockdown (Figure 2.8E). Likewise, in a broader consideration of all phospho-SMAD1/5/8 bound regions, knockdown of *GDF6* caused a general reduction in binding (Figure 2.9A). Reduction in binding was in many cases accompanied by transcriptional changes; for example, reduced binding and transcriptional downregulation co-occurred at the well-established phospho-SMAD1/5/8 target genes *ID1* and *ID3* (Figure 2.9, B and C). Based on these results, BMP signaling is active in melanomas, and much of this activity is driven by *GDF6.*

GDF6 **acts via the BMP-SMAD pathway to promote tumor progression**

To test if the role of *GDF6* in promoting melanoma progression is mediated by the SMAD1/5/8 axis of BMP signaling, we modulated pathway activity in A375 cells. Knockdown of *SMAD1* led to defects in cell growth and tumorigenic potential (Figure 2.10, A-C), like what was observed in *GDF6*

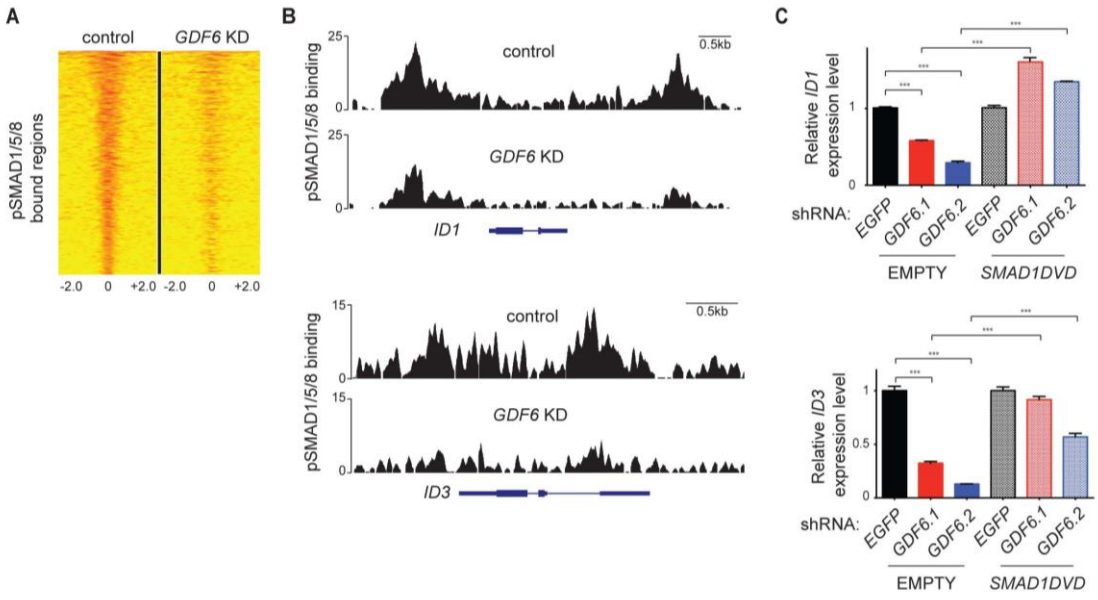

Figure 2.9: *GDF6* knockdown impairs BMP pathway activity
(**A**) Comparison of ChIPseq maps of phospho-SMAD1/5/8 binding in control and *GDF6*-depleted cells. The heat map extends from -2kb to +2kb from the center of each bound region, with each row representing a unique bound region and enrichment denoted in red. The heat map is sorted based on phsopho-SMAD1/5/8 binding in control cells. (**B**) phospho-SMAD1/5/8 binding to the *ID1* locus (top) and *ID3* locus (bottom) in A375 melanoma cells expressing *shEGFP* or *shGDF6.1.* (**C**) qRT-PCR showing expression of *ID1* (top) and *ID3* (bottom) in A375-empty or A375-*SMAD1DVD* cells expressing an shRNA targeting *EGFP* or two independent *GDF6*-targeted shRNAs. Left two brackets, *ID* gene expression is downregulated upon *GDF6* knockdown. Right two brackets, downregulation of *ID* gene expression is reversed in *SMAD1DVD*-expressing cells upon *GDF6* knockdown. Error bars indicate s.e.m.; *n*=3. Two-tailed Student's *t*-test, ***$P<$ 0.001.

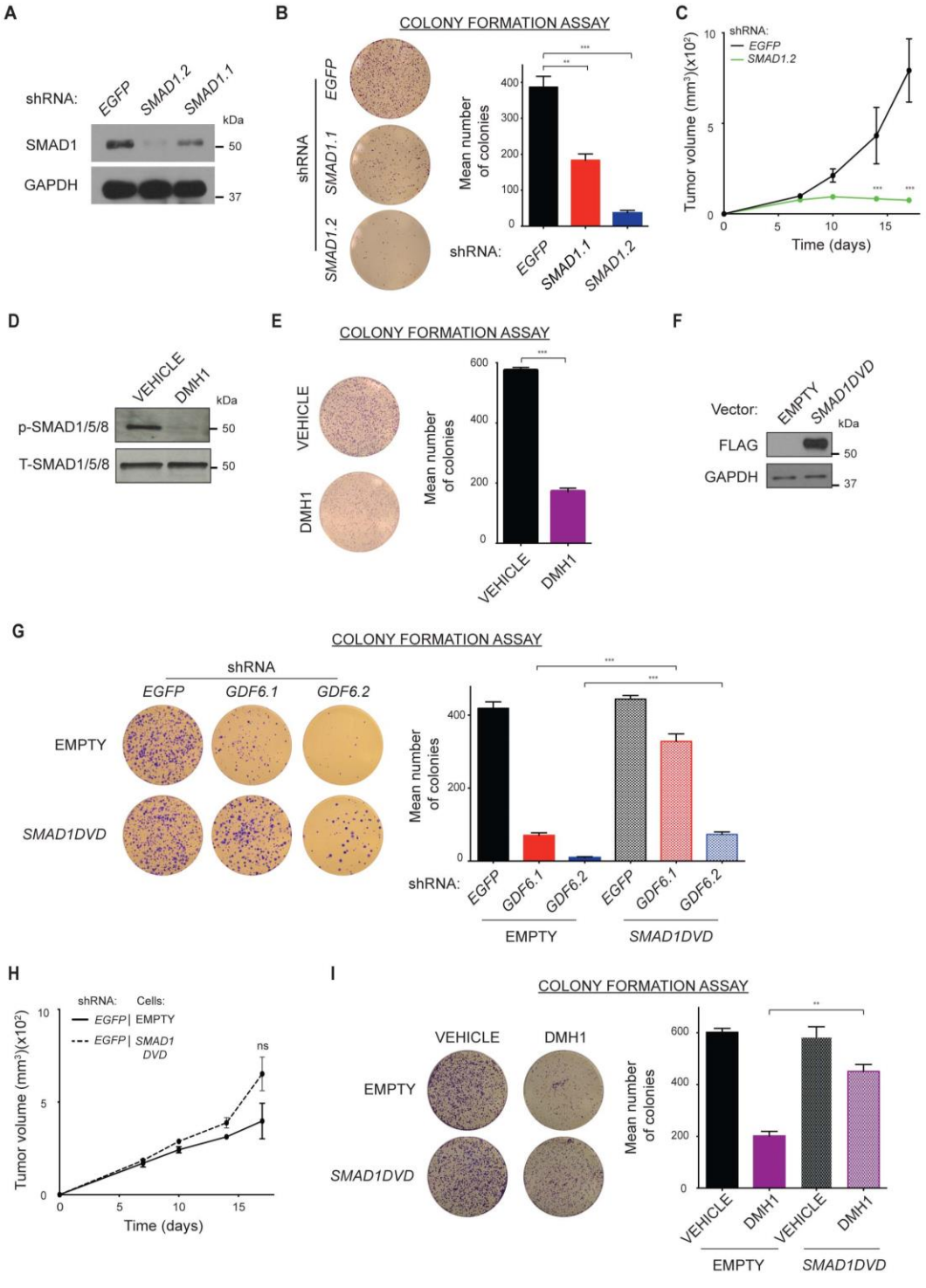
A
shRNA:
EGFP
SMAD1.2
SMAD1.1
kDa
SMAD1
50
GAPDH
37
B
COLONY FORMATION ASSAY
shRNA
EGFP
SMAD1.1
SMAD1.2
Mean number of colonies
shRNA:
EGFP
SMAD1.1
SMAD1.2
C
shRNA:
EGFP
SMAD1.2
Tumor volume (mm³)(x10²)
Time (days)
D
VEHICLE
DMH1
kDa
p-SMAD1/5/8
50
T-SMAD1/5/8
50
E
COLONY FORMATION ASSAY
VEHICLE
DMH1
Mean number of colonies
VEHICLE
DMH1
F
Vector:
EMPTY
SMAD1DVD
kDa
FLAG
50
GAPDH
37
G
COLONY FORMATION ASSAY
shRNA
EGFP
GDF6.1
GDF6.2
EMPTY
SMAD1DVD
Mean number of colonies
shRNA:
EGFP
GDF6.1
GDF6.2
EGFP
GDF6.1
GDF6.2
EMPTY
SMAD1DVD
H
shRNA:
Cells:
EGFP | EMPTY
EGFP | SMAD1 DVD
ns
Tumor volume (mm³)(x10²)
Time (days)
I
COLONY FORMATION ASSAY
VEHICLE
DMH1
EMPTY
SMAD1DVD
Mean number of colonies
VEHICLE
DMH1
VEHICLE
DMH1
EMPTY
SMAD1DVD

Figure 2.10: *GDF6* acts through SMAD1 to promote melanoma progression (**A**) Immunoblots showing expression of SMAD1 and GAPDH in A375 melanoma cells expressing *shEGFP*, *shSMAD1.1* or *shSMAD1.2*. (**B**) Colony formation assay with A375 cells expressing *shEGFP*, *shSMAD1.1* or *shSMAD1.2*. Error bars indicate s.e.m.; *n*=3. (**C**) Tumor formation in mice injected with A375 cells expressing *shEGFP* or *shSMAD1.2*. Error bars indicate s.e.m.; *n*=3. (**D**) Immunoblots showing expression of phospho-SMAD1/5/8 and total SMAD1/5/8 in A375 melanoma cells after treatment with 0.1% DMSO (vehicle) or 10μM DMH1 in 0.1% DMSO. (**E**) Colony formation assay with A375 cells treated with 0.1% DMSO (vehicle) or 10μM DMH1 in 0.1% DMSO. Error bars indicate s.e.m.; *n*=3. (**F**) Immunoblots showing expression of Flag-tagged SMAD1DVD and GAPDH in control and A375-*SMAD1DVD* cells. (**G**) Colony formation assay with A375-EMPTY or A375-*SMAD1DVD* cells expressing *shEGFP*, *shGDF6.1* or *shGDF6.2*. Error bars indicate s.e.m.; *n*=3. (**H**) Tumor formation in mice injected with A375-empty or A375-*SMAD1DVD* cells expressing an *EGFP*-targeted shRNA**.** Each mouse was injected with $1x10^7$ cells. Error bars indicate s.e.m.; *n*=3. (**I**) Colony formation assay with A375-empty or A375-*SMAD1DVD* cells treated with 0.1% DMSO (vehicle) or 10μM DMH1 in 0.1% DMSO. Error bars indicate s.e.m.; *n*=3. Two-tailed Student's *t*-test, ***P*< 0.01, ****P*< 0.001, ns, not significant.

knockdown cells. We also used a small molecule inhibitor of BMP signaling, DMH1, to block pathway activity. DMH1 can suppress growth of BMP-dependent ovarian and lung cancer cells (Hao et al., 2014; Hover et al., 2015), but its efficacy in melanoma has not been reported. DMH1 inhibits kinase activity of ALK2 and BMPR1A (ALK3) receptors but not of BMPR1B (ALK6), thereby abrogating phosphorylation and activation of the SMAD1/5/8 transcriptional cascade (Hao et al., 2010). GDF6 has been shown to act through BMPR1A (ALK3) (Wang et al., 2013b), and we found that treatment with DMH1 reduced phospho-SMAD1/5/8 levels and decreased cell growth and tumorigenicity (Figure 2.8F and Figure 2.10, D and E). To test the relationship of *GDF6* to *SMAD1* in genetic epistasis analyses, we expressed a phosphomimetic variant of *SMAD1*, *SMAD1DVD*, in A375 cells (Figure 2.10F)(Tsukamoto et al., 2014). Whereas *GDF6* knockdown abrogated cell growth and tumorigenic potential of A375 control cells, A375-*SMAD1DVD* cells subjected to *GDF6* knockdown were rescued, exhibiting robust growth in colony formation and xenotranplantation assays (Figure 2.8G and Figure 2.10, G and H) Growth defects caused by treatment with DMH1 were also reversed by *SMAD1DVD* (Figure 2.10I). Together these data indicate that *GDF6* signals via SMAD-dependent BMP signaling to promote tumorigenesis, and inhibition of this signaling achieves a reduction in tumor growth.

GDF6-dependent BMP signaling maintains a trunk neural crest gene signature

Since *GDF6* acts through SMAD transcription factors, we were interested in identifying gene expression changes that could illuminate how this signaling axis regulates tumorigenesis. To do this, we modulated *GDF6* and *SMAD1* and sought genes commonly regulated by both. Based on our genetic epistasis results, we predicted that expression of important genes would change upon *GDF6* knockdown but such changes would be reversed when *GDF6* knockdown was rescued by *SMAD1DVD*. Using RNAseq, we defined the set of genes that was differentially regulated upon *GDF6* knockdown and showed reciprocal differential regulation in *SMAD1DVD*-expressing cells that were subjected to *GDF6* knockdown (Figure 2.11A). Pathway analysis showed that this gene set most significantly overlapped with genes involved in ossification and neural crest development (Figure 2.11B). GDF6-SMAD regulation of neural crest genes is intriguing since melanocytes initially develop from this embryonic tissue. Several genes upregulated by *GDF6* and *SMAD1DVD* – *SOX10, TFAP2B, FOXD3, SNAI2* - are neural crest 'specifiers', genes that are expressed broadly in the neural crest and help to maintain neural crest identity (Figure 2.11C)(Sauka-Spengler and Bronner-Fraser, 2008). *SOX9* is initially broadly expressed in the neural crest, but as development proceeds its expression becomes excluded from trunk neural crest and limited to cranial neural crest, from which mesenchymal tissues such as craniofacial cartilage are derived. Conversely,

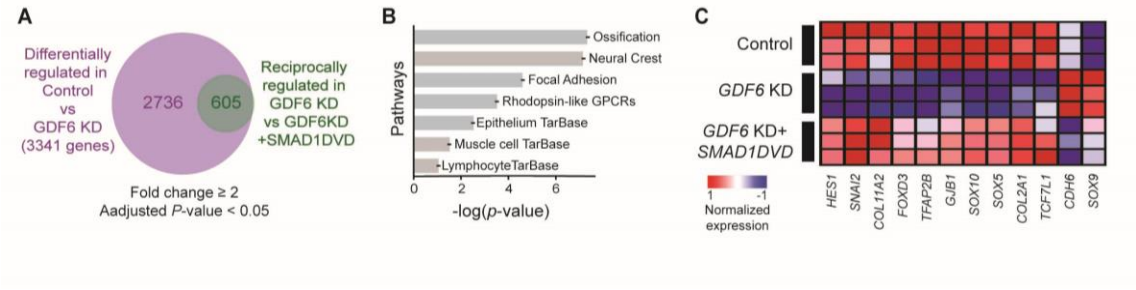

Figure 2.11: *GDF6* and *SMAD1* regulate a neural crest gene signature in melanomas

(**A**) Genes differentially regulated in A375 melanoma cells upon *GDF6* knockdown (purple circle) and genes reciprocally regulated in *SMAD1DVD*-expressing A375 cells upon *GDF6* knockdown (green circle). (**B**) Pathway analysis with the 605 reciprocally regulated genes (minimum overlap ≥ 10 genes; adjusted *P*-value < 0.01). (**C**) Heat map of neural crest genes identified in pathway analysis.

SOX10 expression becomes restricted to trunk neural crest from which non-mesenchymal cells, including melanocytes, develop. Since *SOX10* is upregulated and *SOX9* is downregulated by GDF6-SMAD signaling, the pattern of gene regulation most closely resembles trunk neural crest tissue. Adopting a neural crest-like identity can contribute to the aggressive nature of melanoma cells (Hendrix et al., 2007; Hoek and Goding, 2010). For these reasons we hypothesized that *GDF6*-driven BMP signaling (GDF6-SMAD), by promoting a trunk neural crest gene signature, enables melanoma cells to adopt and maintain an undifferentiated, pro-tumorigenic state.

GDF6* inhibits melanoma cell differentiation by repressing *MITF

To determine how GDF6-driven BMP signaling could regulate the differentiation of melanoma cells, we considered target genes that were bound by phospho-SMAD1/5/8 and transcriptionally regulated in a *GDF6*-dependent manner. Among these genes was *MITF,* the master regulator of melanocyte differentiation. In control A375 cells, phospho-SMAD1/5/8 binding was observed in the *MITF* locus in a region that is intronic for longer *MITF* isoforms and upstream of the smaller *MITF-M* isoform, the predominant species of *MITF* in melanocytes and melanomas (Figure 2.12A)(Fuse et al., 1996). Binding to this region was abrogated in *GDF6* knockdown cells. This loss of binding in *GDF6* knockdown melanoma cells was coupled with a transcriptional increase in *MITF* (Figure 2.12B)*. MITF* itself is a transcriptional factor that orchestrates

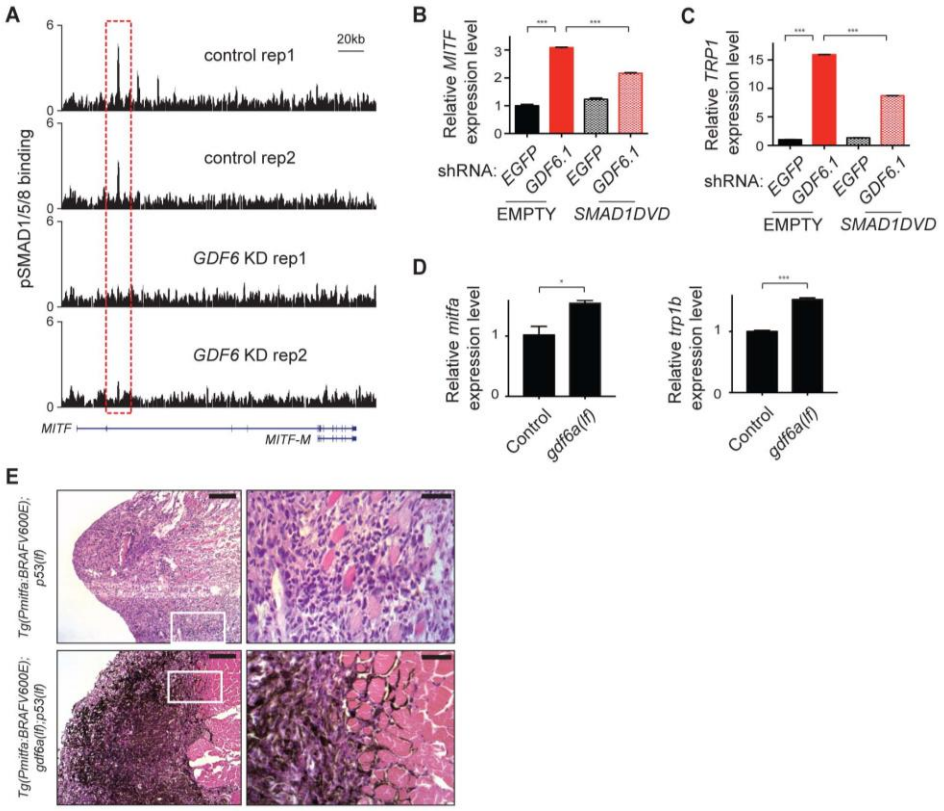

Figure 2.12: *GDF6*-induced BMP signaling blocks melanoma cell differentiation

(**A**) phospho-SMAD1/5/8 binding to the *MITF* locus in A375 melanoma cells expressing an shRNA targeting *EGFP* or the *GDF6*-targeted shRNA, *GDF6.1*. Traces of two independent biological replicates are shown. (**B**) qRT-PCR showing expression of *MITF* in A375-empty or A375-*SMAD1DVD* cells expressing an shRNA targeting *EGFP* or the *GDF6*-targeted shRNA, *GDF6.1*. (**C**) qRT-PCR of *TRP1* under the same conditions. Left brackets, *MITF* or *TRP1* expression is upregulated upon *GDF6* knockdown. Right brackets, *MITF* or *TRP1* expression is less upregulated in *SMAD1DVD*-expressing cells upon *GDF6* knockdown. Error bars indicate s.e.m.; *n*=3. (**D**) qRT-PCR showing expression of *mitfa* (left) and *trp1b* (right) in control and *gdf6a(lf)* zebrafish melanomas. Error bars indicate s.e.m.; *n*=3. (**E**) Hematoxylin and eosin staining of transverse sections from *Tg(mitfa:BRAFV600E);p53(lf)* (top) and *Tg(mitfa:BRAFV600E);p53(lf);gdf6a(lf)* (bottom) zebrafish melanomas invading the dorsal musculature. Left scale bars, 100 µm. Right scale bars, 25 µm. Two-tailed Student's *t*-test, **P*<0.05, ***P*< 0.01, ****P*< 0.001.

differentiation, in part, by activating expression of melanin biosynthesis genes. The increase in *MITF* upon *GDF6* knockdown was accompanied by an increase in the melanin biosynthesis gene *TRP1* (Figure 2.12C), indicating that melanocyte differentiation was invoked upon *GDF6* loss. Upregulation of *MITF* and *TRP1* was less pronounced when *GDF6* knockdown was performed in *SMAD1DVD*-expressing cells (Figure 2.12, B and C). Depending on cofactors involved, phospho-SMAD1/5/8 can promote transcription, as with *ID1* and *ID3*, or repress transcription, as we propose for *MITF* (Massague et al., 2005). To determine if *GDF6* regulates differentiation of melanomas in vivo, we examined tumors that arose in *Tg(mitfa:BRAFV600E); p53(lf); gdf6a(lf)* zebrafish. Melanomas from these animals had increased transcript levels of *mitfa* and *trp1b,* orthologs of the human *MITF* and *TRP1* genes (Figure 2.12D). Furthermore, *gdf6a* mutant tumors exhibited a profound increase in melanization as compared to control tumors (Figure 2.12E). Based on these results, *GDF6* maintains melanomas in an undifferentiated state, and we speculate that preventing differentiation helps melanoma cells retain a neural crest identity.

***GDF6* represses *SOX9* to promote melanoma cell survival**

Knockdown of *GDF6* and *SMAD1* caused defects in melanoma cell growth. We sought to understand this defect and whether the trunk neural crest signature was involved. A variety of analyses suggested that the growth defect was linked to regulation of apoptosis. Specifically, gene set enrichment analysis

(GSEA) revealed that *GDF6* expression negatively correlated with expression of apoptotic pathway genes both in cells with *GDF6* modulation as well as in patient samples (Figure 2.13A and Figure 2.14, A and B). In direct assessments, *GDF6* loss increased apoptotic cell death in A375 cells as well as in vivo in zebrafish melanomas and mouse xenografts (Figure 2.13, B and C, and Figure 2.14, C-E). By contrast, *GDF6* overexpression xenografts showed reduced apoptotic cell death as compared to basal levels of cell death in control xenografts (Figure 2.14, F and G). *GDF6* overexpression xenografts had a slightly increased Ki67 proliferative index, suggesting that the reduction in cell death was not caused by a failure to generate new cells with the potential to die (Figure 2.14H). Finally, the cell death caused by *GDF6* knockdown was rescued by *SMAD1DVD* expression, indicating that *GDF6* acts via BMP signaling to promote melanoma cell survival (Figure 2.13D and Figure 2.15). The involvement of *GDF6* in cell death is consistent with findings in which loss of *GDF6* orthologs in fish and Xenopus caused a substantial increase in apoptosis during eye and neural development (Asai-Coakwell et al., 2013; Hanel and Hensey, 2006; Pant et al., 2013). We speculate that *GDF6* knockdown causes terminal differentiation of melanoma cells, leading to cell cycle exit followed by cell death.

To determine how *GDF6* and BMP signaling regulate melanoma cell survival, we focused on the reciprocally regulated genes defined previously. In particular, *SNAI2* and *SOX9* were assessed because of their importance in specifying neural crest and regulating cell survival

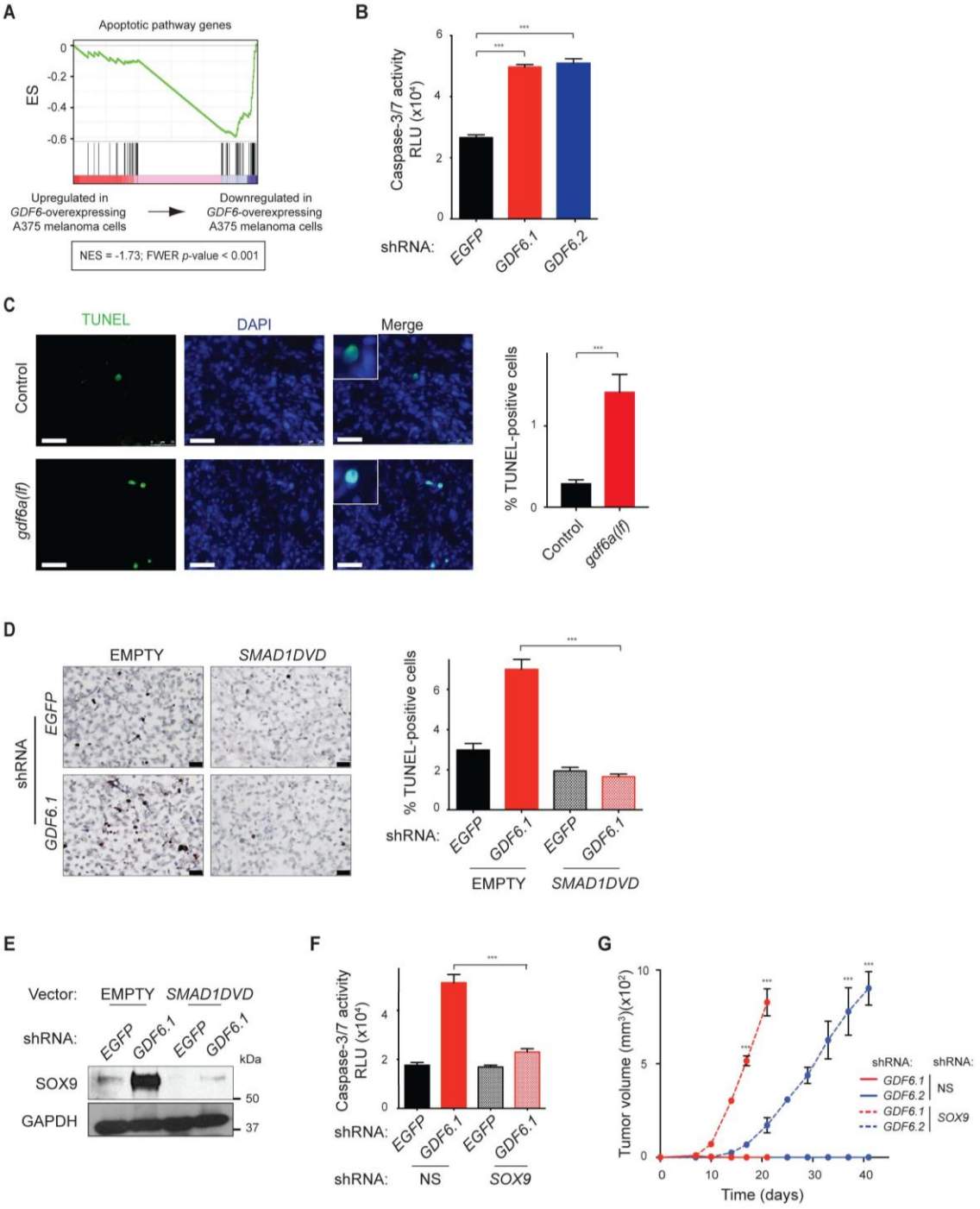

Figure 2.13: *GDF6* and BMP signaling repress *SOX9* to promote melanoma cell survival

(**A**) GSEA shows that expression of an apoptotic gene set (MSigDB- M10169) is negatively enriched in *GDF6*-overexpressing A375 cells. (**B**) Caspase-3/7 activity measured as relative luciferase units (RLU) in A375 cells upon *GDF6*

knockdown. Error bars indicate s.e.m.; *n*=3. (**C**) Fluorescent TUNEL staining of *Tg(mitfa:BRAFV600E);p53(lf)* (left) or *Tg(mitfa:BRAFV600E);p53(lf);gdf6a(lf)* (right) zebrafish melanoma sections. TUNEL (green), DAPI (blue), and a merged image of both channels is shown. Scale bar, 25 μm. Error bars indicate s.e.m.: n= 100 fields. (**D**) TUNEL staining of mouse xenografts of A375 cells expressing *SMAD1DVD* upon *GDF6* knockdown. Scale bar, 25μm. Error bars indicate s.e.m.; *n*=100 fields. (**E**) Immunoblots showing expression of SOX9 and GAPDH in A375-empty or A375-*SMAD1DVD* cells expressing an shRNA targeting *EGFP* or the *GDF6*-targeted shRNA, *GDF6.1*. (**F**) Caspase-3/7 activity measured as relative luciferase units (RLU) in A375-non-silencing (NS) or A375-*shSOX9* cells expressing an shRNA targeting *EGFP* or the *GDF6*-targeted shRNA, *GDF6.1*. Error bars indicate s.e.m.; *n*=3. (**G**) Tumor formation in mice injected with A375-non-silencing or A375-*shSOX9* cells expressing two independent *GDF6*-targeted shRNAs. Each mouse was injected with $1x10^6$ cells. Error bars indicate s.e.m.; *n*=3. Two-tailed Student's *t*-test, $^{**}P< 0.01$, $^{***}P< 0.001$.

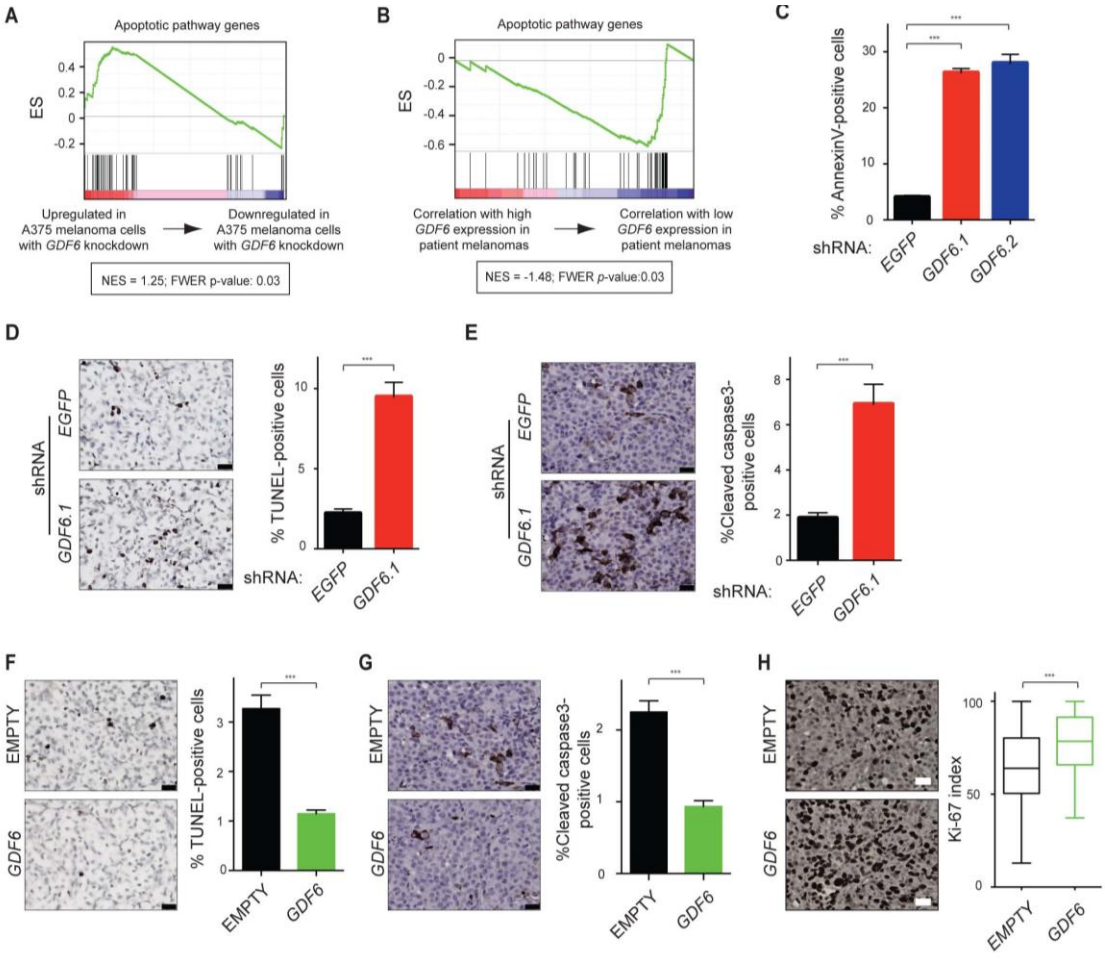

Figure 2.14: *GDF6* knockdown causes melanoma cell death

(**A**) GSEA shows that expression of an apoptotic gene set **(**MSigDB- M10169) is positively enriched in *GDF6*-knockdown A375 cells (**B**) GSEA shows that expression of an apoptotic gene set **(**MSigDB- M10169) is negatively enriched in patient-derived melanomas (TCGA) expressing high levels of *GDF6*. (**C**) Flow cytometry analysis of annexinV-positivity of A375 cells upon *GDF6* knockdown. Error bars indicate s.e.m.; *n*=3. (**D**) TUNEL staining of mouse xenografts of A375 cells upon *GDF6* knockdown. Scale bar, 25µm. Error bars indicate s.e.m.; *n*=100 fields. (**E**) Cleaved Caspase-3-staining of mouse xenografts of A375 cells upon *GDF6* knockdown Scale bar, 25µm. Error bars indicate s.e.m.; *n*=100 fields. (**F**) TUNEL staining of mouse xenografts of A375 cells upon *GDF6* overexpression. Scale bar, 25µm. Error bars indicate s.e.m.; *n*=100 fields. (**G**) Cleaved Caspase-3-staining of mouse xenografts of A375 cells overexpressing *GDF6* or empty vector control. Scale bar, 25µm. Error bars indicate s.e.m.; *n*=100 fields. (**H**) Ki-67 staining of mouse xenografts of A375 cells overexpressing *GDF6* or empty vector control. Scale bar, 25µm. Right, quantification of Ki67-positive cells (Ki-67

index); Error bars indicate s.e.m.; *n*=100 fields. Two-tailed Student's *t*-test, **P*< 0.05, ***P*< 0.01, ****P*< 0.001.

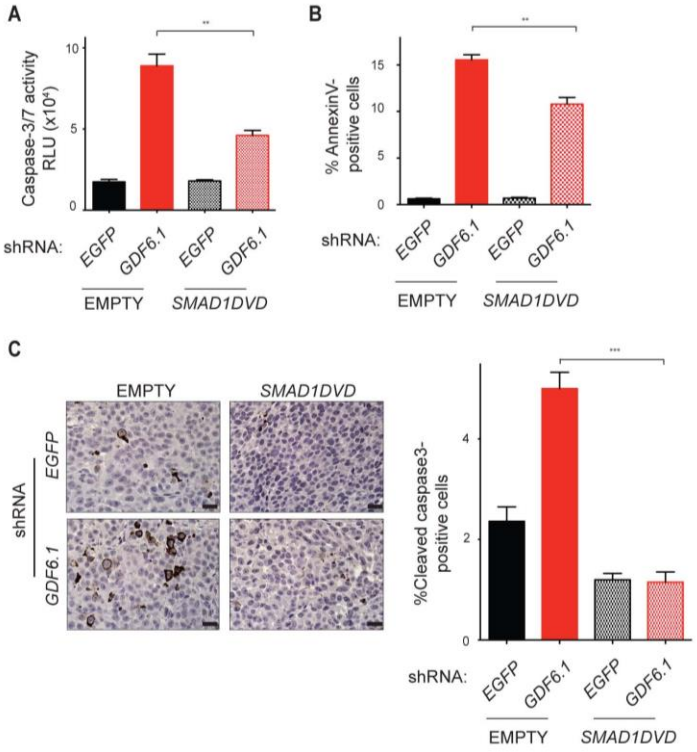

Figure 2.15: *GDF6* knockdown-induced cell death is rescued by *SMAD1DVD*
(**A**) Caspase-3/7 activity measured as relative luciferase units (RLU) in A375-empty or A375-*SMAD1DVD* cells expressing an shRNA targeting *EGFP* or the *GDF6*-targeted shRNA, *GDF6.1*. Error bars indicate s.e.m.; *n*=3. (**B**) Flow cytometry analysis of annexinV-positivity of A375-empty or A375-*SMAD1DVD* cells expressing an shRNA targeting *EGFP* or the *GDF6*-targeted shRNA, *GDF6.1*. Error bars indicate s.e.m.; *n*=3. (**C**) Cleaved Caspase-3 staining of mouse xenografts of A375-empty or A375-*SMAD1DVD* cells expressing an shRNA targeting *EGFP* or the *GDF6*-targeted shRNA *GDF6.1*. Scale bar, 25µm. Error bars indicate s.e.m.; *n*=100 fields. Two-tailed Student's *t*-test, ***P*< 0.01, ****P*< 0.001.

(Cheung and Briscoe, 2003; Greenhill et al., 2011; Kajita et al., 2004; Shakhova et al., 2015). Whereas modulation of *SNAI2* had no effect on *GDF6*-driven survival (Figure 2.16), *SOX9* was intimately involved. In studying *SOX9,* we first confirmed that changes in *GDF6* and BMP signaling affected *SOX9* expression. A375 cells with *GDF6* knockdown had increased *SOX9* RNA and protein levels, and this increase was much less pronounced in *SMAD1DVD* cells that were subjected to *GDF6* knockdown (Figure 2.13E and Figure 2.17A). Additionally, *gdf6a* mutant zebrafish melanomas showed elevated *sox9b* levels (Figure 2.17B). To determine if *GDF6* mediates cell survival by regulating *SOX9* we measured whether knockdown of *SOX9* (Figure 2.17, C and D) could suppress the growth defects and cell death resulting from *GDF6* knockdown. In colony formation assays, cells with combined knockdown of *SOX9* and *GDF6* grew much better than did *GDF6* single knockdown cells (Figure 2.17E). Similarly, cell death, as measured by caspase-3 cleavage and annexinV positivity, was greatly reduced in *GDF6/SOX9* double knockdown cells (Figure 2.13F and Figure 2.17F). Lastly, the ability of *SOX9* knockdown to rescue the tumor-forming capacity of *GDF6* knockdown cells was measured. When performed together with *GDF6* knockdown, *SOX9* knockdown enabled cells to engraft and rapidly grow (Figure 2.13G and Figure 2.17G). These data indicate that a major function of *GDF6* is to repress *SOX9* expression, thereby inhibiting cell death and promoting tumor growth.

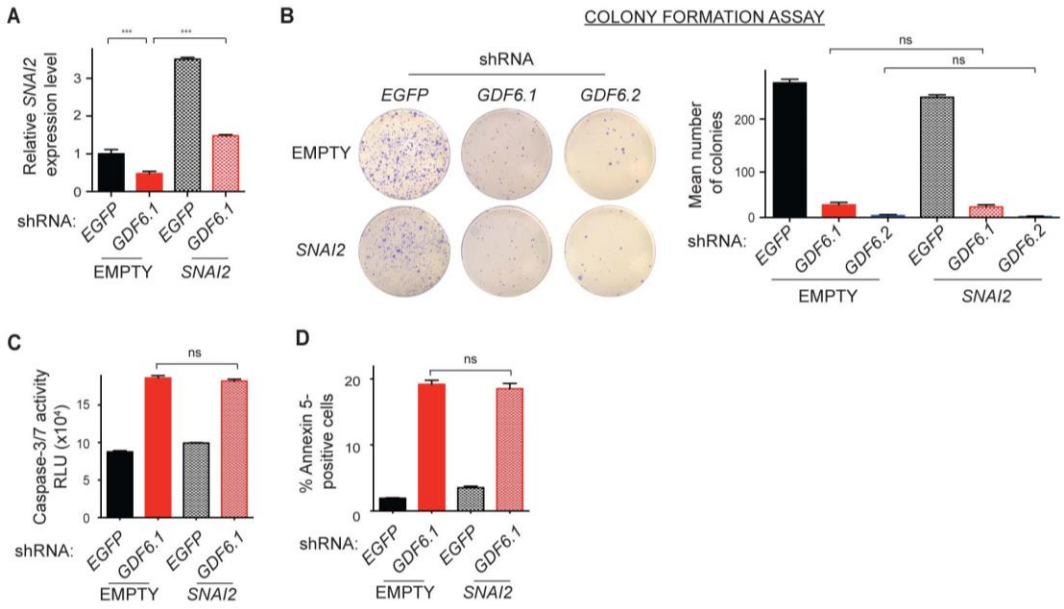

Figure 2.16: *SNAI2* overexpression does not rescue growth defects and cell death caused by *GDF6* knockdown

(**A**) qRT-PCR showing expression of *SNAI2* in A375-empty or A375-*SNAI2* cells expressing *shEGFP* or *shGDF6.1*. Error bars indicate s.e.m.; n=3. Left bracket, *SNAI2* expression is downregulated upon *GDF6* knockdown. Right bracket, *SNAI2* overexpression in *GDF6* knockdown cells. (**B**) Colony formation assay of A375-empty (top) or A375-*SNAI2* (bottom) cells expressing an shRNA targeting *EGFP* or two independent *GDF6*-targeted shRNAs. Error bars indicate s.e.m.; *n*=3. (**C**) Caspase-3/7 activity measured as relative luciferase units (RLU) in A375-empty or A375-*SNAI2* cells expressing *shEGFP* or *shGDF6.1*. Error bars indicate s.e.m.; *n*=3. (**D**) Flow cytometry analysis of annexinV-positivity of A375-empty or A375-*SNAI2* cells expressing *shEGFP* or *shGDF6.1*. Error bars indicate s.e.m.; *n*=3. Two-tailed Student's *t*-test, ***$P < 0.001$. ns, not significant.

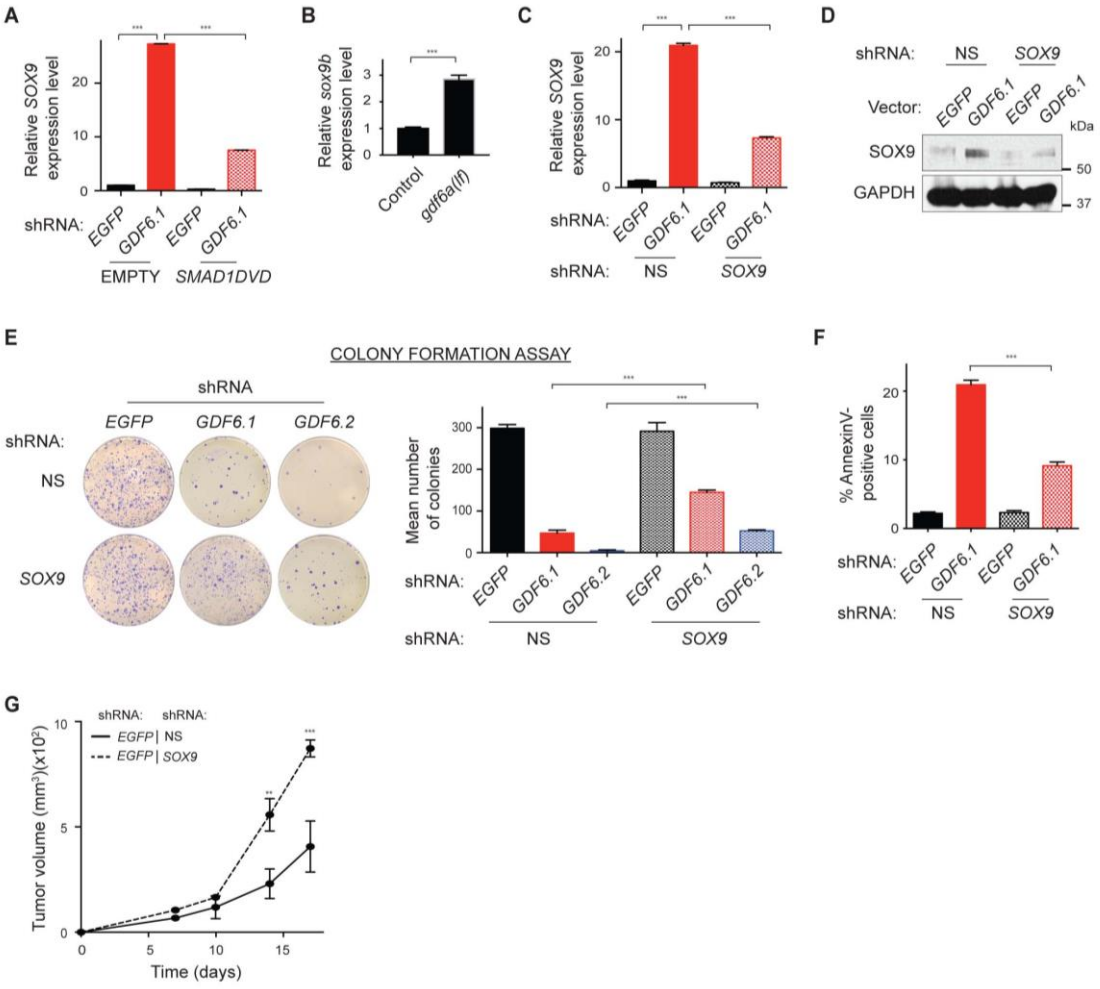

Figure 2.17: *SOX9* knockdown rescues the growth defects and cell death caused by *GDF6* knockdown

(**A**) qRT-PCR of *SOX9* in A375-empty or A375-*SMAD1DVD* cells with *GDF6* knockdown. Error bars indicate s.e.m.; *n*=3. Left bracket, *SOX9* expression is upregulated upon *GDF6* knockdown. Right bracket, *SOX9* expression is less upregulated in *SMAD1DVD*-expressing cells upon *GDF6* knockdown. (**B**) qRT-PCR showing expression of *sox9b* in control and *gdf6a(lf)* zebrafish melanomas. Error bars indicate s.e.m.; *n*=3. (**C**) qRT-PCR showing expression of *SOX9* in A375-non-silencing or A375-*shSOX9* cells with *GDF6* knockdown. Error bars indicate s.e.m.; *n*=3. Left bracket, *SOX9* expression is upregulated upon *GDF6* knockdown. Right bracket, knockdown of *SOX9* expression in *GDF6* knockdown cells. (**D**) Immunoblots showing expression of SOX9 and GAPDH in A375-non-silencing or A375-*shSOX9* cells expressing *shEGFP* or *shGDF6.1*. (**E**) Colony formation assay with A375-non-silencing (top) or A375-*shSOX9* (bottom) cells expressing an shRNA targeting *EGFP* or two independent *GDF6*-targeted

shRNAs. Error bars indicate s.e.m.; *n*=3. (**F**) Flow cytometry analysis of annexinV-positivity of A375-non-silencing or A375-*shSOX9* cells expressing *shEGFP* or *shGDF6.1*. (**G**) Tumor formation in mice injected with A375-non-silencing or A375-*shSOX9* cells expressing an shRNA targeting *EGFP.* Error bars indicate s.e.m.; *n*=3. Two-tailed Student's *t*-test, ***P*< 0.01, ****P*< 0.001.

Clinical significance of GDF6 expression and signaling

We next assessed expression of *GDF6* in human melanomas and examined potential clinical implications. Immunohistochemistry on an initial cohort of patient samples detected high levels of GDF6 protein in melanomas; however, normal melanocytes of adjacent skin (Figure 2.18A) or tumor-infiltrating cells (Figure 2.19) rarely expressed GDF6. In the same cohort, we found high BMP pathway activity, as measured by nuclear phospho-SMAD1/5/8 staining, in tumor cells but not in normal tissue (Figure 2.18A and Figure 2.19). To determine whether expression of GDF6 correlated with melanoma patient clinical characteristics, we performed immunohistochemistry on a microarray with 104 melanoma tissue cores (78 primary and 26 metastatic melanomas). Consistent with the initial cohort, robust GDF6 expression was observed in a majority of melanomas (80% of total; n=104 cases). Importantly, in analyzing clinical aspects of the melanoma tissue microarray, we found that patients whose tumors at diagnosis expressed high amounts of GDF6 had a lower survival probability than did patients whose tumors expressed no or low GDF6 (Figure 2.18B and Table 2.1). This association was mainly driven by patients with primary melanomas (Figure 2.20A). Additionally, GDF6 expression in primary melanomas significantly correlated with lymph node metastasis (Figure 2.18C). In these primary melanomas, expression of GDF6 tended to be higher than in metastatic lesions (Figure 2.20B). Together, these data indicate that GDF6 is a negative prognostic marker for early stage melanomas.

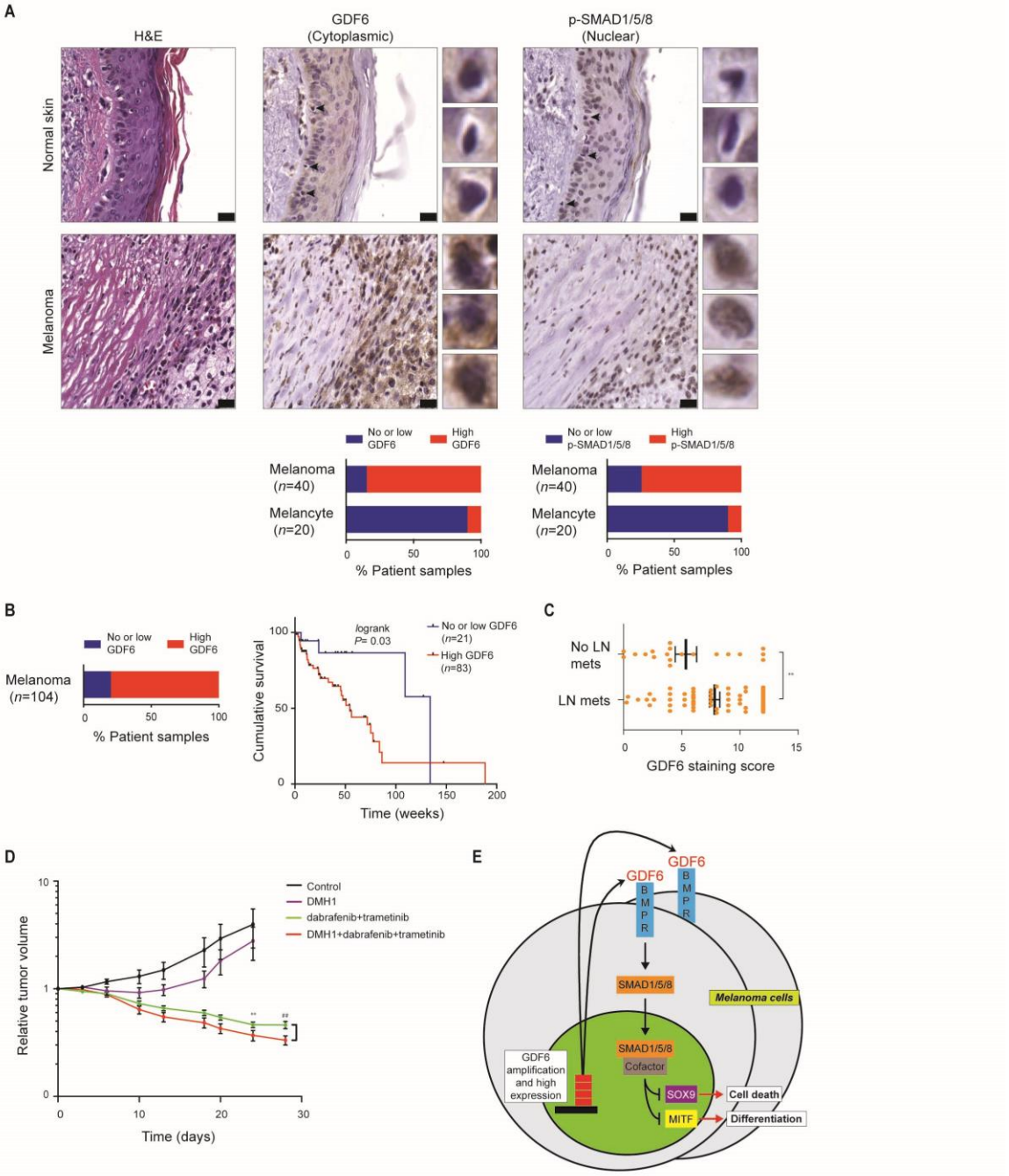
A
H&E
GDF6
(Cytoplasmic)
p-SMAD1/5/8
(Nuclear)
Normal skin
Melanoma
No or low GDF6
High GDF6
Melanoma (n=40)
Melancyte (n=20)
% Patient samples
No or low p-SMAD1/5/8
High p-SMAD1/5/8
B
Melanoma (n=104)
logrank P= 0.03
No or low GDF6 (n=21)
High GDF6 (n=83)
Cumulative survival
Time (weeks)
C
No LN mets
LN mets
GDF6 staining score
D
Control
DMH1
dabrafenib+trametinib
DMH1+dabrafenib+trametinib
Relative tumor volume
Time (days)
E
GDF6
BMPR
SMAD1/5/8
Melanoma cells
Cofactor
GDF6 amplification and high expression
SOX9
MITF
Cell death
Differentiation

Figure 2.18: Clinical impact of GDF6 expression and BMP pathway inhibition

(A) Staining of adjacent normal skin and melanoma tissue from the same section. Left, hematoxylin and eosin. Center, GDF6 immunostaining. Right, phospho-SMAD1/5/8 immunostaining. Melanocytes in normal skin sections are indicated (arrowheads). Scale bar, 25µm. Images of individual cells are shown immediately to the right. Below GDF6 and phospho-SMAD1/5/8 images the percentages of patient samples with no or low, and high expression of these proteins in normal melanocytes and melanomas is indicated. (B) Left, percentages of patient samples with no or low, and high GDF6 expression in the melanoma tissue microarray. Right, Kaplan-Meier analysis for the melanoma tissue microarray samples showing overall survival of patients with no or low GDF6 expression (blue line) versus high GDF6 expression (red line). Statistical analysis was performed with a Mantel-Cox log rank test. (C) GDF6 staining score in patients with primary melanomas with (n=61) or without (n=19) lymph node metastasis. Two-tailed Welch's *t*-test $^{**}P<0.01$. (D) Mice bearing A375 xenografts were treated with vehicle, DMH1, dabrafenib+trametinib or a combination of all three drugs. Normalized tumor volumes following the beginning of drug treatments are shown. Error bars indicate s.e.m.; $n \geq 8$ animals. (E) Model for GDF6 activation and function in melanomas. $^{**}P< 0.01$ two-tailed Student's *t*-test (C) or by one-way ANOVA with Bonferroni test (D). $^{\#\#}P< 0.001$ by one-way ANOVA (D).

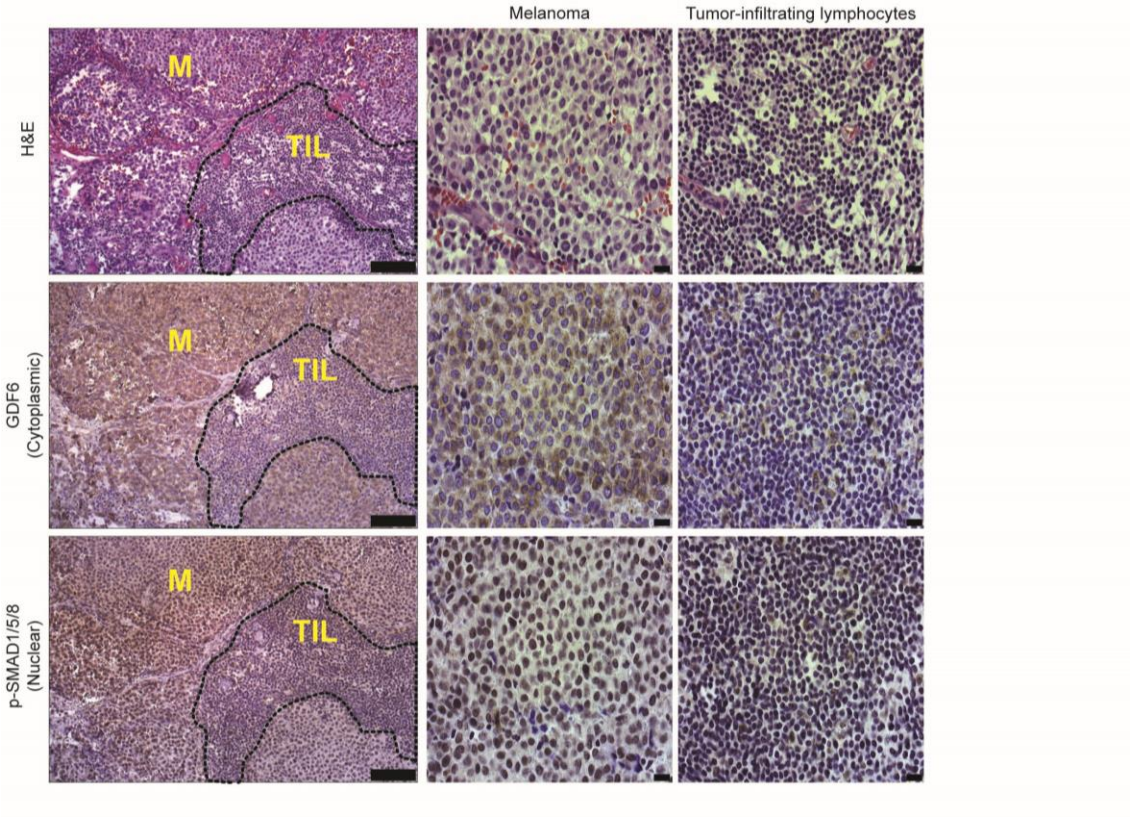

Figure 2.19: GDF6 and phospho-SMAD1/5/8 expression in a patient melanoma section

Section of a metastatic human melanoma (M) with tumor infiltrating lymphoycytes (TIL). Top, hematoxylin and eosin staining. Middle, GDF6 staining. Bottom, phospho-SMAD1/5/8 staining. Left, scale bar, 50 µm. Center and right, melanoma region and TIL region, respectively. Scale bar, 25 µm.

Group	Hazard Ratio	P-value
GDF6 expression	2.07	0.04
Age	1.41	0.16
Sex (Female vs Male)	0.27	0.79
Tstage (3vs2)	-0.44	0.66
Tstage (4vs2)	1.46	0.14
Metastatic vs Primary	0.11	0.91

Table 2.1 Multivariate analysis using the tissue microarray with melanoma patient samples

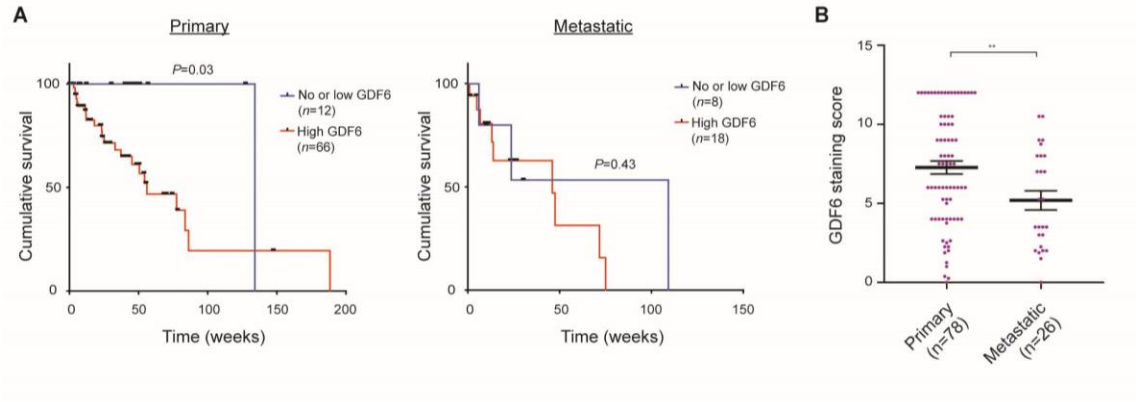

Figure 2.20: Correlation of GDF6 expression with melanoma clinical features

(**A**) Kaplan-Meier analysis showing overall survival of patients (melanoma tissue microarray) with primary melanomas (left) and metastatic melanomas (right) with no or low GDF6 expression (blue line) versus high GDF6 expression (red line). Statistical analysis was performed with a Mantel-Cox log rank test. (**B**) GDF6 expression score in primary and metastatic melanomas from the melanoma tissue microarray. Two-tailed Welch's *t*-test, ***P*< 0.01.

Next, we wanted to test whether targeting GDF6-driven BMP signaling could be combined with existing therapies. We treated established A375 melanoma xenografts with DMH1 or dabrafenib+trametinib or a combination of all three drugs. While treatment with dabrafenib+trametinib caused substantial regression, the combination of DMH1 with dabrafenib+trametinib showed even further regression (Figure 2.18D). Treatment with DMH1 alone had little effect, although we presume that it does not fully inhibit GDF6-driven BMP signaling in vivo, as indicated by our previous experiments. These results indicate that targeting GDF6-driven BMP signaling in combination with current therapeutic strategies may have profound clinical benefits.

Discussion

In this study, genomic and functional analyses identified *GDF6* as a novel melanoma oncogene. Based on these and additional mechanistic studies, we propose the following model for the role of *GDF6* in melanoma tumorigenesis (Figure 7E). First, during the course of melanomagenesis, the *GDF6* locus is transcriptionally activated, in some cases stemming from copy number amplification. Production of GDF6 protein leads to either autocrine or paracrine activation of BMP pathway signaling in nascent melanoma cells. BMP signaling triggers SMAD1/5/8-dependent downregulation of *MITF* and *SOX9*, which inhibits melanoma cell differentiation and death, respectively. *GDF6*-dependent binding of SMAD1/5/8 to the *MITF* locus suggests downregulation in this case is direct. There are no SMAD1/5/8 bound regions in the *SOX9* locus, so its downregulation is either indirect or mediated by long-range interactions with SMAD1/5/8 that is bound, in a *GDF6*-dependent fashion, to sites in neighboring loci. The outcome of this signaling is to promote a neural crest gene signature within melanoma cells, which enables tumor progression.

GDF6 and BMP signaling in melanoma maintenance and initiation

BMP pathway activity has previously been implicated in melanoma progression. BMP4 and BMP7 expression has been shown to promote tumor cell invasion and migration in an autocrine fashion (Rothhammer et al., 2005), whereas BMP2 and BMP4 promote angiogenesis through paracrine signaling

(Rothhammer et al., 2007). Independent studies indicate that BMP7 can block melanoma cell growth and inhibit metastasis (Hsu et al., 2008; Na et al., 2009), suggesting BMP7's effects on melanoma progression may be complex and potentially cell line-specific. More relevant to our studies, BMP signaling has been proposed to promote melanoma survival by inducing the anti-apoptotic factor *DIDO1* (Braig and Bosserhoff, 2013). We tested whether *DIDO1* is involved in the anti-apoptotic role of *GDF6* in melanoma cells. Upon *GDF6* knockdown we did not observe changes in *DIDO1* transcript levels. Furthermore, we found that while phospho-SMAD1/5/8 bound to a site within the *DIDO1* gene, this site was not differentially bound upon *GDF6* knockdown. Thus *GDF6,* via *SOX9,* likely interfaces with the cell death machinery through other factors.

Along with preventing cell death, our studies indicate that *GDF6* and BMP signaling promote melanoma maintenance through additional mechanisms. *GDF6* downregulates expression of *MITF*, which is likely accomplished by induction of phospho-SMAD1/5/8 and its direct binding to the *MITF* gene. *MITF* is a master regulator of the melanocyte lineage, and its regulation is critically important for the behaviors of cells within this lineage. *MITF* expression is governed by a variety of signals that ultimately produce an expression level that dictates cellular phenotype. In this way *MITF* is proposed to act as a rheostat (Carreira et al., 2006; Goding, 2011; Hoek and Goding, 2010). Specifically, high levels of *MITF* promote cell cycle arrest and terminal differentiation, whereas lower expression levels stimulate proliferation. Even lower levels endow cells

with stem cell-like and invasive properties. We speculate that by repressing *MITF*, *GDF6* and BMP signaling keep *MITF* expression in a range that not only inhibits terminal differentiation but also protects against cell death and endows cells with properties important for tumor maintenance.

Our data also implicate *GDF6* and BMP signaling in melanoma initiation. In zebrafish, cells in the melanocyte lineage that expressed *gdf6b* gave rise to melanomas more rapidly than did control cells. Furthermore, melanoma onset was delayed in *gdf6a* mutant zebrafish. Recently it was shown that cells of origin for zebrafish melanomas adopt neural crest characteristics that distinguish them from normal melanocytes (Kaufman et al., 2016). These neural crest characteristics are proposed to be instrumental in melanoma initiation. Given that *GDF6* and its orthologs are melanoma oncogenes and they promote a neural crest gene signature, we speculate that *GDF6* and BMP signaling are important at the earliest stages of melanoma formation.

Reiteration of embryonic *GDF6* activities in melanomas

GDF6 is expressed during embryogenesis, and its functions during development mirror those upon its reactivation in melanomas. In *Xenopus* and zebrafish embryos, *GDF6* is expressed at the edges of the neural plate and in the eye fields of the anterior neural plate. Upon neural tube closure, expression is prominent in the dorsal neural tube and neural crest (Bruneau and Rosa, 1997; Hanel and Hensey, 2006; Reichert et al., 2013). Loss-of-function studies in both

species suggest that *GDF6* promotes ectodermal cell survival (Delot et al., 1999; Hanel and Hensey, 2006). In *Xenopus* and zebrafish, knockdown of *GDF6* and *gdf6a*, respectively, caused a reduction in eye size that resulted from inappropriate death of retinal neuron progenitor cells (Asai-Coakwell et al., 2009; Asai-Coakwell et al., 2013; Pant et al., 2013). *GDF6* also acts during embryogenesis to regulate cell differentiation. In the mouse, *Gdf6* inhibits differentiation of the mesenchymal progenitors that develop into the coronal suture, and precocious differentiation of these cells results in fusion (Clendenning and Mortlock, 2012; Settle et al., 2003). Thus, in certain tissues GDF6 can promote cell survival during development as well as regulate terminal differentiation.

We have found that *GDF6* promotes a neural crest signature in melanoma cells. In particular, *GDF6* maintains expression of the trunk neural crest factor *SOX10* while repressing the cranial neural crest factor *SOX9*. Some data support a similar function for *GDF6* in embryogenesis. As noted above, *GDF6* orthologs in *Xenopus* and zebrafish are expressed in the neural crest and adjacent dorsal neural tube. In zebrafish, knockdown of *gdf6a* reduces expression of *sox10* in neural crest cells (Reichert et al., 2013), consistent with a function in maintaining a trunk neural crest gene signature. As development proceeds, *gdf6* paralog expression is progressively lost in a rostrocaudal direction, which occurs concomitantly with rostrocaudal differentiation of crest cells, including melanocytes. Perhaps the loss of *gdf6* expression removes a barrier to

melanocyte differentiation. Support for such a barrier has been shown in avian embryos, where BMP4-driven pathway activity inhibits melanocyte fate specification during neural crest lineage segregation (Jin et al., 2001). We speculate that *GDF6* may activate BMP signaling in the neural crest to repress *MITF*. With *MITF* repressed, neural crest cells can remain undifferentiated and responsive to proliferative signals as well as those that specify alternative cell fates. In melanomas BMP signaling likewise could promote a neural crest cell identity that is not terminally differentiated and therefore conducive to proliferation.

Targeting GDF6 and BMP signaling in melanoma

Our patient cohort analyses show that a major fraction of melanomas express *GDF6* and have an active BMP pathway. Since *GDF6* expression is correlated with poor patient survival and inhibition of *GDF6* leads to cell death, targeting this gene or the BMP pathway may prove to be an effective therapeutic intervention for melanomas. *GDF6* itself is an attractive target since its expression is very low or undetectable in most adult tissues (2013). The knockout of mouse *Gdf6* indicates that it is a non-essential gene, although it is necessary for the development of certain joints, ligaments and cartilage (Settle et al., 2003). These developmental activities of GDF6 would likely not complicate treatment of adult patients with anti-GDF6 therapy, although it is not known whether GDF6 inhibition would affect the limited repair of connective tissues that

occurs in adults. On the other hand, BMP signaling regulates the function or repair of some adult tissues, including muscle, bone and lung (Cai et al., 2012; Sartori et al., 2013; Tsuji et al., 2006). Thus, GDF6 inhibition could be more specific to melanoma tissue as compared to a broad BMP pathway inhibitor such as DMH1, which would block BMP signaling in normal tissues. As a secreted molecule, GDF6 inhibition could be accomplished by a variety of means, including cell-impermeable therapies. Such therapies could be used in different molecular subtypes of melanoma, as cell death caused by *GDF6* inhibition does not depend on underlying *BRAF*, *NRAS* or other driver mutations. Our data do suggest that tumors expressing high levels of GDF6 would be particularly sensitive to GDF6 inhibition. This elevated expression correlates with *GDF6* gene amplification, which is present in 38% of melanomas (Akbani R, 2015). However, 80% of the melanomas we analyzed showed high GDF6 expression, suggesting that mechanisms other than amplification can lead to higher expression. Ultimately it would be useful to determine if the level of GDF6 expression is predictive of therapeutic response to a GDF6 or BMP inhibitor. As indicated by the potent activity against xenografts of DMH1 with dabrafenib+trametinib, such an inhibitor could be used in conjunction with BRAF inhibitors and other MAPK pathway inhibitors to treat this lethal disease.

CHAPTER III

Zebrafish melanoma-derived neural crest signature predicts melanoma patient survival

INTRODUCTION

Melanomas are highly aggressive skin cancers that arise from pigment-producing melanocytes. Melanocytes develop from an embryonic tissue-type called the NC. The NC is a multipotent tissue type that has a remarkable potential to proliferate, migrate and give rise to different cell types. A highly complex network of signaling factors orchestrates these processes in the NC. Several of these factors are expressed in the NC, and their expression is turned off upon terminal differentiation to different lineages. However, tumors originating from these lineages, like melanomas, reexpress some of these factors (Bhaskara et al., 2012; Gupta et al., 2005; Hohenauer et al., 2013; Kuphal and Bosserhoff, 2006). It is predicted that expression of these factors endows pro-tumorigenic features to these cancer cells.

Melanomas have been associated with expression of NC factors that are usually not expressed or lowly expressed in the parental melanocytic lineage. Analyses of these factors have indicated that pathways specific to the NC can play a wide range of pro-tumorigenic roles in melanoma cells. NC factors like *SOX10* and *BRN3a* promote tumor cell survival, whereas expression of endothelial-to-mesenchyme promoting factors like *SNAIL*, *SLUG* and *PAX3* induce migratory behaviors in melanoma cells (Eccles et al., 2013; Hohenauer et al., 2013; Shakhova et al., 2015; Shakhova et al., 2012). Recently, studies have also shown involvement of neural crest factors like *FOXD3* and *ZEB1* in

resistance to the BRAF and MEK inhibitors in melanomas (Basile et al., 2012; Richard et al., 2016). These studies have defined diverse roles for NC factors in melanomas. However, there are no known gene signatures that represent the existence of NC identities in patient melanomas. Furthermore, whether the presence of such a NC gene signature has any prognostic value is also largely unknown for patients with melanomas.

RESULTS & DISCUSSION

Although roles for NC factors in melanomas have been identified using cell-based assays and in animal models, very few studies have investigated expression of NC factors in patient melanomas. Moreover, it is unclear whether expression of NC factors correlates with clinical features of melanoma patients. To test this, we analyzed if expression of NC factors known to be involved in melanoma progression correlated with patient survival. Using publically available The Cancer Genome Atlas (TCGA) database, we correlated NC factor expression with patient survival and found that independently these factors failed to predict survival outcome of patients (Table 3.1). Since the roles of NC factors in melanomas are multifaceted, we hypothesized that NC identities in melanoma can be better represented by a set of NC genes rather than individual factors. Therefore we sought to identify such a NC gene set and assess whether such a gene signature would show any clinical correlation.

In order to seek a melanoma-specific NC gene signature, we used a zebrafish model of melanoma that combines melanocyte-specific expression of *BRAF*^{V600E} along with a loss-of-function *P53.* Melanomas in this model of zebrafish initiate from melanocytic cells that have neural crest identities (Kaufman et al., 2016). Therefore, we hypothesized that this melanoma model would be ideal to obtain a NC gene signature. We isolated melanomas and

Gene	Hazard Ratio	LCL (95%)	UCL (95%)	Log rank *P*-value
SOX10	1.07	0.93	1.23	0.36
FOXD3	0.98	0.87	1.11	0.73
SNAI1	0.98	0.9	1.07	0.65
SNAI2	1.11	0.99	1.25	0.07
MITF	1.09	0.99	1.21	0.07
PAX3	1.09	0.97	1.23	0.14
ZEB1	0.90	1.1	0.78	0.03

Table 3.1: Correlation of neural crest gene expression with overall melanoma patient survival

scale-associated normal melanocytes from these zebrafish and performed RNA sequencing and differential analysis (Figure 3.1A). Pathway analysis of genes differentially regulated genes in zebrafish melanomas as compared to normal melanocytes showed an enrichment of NC factors, emphasizing the role of NC identities in zebrafish melanomas (Figure 3.2B). Since neural crest factors are known to act via elevated expression in melanomas, we identified NC genes that are upregulated in zebrafish melanomas as compared to normal melanocytes and defined a 15-gene NC signature (Figure 3.3C).

In assessing this signature, we first tested the presence of this zebrafish melanoma-derived NC gene signature in patient melanomas (TCGA database). We probed the expression of the gene signature in patient-derived melanomas and found that they positively correlate with *SOX10* (Figure 3.2A), a factor that has been implicated with NC identities in melanoma (Kaufman et al., 2016). These results indicate that melanomas arising in this zebrafish model would represent NC identity-positive melanomas arising in human patients. These results support the use of zebrafish melanoma model to study the subset of melanomas that harbor neural crest features. This model could help gain insight into tumor mechanisms relating to NC features and provides an ideal model for therapeutic targeting of these mechanisms.

Next, we wanted to assess whether the NC gene signatures could predict melanoma patient survival. After normalizing for age and sex of patients, we segregated overall survival of patients based on the average expression of

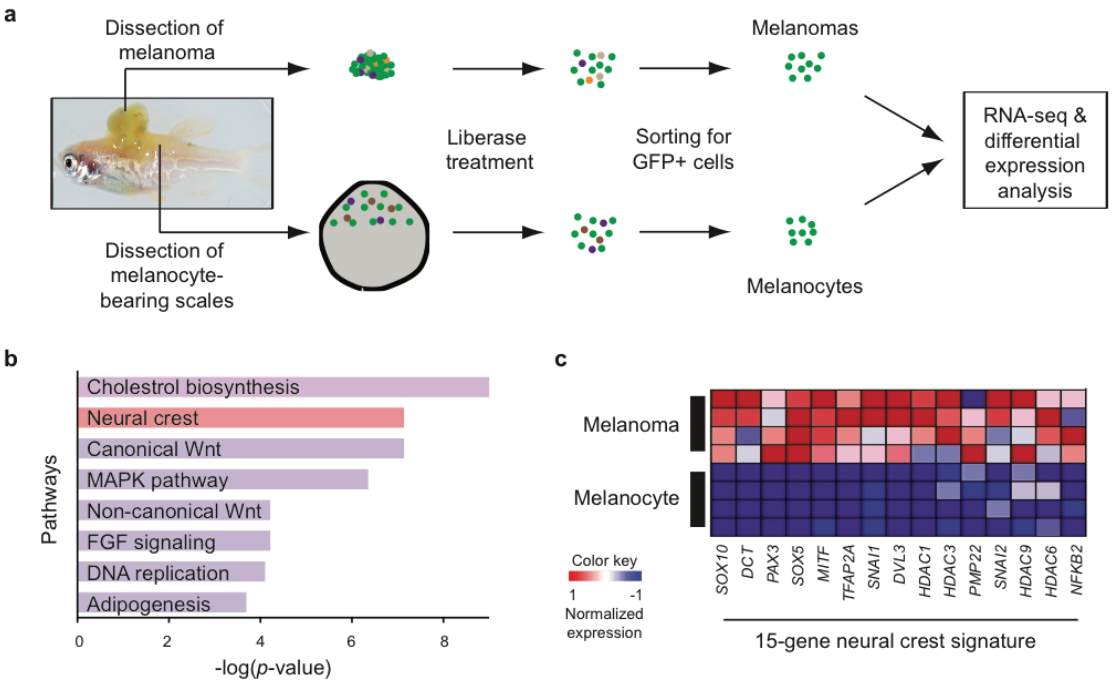

Figure 3.1: Transcriptome analysis of zebrafish melanomas to identify a NC gene signature

(a) Schematic showing isolation of melanoma cells and scale-associated melanocytes from *Tg(Pmitf:BRAFV600E);p53(lf)* zebrafish to perform comparitive transcriptome analysis. (b) Pathway analysis with genes differentially regulated in zebrafish melanomas as compared to normal melanocytes (minimum overlap ≥ 10 genes; adjusted *P*-value < 0.01). (c) Heat map of neural crest genes upregulated (≥ 2 fold) in zebrafish melanomas as compared to normal melanocytes.

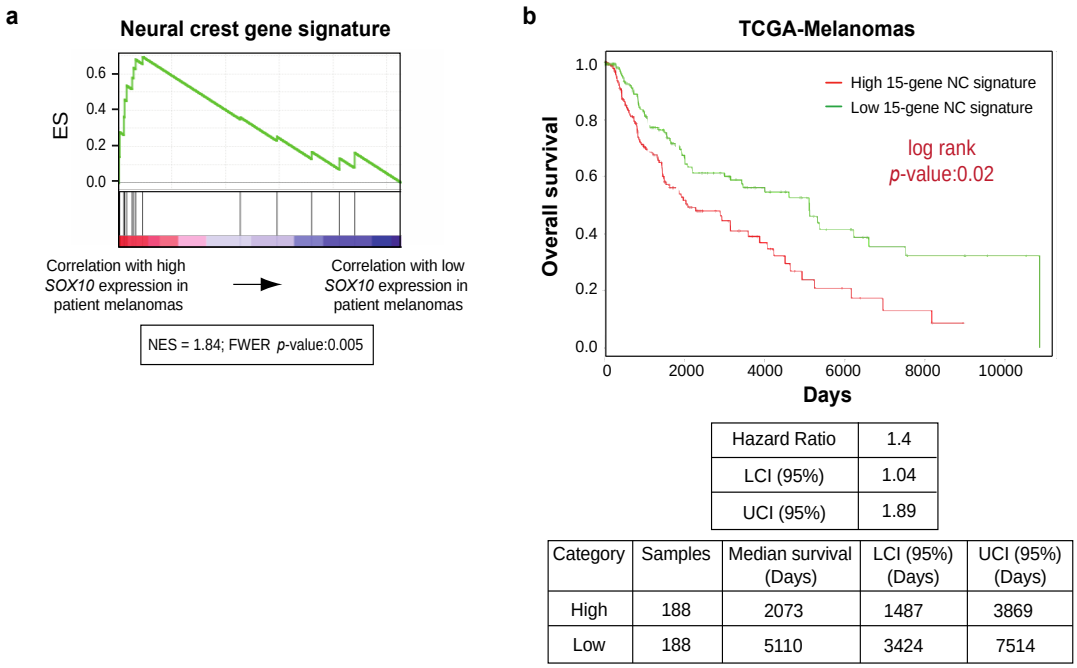

Hazard Ratio	1.4
LCI (95%)	1.04
UCI (95%)	1.89

Category	Samples	Median survival (Days)	LCI (95%) (Days)	UCI (95%) (Days)
High	188	2073	1487	3869
Low	188	5110	3424	7514

Figure 3.2: Correlation of zebrafish-derived NC signature with human melanomas

(a) GSEA shows that average expression of genes in the NC gene signature (excluing *SOX10*) positively correlates with expression of SOX10 in patient-derived melanomas. (b) Kaplan-Meier analysis showing overall survival of patients with low 15-gene NC signature expression (green line) versus high 15-gene NC signature expression. The survival outcome has been adjusted for age and sex of the patients. Statistical anlaysis was performed with Manter-Cox log rank test.

the 15-gene NC signature. Patients whose tumors had high expression of this 15-gene NC signature showed lower survival probability than did patients whose tumors had low expression of the signature (Figure 3.2B). Furthermore, the expression of this signature had no bias towards the stage of the disease (Figure 3.3), implying that the signature could independently predict patient survival.

Here, we identify a NC gene signature for melanomas that can be used as a prognostic marker. These results add to the growing evidence of the importance of neural crest programs in melanoma. Drugs like Leflunomide that specifically target transcriptional programs common to both, the neural crest and melanomas have shown great promise in abrogating tumor growth (White et al., 2011). Use of this drug in combination with Vemurafenib, a mutant-*BRAF* inhibitor, for treatment of melanomas is currently being tested in clinical trials (Kraehn et al., 2001). With further studies, this signature could potentially be used to predict response to such treatment modules.

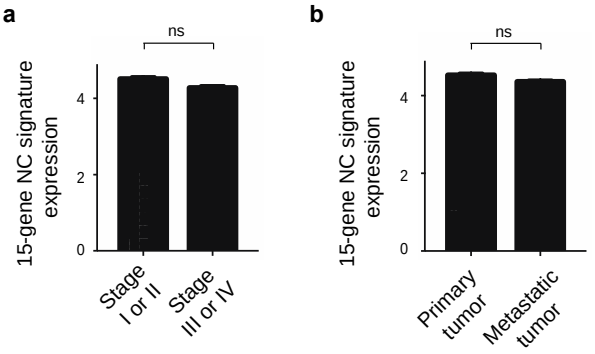

Figure 3.3: Correlation of 15-gene NC signature with clinical stage of patient melanomas

(a) Comparison of15-gene NC signature in ealry stage melanomas (Stage I or II) versus late stage melanomas (Stage III or Stage IV). (b) Comparison of 15-gene NC signature in primary versus metastatic melanomas. ns, not significant. 15-gene NC signature was calculated by averaging the log2-transformed expression values of the 15 neural crest genes.

CHAPTER IV

METHODS

Cell lines and cell culture

A375, M14, C32 and HEK293T cells (ATCC) were maintained in Dulbecco's Modified Eagle's Medium (DMEM) and SK-MEL-28, SK-MEL-5 cells (ATCC) were maintained in Roswell Park Memorial Institute (RPMI) 1640 media supplemented with 10% fetal bovine serum (FBS) and 2 µg/ml Pen Strep (Gibco) at 37°C and 5% CO_2. Cells cultured at the same time were pooled, counted and then seeded in a 10cm dish. Wells/dishes were then subjected to treatment with lentiviral vectors.

Lentiviral infection

Lentiviral infections were performed as described previously (Ceol et al., 2011). For stable gene knockdowns, we used pLKO-1 lentiviral vectors to deliver short hairpin sequences (shRNAs) (obtained from the RNAi Consortium (TRC)/Broad Institute through the UMMS RNAi core facility) specific for *GDF6* (GDF6.1: TRCN0000141818, target sequence: GCCAAGTGTTACATTGAGCTT; GDF6.2: TRCN0000140097, target sequence: GTGTCCATGCTCTCAGACAAA) or *SMAD1* (SMAD1.1: TRCN0000021781, target sequence: CGGTTGCTTATGAGGAACCAA; SMAD1.2: TRCN0000021782, target sequence: GCCGATGGACACAAACATGAT) or *EGFP* (TRCN0000072181,

target sequence: ACAACAGCCACAACGTCTATA). Virus was made using a second generation lentiviral packaging system in HEK293T cells and quantified using a p24 ELISA kit (Clontech). Cells were infected with virus at a multiplicity of infection of 2.5 with 8 µg/ml polybrene followed by puromycin selection (2 µg/ml) for 2 days in appropriate media. For genetic epistasis experiments with *SOX9,* we used the pGIPZ lentiviral vectors (obtained from Thermofisher Scientific through the UMMS RNAi core facility) to deliver shRNAs specific for *SOX9* (V3LHS_396212, target sequence: AGTCGTACTGTGAGCGGGT) or used the non-silencing control (target sequence: CTTACTCTCGCCCAAGCGAGAG) (Deng et al., 2015). A375 melanoma cells expressing an shRNA targeting *GDF6* or *EGFP* were treated with virus delivering *SOX9* or non-silencing shRNA. The viral dosage was determined such that 100% of the cells were EGFP-positive and therefore contained the pGIPZ vector expressing either *SOX9* or non-silencing shRNA. For transgene expression, we used Gateway cloning (Life Technologies) to insert the *GDF6* or *SNAI2* ORF (GE life sciences) or *SMAD1DVD* ORF (provided by Takenobu Katagiri, Saitama Medical University, Saitama, Japan) into the pLenti CMV Hygro DEST (w117-1) vector (provided by Paul Kaufman, University of Massachusetts Medical School, Worcester, USA). Infection and monitoring was performed as described (Ceol et al., 2011), except that selection was done with 300 ug/ml hygromycin for 10 days.

Mouse xenografts

A375 cells stably expressing an *EGFP* or *GDF6* or *SMAD1* shRNA and/or empty vector or *GDF6*-expressing vector or *SMAD1DVD*-overexpressing vector were subcutaneously injected into the flanks of 6-8-week-old BALB/c nu/nu female mice (Taconic Farms) to produce orthotopic primary tumors. Primary tumor growth was monitored every 3 days with calipers, and tumor volume was calculated as described previously (Gazin et al., 2007). For *GDF6* knockdown, *SMAD1* knockdown and epistasis experiments with *SMAD1DVD* overexpression, 1 x 10^7 live cells were injected. For *GDF6* overexpression experiments and epistasis experiments with *SOX9* knockdown, 1 x 10^6 live cells were injected. For *GDF6* overexpression and *GDF6* knockdowns, a representative of two independent experiments (*n*=3 animals per experiment) is shown. For DMH1 drug experiments shown in Figure 3F, 1 x 10^6 live A375 cells were subcutaneously injected in the flanks of BALB/c nu/nu female mice. Beginning on the day cells were injected, mice were injected intraperitoneally with vehicle (12.5% 2-hydroxypropyl-β-cyclodextrin) or 25 mg/kg DMH1 in vehicle every other day. This experiment was repeated twice and the weighted average of both experiments (*n*=8 animals total) is represented. For drug experiments in Figure 7D, 1 x 10^6 A375 cells were subcutaneously injected in the flanks of BALB/c nu/nu female mice. Once the tumors volumes reached 75 mm^3, groups of mice were treated with vehicle, DMH1, dabrafenib+trametinib or a combination of all three drugs. DMH1 was administered intraperitoneally in seven day cycles with 25 mg/kg given twice a day for 5 days and once a day for 2 days. Dabrafenib

(300 mg/kg) + trametinib (0.3 mg/kg) were administered by oral gavage once per day. The control group received the vehicle 12.5% 2-hydroxypropyl-β-cyclodextrin intraperitoneally in seven day cycles with 25 mg/kg given twice a day for 5 days and once a day for 2 days. Control animals also received 0.5% hydroxypropyl methylcellulose once a day by oral gavage. These treatment regimens were continued until the end of study or until tumors reached 400 mm^3. A total of 8 or 9 animals were used in each group.

Zebrafish stocks and husbandry

Zebrafish were maintained at 28.5°C with a 14 hours ON: 10 hours OFF light cycle. *Tg(mitfa:BRAF^{V600E})*(Patton et al., 2005)*, p53(lf)*(Berghmans et al., 2005)*, mitfa(lf)*(Lister et al., 1999) *and gdf6a(lf)*(Gosse and Baier, 2009) zebrafish strains were used. *gdf6a(lf)* mutants were generously provided by Dr. Herwig Baier, Max Plank Institute of Neurobiology, Martinsried, Germany. AB was used as the wild-type strain.

miniCoopR assay

The miniCoopR assay measuring the effect of *gdf6b* on melanoma onset in zebrafish was performed as previously described (Ceol et al., 2011). For miniCoopR-*EGFP* experiments a weighted average of two independent experiments is represented, and for miniCoopR-*gdf6b* experiments a weighted average of four independent experiments is represented. For the embryonic

melanocyte rescue analysis, embryos were treated with epinephrine (1 mg/ml) at 4 days post fertilization to contract pigment to distinguish any overlapping cells, and melanocytes were counted manually.

cDNA synthesis and qRT-PCR

For adult zebrafish, total RNA was extracted from melanoma cells and from normal scale-associated melanocytes of *Tg(mitfa:BRAF(V600E)); p53(lf); alb(lf); Tg(mitfa:EGFP)* zebrafish. For isolation of melanoma cells, melanomas were dissected, dissociated using Liberase TH treatment and subjected to fluorescence activated cell sorting (FACS) to isolate EGFP-positive cells. The same protocol was used for normal melanocytes, except dorsal scales from zebrafish were plucked to isolate melanocytes. Total RNA from zebrafish melanomas and melanocytes was isolated using Trizol-chloroform extraction, followed by RNA clean up (Qiagen RNeasy). Total RNA was reverse transcribed using the Superscript 2 Reverse Transcriptase kit (Invitrogen). qRT-PCR with SYBR green master mix (Biorad) was performed using the following primers: *gdf6a* F: CTGAGAAACTGGGGCTCAAT, *gdf6a* R: CGACCAGCTCCTCTTTGTCT, *gdf6b* F: CGTCTAAAGCAGCAAACACC, *gdf6b* R: CCAAAGTGGAGAGTTCAAATGG, *actb1* F: CGAGCAGGAGATGGGAACC, *actb1* R: CAACGGAAACGCTCATTGC. For zebrafish embryos, drug treatment was performed as mentioned in Experimental Procedures, except 10μM DMH1 was used and total RNA was isolated at 20 hpf in the same manner. qRT-PCR

was performed using the following primers: *mitfa* F*:* CTGGACCATGTGGCAAGTTT*, mitfa* R: GAGGTTGTGGTTGTCCTTCT, *tyrp1b* F: CGACAACCTGGGATACACCT, *tyrp1b* R: AACCAGCACCACTGCAACTA*.*

For A375 human melanoma cells with *GDF6* and/or *SMAD1DVD* modulation, total RNA was prepared in the same manner, and qRT-PCR was performed using the following primers: *ID1* F: CCAACGCGCCTCGCCGGATC, *ID1* R: CTCCTCGCCAGTGCCTCAG, *ID3* F: CTGGACGACATGAACCACTG, *ID3* R: GTAGTCGATGACGCGCTGTA, *SNAI2* F: TGTTGCAGTGAGGGCAAGAA, *SNAI2* R: GACCCTGGTTGCTTCAAGGA, *SOX9* F: GTACCCGCACTTGCACAAC, *SOX9* R: TCTCGCTCTCGTTCAGAAGTC, *MITF* F: AAACCCCACCAAGTACCACA, *MITF* R: ACATGGCAAGCTCAGGAC, *TRP1* F: GTAACAGCACCGAGGATGG, *TRP1* R: TCCAAGCACTGAGCGACAT, *GAPDH* F: TGCACCACCAACTGCTTAGC, *GAPDH* R: GGCATGGACTGTGGTCATGAG.

Gene set enrichment analysis (GSEA) and pathway analysis

For GSEA, the enrichment score (ES), normalized enrichment score (NES) and familywise error rate (FWER) were calculated based on a running metric, which increased when a gene (vertical line in the graphical representation) in the gene set was encountered and decreased when one was not. For GSEA of the apoptotic pathway gene signature (MSigDB- M10169) (Wu et al., 2002), a rank-ordered gene list was made with FPKM values from *GDF6*-overexpressing A375

melanoma cells as compared to empty vector control cells or A375 cells expressing an shRNA targeting *EGFP* as compared to *GDF6.1* shRNA-expressing cells. Default parameters of GSEA were used and the Student's *t*-test was used to calculate significance. For GSEA based on TCGA samples, a rank-ordered gene list was derived from the expression profiles of 385 melanoma samples, using *GDF6* expression level as a continuous variable. Default parameters of GSEA were used, and Pearson correlation was used to calculate significance. Pathway analysis was performed using the WEB-based Gene SeT AnaLysis Toolkit (WebGestalt) (Wang et al., 2013a). Default parameters were used, except the minimum number of genes for a category was set to 10.

Statistics

Data are presented as mean ± s.e.m. Differences between groups were assessed by a two-tailed Student's *t* test, except in Figures 2G, 2H (left), 3G, 5B, 5C, 6B, 6D, 6F, 6G, 7D and Supplemental Figures S4A, S4B, S6C, S7B, S7G, S7I, S8C, S9A, S9B, S9C, S10A-D, S11A, S11C, S11E, and S11F where a one-way ANOVA test was used (GraphPad Prism 7 software). In Figure 7C, Supplemental Figures S1C and S13B a two-tailed Welch's *t* test was used (GraphPad Prism 7 software) In Figure 3E a two-sample Kolmogorov-Smirnov test was used. In Figures 1C, 3C, 4A, 6A and Supplemental Figures 8A and 8B we used a family-wise error rate (FWER) *P* value to account for multiple comparisons. For multiple comparisons Dunnett or Bonferroni tests were used as

appropriate. Kaplan-Meier curves were generated using GraphPad Prism 7 software and the differences between groups were assessed by Wilcoxon rank sum analysis for Figures 2A and 2H and by Mantel-Cox log-rank analysis for Figure 7B and Supplemental Figure 12. A *P* value less than 0.05 was considered significant.

Study approval

All zebrafish and mouse studies were performed according to Institutional Animal Care and Use Committee (IACUC) guidelines and University of Massachusetts Medical School Animal Care Committee protocols. Approval for the tissue microarray study was granted by the Brigham and Women's Partners Human Research Committee. Informed consent was not necessary as all samples were discardable tissue and deidentified.

Growth curve, clonogenic and soft agar assays

For growth curves 50,000 live cells were seeded per well in a 6-well tissue culture plate on day 0. The numbers of live cells were calculated every day using an automated cell counter (Nexcelom Bioscience Cellometer Auto T4) following standard procedures. All assays were performed with technical replicates. For clonogenic assays, 3,000 live cells were seeded in a 10 cm tissue culture plate. After 3 weeks, colonies were fixed and stained using bromophenol blue in acetone. ImageJ was used to quantify the number of colonies. In assays with

DMH1 treatment, control or DMH1-containing media was replaced every other day. For soft agar assays a 0.5% bottom layer (1:1 with 1% agar and 2XDMEM with 20% FBS) and a 0.3% top layer (1:1 with 0.6% agar and 2XDMEM with 20% FBS) were used. 3,000 live cells per well of a 6-well tissue culture plate were added in the top layer. Media was added initially then replaced every 3 days. After 3 weeks, colonies were stained with nitroblue tetrazolium chloride overnight at 37°C. Once stained, individual wells were photographed, and ImageJ was used to count the number of colonies. All these assays were done in triplicate, and experiments were repeated at least twice.

Cell death assays

A375 melanoma cells after stable knockdown and/or overexpression were stained for Annexin V and 7-AAD (BD Pharmingen PR Annexin V Apoptosis Detection kit) as per manufacturer's instructions, followed by flow cytometry using a FACSCalibur instrument (BD Biosciences). Caspase3/7 activity was measured using the Caspase-Glo 3/7 assay (Promega) as per manufacturer's instructions.

Animal experiments

All animal protocols were approved by the UMMS Institution Animal Care and Use Committee (A-2016, A-2171). Mice were randomly allocated to individual experimental groups. No blinding was done as animal groups were identified by

tagging and cage labeling. Animals were excluded, according to pre-established criteria, if the tumor volume reached >1,000 mm^3; if tumor size or location affected the mobility or general health of animal, the animal was euthanized and excluded from the experiment or the complete experiment was terminated.

Antibody production

Antibodies recognizing Gdf6b were generated by injecting a glutathione S-transferase-tagged *gdf6b*, GST-*gdf6b*, into two guinea pigs. Antibodies were validated by comparing reactivity of pre- and post-immune sera to bacterially-expressed GST-*gdf6b*. Results from one of the antibodies are shown.

Immunofluorescence

For adults, dorsal scales bearing normal melanocytes or melanomas were plucked from anesthetized zebrafish. After fixation, scales were bleached of melanin pigment to visualize fluorescence after staining. Scales were incubated with primary antibody (Gdf6b (1:250), Mitfa (1:250)) overnight. Subsequently the scales were washed, incubated in appropriate secondary antibodies (Jackson Labs), incubated with DAPI, mounted on slides with Vectashield (Vectorlabs), and visualized using confocal fluorescence microscopy.

Immunoblotting

Protein extracts were separated on 12% SDS-PAGE gels. Blots were probed with primary antibodies (GDF6 (Sigma PRS4691; 1:1000), phospho-SMAD1/5/8 (Cell Signaling 13820; 1:1000), SMAD1 (Cell Signaling 9743; 1:500), Total SMAD1/5/8 (Santa Cruz sc-6031-R; 1:1000), FLAG (Sigma F3165, 1:2000), SOX9 (Cell Signaling 82630S; 1:1000), GAPDH (Abcam 8245; 1:2000)) overnight at 4°C, washed five times in TBS plus 0.1% Tween (TBST) and then incubated with the appropriate HRP-conjugated secondary antibody (Jackson Labs) for 1 hour at room temperature. Membranes were washed five times in TBST and visualized on autoradiography film after incubating with ECL reagent (Supersignal West Pico or Supersignal West Femto; Thermo Scientific).

Immunohistochemistry (IHC) and TUNEL staining

From mouse xenografts, formalin-fixed, paraffin-embedded tissues were processed to obtain 5µm sections. Sections were stained with H&E, cleaved Caspase-3 (Cell signaling 9664; 1:100), Ki-67 (Dako M7240; 1:100) and evaluated. TUNEL staining was performed on sections using the In Situ Cell Death Detection kit (Roche) as per manufacturer's protocol. The numbers of TUNEL-positive or cleaved Caspase-3-positive or Ki67-positive cells were counted manually and the total number of cells in each field was calculated using ImageJ software.

Individual patient melanoma and tissue microarray cores consisted of 5 µm sections of formalin-fixed, paraffin-embedded tissues. Slides were first

deparaffinized with two changes of xylene, and rehydrated with changes of decreasing concentrations of alcohols, then rinsed in distilled water. Antigen retrieval was carried out with 0.01M citrate buffer at pH 6.0, or 0.001M EDTA at pH 8.0. Slides were heated in a 770W microwave oven for 14 minutes, cooled to room temperature, and rinsed in distilled water. The sections were first blocked for endogenous non-specific protein and peroxidase activity with an application of Dual Endogenous Block (Dako) for 10 minutes, followed by a buffer wash, followed by staining with antibodies recognizing GDF6 (Sigma PRS4691; 1:1000) and p-SMAD1/5/8 (Cell signaling 9664; 1:100) for 30 minutes. Staining with a second antibody recognizing GDF6 (Sigma HPA045206; 1:100) yielded concordant results. For negative controls, non-immune immunoglobulin G (a cocktail of Mouse Whole IgG and Rabbit Whole IgG (Pierce antibodies 31204 and 31207, respectively; both 1ug/ml)) staining was used. Following a buffer wash, sections were incubated with the EnVision+ Dual Link (Dako) detection reagent for 30 minutes. The sections were washed, and treated with a solution of diaminobenzidine and hydrogen peroxide (Dako) for 10 minutes, to produce the visible brown pigment. After rinsing, a toning solution (DAB Enhancer, Dako) was used for 2 minutes to enrich the final color. The sections were counterstained with hematoxylin, dehydrated, and coverslipped with permanent mounting media. Positive signal was defined as dark brown staining. Scant, or fine granular background staining, or no staining was considered negative.

Zebrafish formalin-fixed, 5mM EDTA treated, paraffin-embedded tissues were processed to obtain 5µm transverse sections. Sections were stained for H&E and as mentioned above with p-SMAD1/5/8 (Cell Signaling 9511; 1:150) and coverslipped with permanent mounting media. TUNEL staining was performed on sections with fluorescein-dUTP using In Situ Cell Death Detection kit (Roche) as per manufacturer's protocol. For TUNEL staining, sections were bleached in bleaching solutions (3% hydrogen peroxide 1% Potassium hydroxide) to remove the melanin pigment. The numbers of TUNEL-positive were counted manually and the total number of cells (DAPI positive) in each field was calculated using ImageJ software.

IHC scoring

For both the UMass patient cohort and the tissue microarray, a modified visual semi-quantitative method was used. Sections were scored for immunointensity (0-4) and immunopositivity (0-3), which were then multiplied. For the UMMS patient cohort, scoring was done by C.J.C. and A.M.V., and the scores were averaged. Scores were verified by A.D. For the tissue microarray cohort, scoring was conducted independently by C.L. and C.B.F.G. and the scores were averaged. Sections with scores less than or equal to four were binned into the low or no staining group and sections with scores greater than four were binned into the high staining group.

in situ hybridization

Embryos were grown at 28.5°C until the desired stage, then dechorionated and fixed in 4% PFA/PBS for 24 hours at 4°C. Following fixation, embryos were dehydrated in methanol and stored at -20°C. For *in situ* hybridization, embryos were rehydrated, permeabilized with proteinase K, and hybridized with digoxigenin-labeled probes in hybridization solution (1:100) overnight at 68°C. Probe mixes were removed, embryos were washed in TBST, and then incubated in blocking solution (0.5% Roche Blocking Reagent in TBST) at room temperature. Subsequently the embryos were incubated in anti-digoxigenin-AP conjugated antibody (Roche) diluted in blocking solution (1:400) overnight at 4°C. Following antibody incubation, the embryos were washed in TBST, and the RNA probes were visualized by incubation in NBT-BCIP solution (NBT-BCIP stock solution from Roche, diluted 1:200 in TBST with 50 mM MgCl2). After staining, embryos were washed in PBS and stored in 4% PFA/PBS at 4°C, then mounted 3% methylcellulose for imaging.

Quantifying melanocyte numbers in embryonic zebrafish

Zebrafish embryos were injected with miniCoopR-*EGFP,* miniCoopR-*gdf6a* or miniCoopR-*gdf6b* at the single-cell stage and then grown at 28.5°C. At 4 days post-fertilization, embryos were visualized under a light microscope to identify ones that had a chimeric pattern of melanocyte rescue. Additionally, the number of melanocytes per rescued embryo was counted manually.

Chromatin immunoprecipitation (ChIP) sequencing and analysis

ChIP was performed using the Simple ChIP Plus Enzymatic Chromatin IP kit as per manufacturer's instructions (Cell Signaling 9001) with the p-SMAD1/5/8 antibody (Cell Signaling 11971; 1:100). ChIP-DNA from A375 melanoma cells expressing an shRNA targeting *GDF6, GDF6.1* or *EGFP* or a 2% input control was used for library preparation using the TruSeq ChIP Library Prep Kit for ChIP-Seq (Illumina). Fastq files were aligned to the human reference genome (ENSEMBL GRCH37) by Bowtie (version 1.0.0) (Langmead et al., 2009) allowing uniquely mapped reads and removing PCR duplicates. For aggregation plotting, aligned reads were processed in HOMER (Heinz et al., 2010) using annotatePeaks to bin the regions of interest in 20-bp windows resulting in average enrichment with normalized reads for all genes. MACS2 (version 2.1.1.20160226) (Feng et al., 2012) was used for peak calling. Peaks with a false discovery cutoff of 1% were used. The alignment files were converted to bedGraph files and loaded as custom tracks in the UCSC genome browser to visualize regions of interest. ChIPpeakAnno (version 3.5.12) (Zhu et al., 2010) was used to visualize and compare the overlapping pSMAD1/5/8 peaks for genes bound by pSMAD1/5/8 in wild-type and *GDF6* knockdown A375 cells.

aCGH probe design

We custom designed the G3 array format of 2x400K probes for the Zebrafish ZV9 genome assembly using Agilent's eArray (eArray ID 036041). The array has 398426 unique probes covering 97% of the zebrafish genome (based on Zv9 assembly). The probes are 60 bases long and are spaced across the genome with an average separation of 3550 bases.

aCGH, JISTIC analysis and comparative analysis

aCGH was performed as per Agilent's array-based genomic DNA hybridization protocol. Briefly, genomic DNA was extracted from zebrafish melanomas or a normal region of the same fish using the Qiagen DNeasy Blood and Tissue kit. 5 µg of tumor or matched normal gDNA was fragmented to 200-500bp by sonication (Covaris S220R High Performance Sample Preparation Ultrasonicator System 220x S), labeled in a random-primed reaction using Cy5-dCTP or Cy3-dCTP, respectively, and hybridized in Agilent's hybridization buffer with Cot1 DNA (1mg/ml) at 65°C overnight. Arrays were then washed, and Cy5 and Cy3 signals were measured using an Agilent G2565 Microarray Scanner. Raw data was generated from scanned images with the Agilent Feature Extraction software (v10.7). Raw values were normalized using the Agilent Genomic workbench and copy number alterations were detected. The JISTIC algorithm was used in limited peel-off mode to calculate significantly altered regions, and peak calling was done using a q-value cut-off of 0.25. Gene-based JISTIC G-scores and –log10 transformed q-values are represented using the Circos package (Krzywinski et

al., 2009). For representation of data, the G-score scale for amplifications was 0 (minimum) and 1550 (maximum), and for deletions it was 0 (minimum) and 2150 (maximum). The log10-transformed q-value scale for both amplifications and deletions was 0 (minimum) and 11 (maximum). For human melanomas, copy number data was downloaded from Tumorscape (Beroukhim et al., 2010; Lin et al., 2008), and JISTIC analysis was conducted as described above. Genes from within peaks were pooled to define species-specific sets of recurrently amplified genes. Human orthologs of zebrafish genes were determined using Ensembl (Collins et al., 2012; Howe et al., 2013) and supplemented by performing BLAST (Altschul et al., 1990). Recurrently amplified zebrafish and human genes, as determined by JISTIC, were compared to find the overlapping set of commonly amplified genes.

cDNA amplification and microarray analysis

Total RNA was extracted and prepared from melanoma cells and from normal scale-associated melanocytes of *Tg(mitfa:BRAF(V600E)); p53(lf); alb(lf); Tg(mitfa:EGFP)* zebrafish as described above. Total RNA was amplified using the Nugen Ovation RNA Amplification system V2 as per manufacturer's protocol. For microarrays, amplified cDNA was hybridized to a 385K microarray (NimbleGen 0711105Zv7EXPR) as per manufacturer's protocol. Briefly, amplified cDNA from melanomas and melanocytes were labeled with Cy3 independently, hybridized to the microarray, washed and scanned with a GenePix 4000B

Scanner. Images were analyzed and normalized using NimbleScan software, and differentially expressed genes were identified.

Massively parallel RNA sequencing

For zebrafish melanomas and melanocytes, total RNA was isolated as described above and libraries were prepared using the TrueSeq Stranded mRNA Library Prep Kit as per manufacturer's protocol (Illumina). FASTQ files were analyzed using FASTQC v0.10.1(S, 2010) to ensure uniform read quality (phred>30). Paired-end reads were aligned to the zebrafish genome using STAR v2.3 (Dobin et al., 2013) (Zv9). The mapped reads were counted using htseq-count (v0.6.0, parameters –t exon) (Anders et al., 2015) and gene models from the Ensembl transcriptome (Howe et al., 2013). Analyses of differential gene expression were performed using DESeq2 (Ritchie et al., 2015). Orthology to human genes was determined using Ensembl (Collins et al., 2012; Howe et al., 2013) and supplemented by performing BLAST (Altschul et al., 1990). The heatmap of BMP pathway genes (REACTOME_SIGNALING_BY_BMP; MSigDB (Broad Institute)) was created using human orthologs of differentially expressed BMP pathway genes. The fish orthologs of human genes represented are *SMAD5=smad5, SMAD4=si:dkey-239n17.4, ACVR2A=acvr2a, ACVR2B=acvr2b, BMPR1A=bmpr1aa, FSTL1=fstl1b, SMAD7=smad7, BMPR2=bmpr2a, SMURF2=smurf2, SMAD6=smad6b, ZFYVE16=zfyve16, SKI=skib, GREM2=grem2, SMURF1=smurf1, UBE2D1=ube2d1, CER1=dand5, NOG=nog,*

BMP2=bmp2b, BMPR1B=bmpr1bb. For A375 human melanoma cells with *GDF6* and/or *SMAD1DVD* modulation, total RNA was isolated and libraries prepared as described above. Prepared libraries were sequenced using Illumina Hiseq technology (NY Genome Center). FASTQC v0.10.1 (S, 2010) was used on the FASTQ sequences for the A375 samples to generate sequence quality reports. Data were analyzed using two different bioinformatics pipelines. In the first pipeline, reads were aligned to the human reference genome (Ensembl GRCh37) using Bowtie2 (v 2-2.1.0) (Langmead and Salzberg, 2012) and Tophat2 (v 2.0.9) (Kim et al., 2013). Samtools (v 0.0.19) (Li et al., 2009) and IGV (v 2.3.60) (Thorvaldsdottir et al., 2013) were used for indexing the alignment files and viewing the aligned reads, respectively. Gene expression was quantitated as fragments per kilobase of exon model per million mapped fragments (FPKM) using Cufflinks (v 2.2.0) (Trapnell et al., 2012). Differentially-expressed genes were identified using the Cufflinks tools (Cuffmerge and Cuffdiff). cummeRbund (v 2.4.1) (Trapnell et al., 2012) was used to assess replicate concordance. In the second pipeline, reads were mapped against the human reference genome (Ensembl GRCh37) using the aligner STAR (v 2.4.2a), and gene level counts of uniquely mapped reads were obtained using htseq-count (v 0.6.1) (Anders et al., 2015). Differential expression analysis was performed using DESeq2 (Love et al., 2014) for each pairwise condition using a p-adj threshold of 0.05. The FPKM-based method and the counts-based method generated concordant results. Analyses using the FPKM-based method have been represented in results.

Human melanocyte and melanoma transcriptome analysis

Three hundred and eighty-five human RNA-seq samples were downloaded from the Cancer Genomics Hub (CGHub) (https://cghub.ucsc.edu) using GeneTorrent (v 3.8.5a) (Wilks et al., 2014). The RNAseq TCGA dataset is comprised of three sample types: 302 metastatic melanoma samples, 82 primary melanomas, and 1 solid tissue normal (2015). For the normal melanocyte datasets, two RNAseq samples were downloaded from the Short Read Archive (SRA) (https://www.ncbi.nlm.nih.gov/sra/; accession codes: SRR522118, SRR522119)(Barrett et al., 2013) and two from the ENCODE project (https://www.encodeproject.org/; experiment: ENCSR000CUQ) (2012). The datasets downloaded from TCGA, SRA and ENCODE were aligned to the human reference genome (Ensembl GRCh37) and analyzed using the FPKM-based method described above.

The accession number for the RNAseq, ChIPseq and gene expression microarray datasets reported in this paper is GEO: GSE83400

CHAPTER V
FINAL SUMMARY AND DISCUSSION

Summary

This study (1) used a cross-species comparative genomics approach with zebrafish melanoma to identify the novel melanoma oncogene *GDF6*, (2) defined the a role of GDF6-induced BMP signaling in inhibiting MITF and SOX9 to maintain melanoma cells undifferentiated and alive, (3) reported the clinical relevance of *GDF6* expression in patients with melanoma, and (4) generated a prognostic NC identity for melanomas.

In the first part, a comparative genomic approach was used on human and zebrafish melanomas to identify cancer genes dysregulated by CNVs. By integrating transcriptome analysis, I identified *GDF6* as a recurrently amplified and transcriptionally upregulated melanoma oncogene. In zebrafish, the overexpression of a *GDF6* ortholog accelerated melanoma onset, whereas the loss of an ortholog delayed disease onset, indicating the role of GDF6 in tumor initiation. In established human melanoma cell lines and mouse xenografts, *GDF6* overexpression promoted tumor growth, whereas its knockdown abrogated growth. By using mechanistic analysis, I observed that *GDF6* acts via the BMP-SMAD1 signaling axis to invoke trunk NC identity in melanoma cells. As a part of this signaling axis, *GDF6*-activated BMP signaling repressed the melanocyte differentiation gene *MITF* and the proapoptotic melanoma gene *SOX9*, aiding the melanoma cells in remaining undifferentiated and alive. During

the analysis of the clinical relevance of GDF6 expression in patients with melanoma, I identified GDF6 expression as a prognostic indicator of lymph node metastasis, which was inversely correlated with melanoma patient survival. During the identification of the role of GDF6 in melanomas, I also noted a novel role of GDF6 in regulating melanocyte development. Although the overexpression of *gdf6* orthologs reduced the number of differentiated melanocytes, the loss of *gdf6a* caused an evident increase in the number of melanocyte. Taken together, these findings suggest that developmental functions of GDF6 and BMP signaling are reestablished in melanomas to promote tumor initiation and maintenance.

In the second part, the transcriptome data from zebrafish tumors were exploited further to generate a prognostic NC signature for melanoma. Compared with normal melanocytes, differentially regulated genes in zebrafish melanomas are enriched for NC pathway genes, indicating the activation of NC identities in these melanomas. By using this transcriptome data, I generated a 15-gene NC gene signature. This gene signature correlated with the expression of *SOX10*, a previously defined NC marker in human melanoma. Patients with melanomas having a high expression of this NC gene signature had low overall survival. These analyses indicate the clinical relevance of NC identities in melanomas, and also establish, for the first time, a prognostic NC gene signature for melanomas.

Overall, this study emphasizes the importance of NC identities in melanoma and identifies a new signaling pathway that establishes these identities in tumor cells. In addition to providing insight into a fundamental process of cancer biology, this study provides new targeting opportunities for melanoma therapy.

Comparative Genomics Using Zebrafish as a Gene Discovery Tool

Several fundamental aspects of cancer biology have been revealed by using zebrafish cancer models, particularly through comparative genomics (Lam and Gong, 2006; Zhang et al., 2013; Zhang et al., 2010). Since the advent of next-generation sequencing, several cancer genomes have been comprehensively analyzed and consequently several tumor-associated genetic alterations have been identified. Functional analysis of these aberrations to identify their role in tumorigenesis has been a major focus. Comparative oncogenomics using zebrafish has aided in identifying such driver alterations and their roles in tumorigenesis.

In this study, I used the zebrafish melanoma model to identify driver genes dysregulated by the virtue of CNVs. In human melanomas, approximately 10% of the genome undergoes recurrent CNVs (Beroukhim et al., 2010; Lin et al., 2008). In CNV regions, most genes are predicted to be random passengers, which alter because they are located next to the drivers. I predicted that the evolutionary divergence between humans and zebrafish (of approximately 420 million years)

would frequently place orthologous driver genes next to different set of neighboring genes in each species because of the extensive genomic reorganization present between these species (Catchen et al., 2011). To test this rationale and identify potential melanoma oncogenes, I compared human and zebrafish melanoma copy number amplifications. I assumed the copy number amplification mechanism is conserved between human and zebrafish melanomas on the basis of the following factors: First, known melanoma oncogenes, such as *SETDB1*, *TERT*, and *MYC*, are amplified in human melanomas as well as zebrafish melanomas. Second, genome-wide comparisons demonstrated that the number of genes commonly amplified in melanomas of both species were incidentally much higher than expected. Finally, previous studies have indicated that zebrafish melanomas have a low number of DNA base substitution mutations, unlike human melanoma (Yen et al., 2013). The current study also revealed extensive CNVs in zebrafish melanomas that significantly overlapped with the CNV regions identified in my analysis. Taken together, these findings suggest that zebrafish melanomas are mostly driven by oncogenes located in recurrently amplified regions of the genome, and comparative analysis with human melanoma may aid in elucidating novel oncogenes.

To identify these oncogenes, I next integrated the transcriptome data of zebrafish melanomas with comparative copy number amplification analysis. The use of zebrafish model for analyzing gene expression of melanomas has a unique advantage. Most gene expression studies for melanoma have used either

skin sections or transformed melanocyte cell lines as controls to identify differentially regulated genes. In this study, I compared gene expression of melanoma cells with primary melanocytes directly obtained from zebrafish by using *Tg(mitfa:EGFP)* transgenic zebrafish, the melanocytes of which were labeled with EGFP. By using the transcriptome data from zebrafish melanomas and melanocytes, I found 128 genes that were not only amplified but also transcriptionally upregulated at least 2-fold in the melanomas of both species. Among these genes, I focused on *GDF6* because of its expression in the NC, an embryonic tissue that gives rise to melanocytes. However, because the list identified in this study may contain several other melanoma oncogenes, further functional analysis is required to reveal the driver genes.

I also compared copy number deletions in zebrafish melanomas with those in human melanomas. Unlike amplifications, the number of genes commonly deleted in melanomas of both species were incidentally much lower than expected (Figure 4.1). I speculated that this lack of conservation in copy number deletions across species could be due to the duplication event that occurred in the teleost lineage, causing approximately 40% of human genes to have two zebrafish paralogs. Because the deletion of both paralogs of a tumor suppressor gene may be required for complete inactivation of the pathway, this loss-of-function mechanism may not be opted by zebrafish melanomas. Among the 72 commonly deleted genes, only 16% had two zebrafish paralogs compared

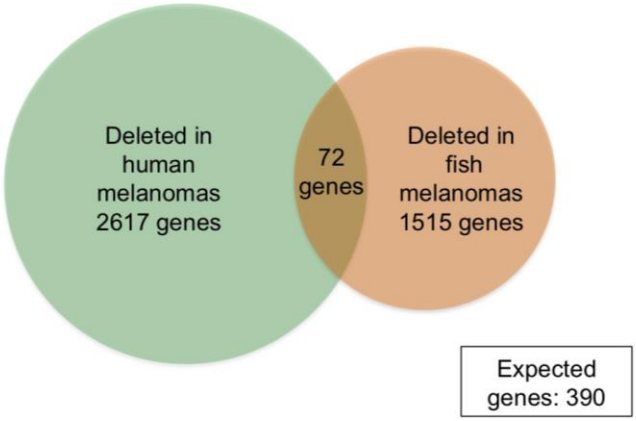

Figure 4.1: Genes deleted in human and zebrafish melanomas

Venn diagram of orthologous genes significantly deleted in human and zebrafish melanomas from a total of 10380 human-zebrafish gene pairs (hypergeometric test, *P*-value: $4.0e^{-22}$).

with the expected 40%. Nevertheless, some of these commonly deleted genes are potential tumor suppressors; functional analysis using these genes may aid in inferring their role in melanomagenesis.

BMP Signaling in Melanoma

BMP Signaling Invokes an Undifferentiated NC Identity in Melanomas

In several cancers, a low degree of differentiation is correlated with increased tumor initiation capability of transformed cells. A hallmark study linking cell differentiation and tumor initiation was performed by the Petrenko lab, wherein they used a conditional mouse model to express oncogenic $KRAS^{G12D}$ in the pancreas and traced the cellular and molecular changes that occurred during different transformation stages (Ischenko et al., 2013). The authors noted that activated $KRAS^{G12D}$ rendered plasticity to differentiated cells, which acquired stem cell-like features and transformed into neoplastic cells. Another study found cellular dedifferentiation and awakening of stem cell-like features to be involved in the initiation of intestinal tumors (Schwitalla et al., 2013). In these tumors, the Wnt pathway promotes dedifferentiation-induced tumor initiation. The Wnt pathway regulates the fate specification of the intestinal stem cell pool (Tian et al., 2016), and this function is potentially invoked during the early stages of tumorigenesis.

In melanomas, embryonic identities have been implicated in tumor initiation (Boiko et al., 2010; Kaufman et al., 2016), but the mechanisms involved

in regulating these embryonic identities are largely unknown. In the present study, I demonstrated that GDF6 promotes melanoma initiation, potentially by inducing embryonic NC identities. In zebrafish, *gdf6b* overexpression accelerates melanoma onset, whereas its loss delays the onset, indicating that GDF6 is important during tumor initiation in zebrafish. GDF6 regulates an NC identity in melanoma cells. Thus, I speculated that the cell-of-origin for zebrafish melanomas is an undifferentiated melanocytic cell that has adopted an embryonic identity. Corroborating this hypothesis, I reported that GDF6 can regulate the differentiation of the melanocyte lineage. During normal development, the overexpression of *gdf6* orthologs reduced the number of differentiated melanocytes in zebrafish embryos, whereas the loss of *gdf6a* caused an evident increase in the number of melanocytes in adult zebrafish, thus suggesting that GDF6 inhibits melanocyte differentiation. In human melanoma cells, GDF6 directly represses *MITF* and *SOX9*, both of which are regulators of melanocyte and melanoma differentiation. Thus, GDF6 potentially acts through BMP signaling to suppress differentiation signaling in melanocytes, leading to the expression of NC factors that induce dedifferentiation and promote tumor initiation. In the absence of GDF6, zebrafish develop fewer melanomas; these melanomas are highly differentiated and potentially less aggressive.

The experiments performed in this study determined the role of GDF6 and BMP signaling in melanoma initiation in a zebrafish model; however, identifying similar mechanisms in a mammalian setting is essential. Such studies are

challenging in part because of the lack of available NC reporters for assessing changes in the cellular identities of mammalian melanoma models. However, here, I detected GDF6 and active BMP pathway in a majority of the melanomas (approximately 80%). Moreover, patients with primary melanomas containing higher GDF6 levels had an increased likelihood of metastasis and experienced shorter survival compared with patients with melanomas containing no or lower levels of GDF6. On the basis of these findings, I predicted that even in humans, GDF6 is important during the early stages of melanomagenesis and is a prognostic predictor of tumor aggressiveness.

BMP Signaling Promotes Melanoma Cell Survival

Bernard Weinstein coined the term “oncogene addiction,” which refers to the dependency of a cancer on the continued activity or expression of a particular oncogene (Weinstein, 2002). In this model, an oncogene provides aberrant proproliferative or prosurvival benefits, specifically to the tumor cells and not to the corresponding normal tissue. The tumors cannot sustain the loss of this oncogene. The biological significance and clinical impact of this model has been exemplified by several reports, such as *KIT* mutations in gastrointestinal stromal tumors, *EGFR* mutations in non–small-cell lung cancers and *BCR-ABL* translocations in acute myeloid leukemia (Demetri et al., 2002; Kantarjian et al., 2002; Lynch et al., 2004; Paez et al., 2004; Xu et al., 2014). In the present study, I observed that melanoma-specific expression of GDF6, either by amplification or

transcriptional upregulation, provides prosurvival signals to tumors cells, whereas its loss abrogated tumor growth. Thus, the *GDF6*-expressing melanoma cells are addicted to GDF6 activity.

The potential of GDF6 and BMP signaling to promote melanoma cell survival is owing to its ability to regulate SOX9 and SOX10. In melanomas, SOX10 is a prosurvival factor, whereas SOX9 is a proapoptotic factor; these factors antagonistically crossregulate each other (Shakhova et al., 2015; Shakhova et al., 2012). On the basis of gene expression analysis, I noted that that GDF6 induces *SOX10* expression and represses *SOX9* expression, a pattern of regulation promoting tumor cell survival. Whether GDF6-activated BMP signaling regulates one or both the factors directly requires elucidation. According to the current ChIPseq data, GDF6-dependent phosphoSMAD1/5/8-binding peaks at distal regions upstream of *SOX9*, thus suggesting direct regulation. In the SOX10 promoter, phosphoSMAD1/5/8 peaked, but the binding was not abrogated by *GDF6* knockdown. Thus, I speculated that GDF6 promotes melanoma cell survival by directly repressing *SOX9* expression and indirectly regulating that of *SOX10*.

Role of BMP Signaling in Melanocyte Development

Several studies have investigated the roles of known developmental factors in cancer progression (Gupta et al., 2005; Mack et al., 2016; Maguire et al., 2015; Wong et al., 2015). Given the role of GDF6 and BMP signaling in

regulating differentiation and NC identity within melanomas, I hypothesized that GDF6 have a developmental role during melanocyte development.

A conglomerate of transcription factors orchestrates melanocyte differentiation; in melanomas, GDF6-activated BMP signaling regulates several of these factors. Through mathematical modeling and *in vivo* analysis in zebrafish embryos, the Kelsh lab reported a gene regulatory network for melanocyte differentiation (Greenhill et al., 2011). According to this model, orthologs of MITF and SOX9 (*mitfa* and *sox9b,* respectively) are critical for the initiation of melanocyte differentiation. GDF6 and BMP signaling repress both of these factors in human and zebrafish melanomas. Thus, the ability of GDF6 to inhibit melanocyte differentiation in embryos may be resulting from its potential to repress *mitfa* and *sox9b* expression during zebrafish development. The expression of *GDF6* orthologs in zebrafish during this time further supports the role of this pathway in blocking melanocyte differentiation. *GDF6* orthologs are expressed in the NC and adjacent tissues; however, during melanocyte differentiation, their expression is turned off, potentially enabling *mitfa* and *sox9b* expression and thereby initiating melanocyte differentiation. Zebrafish with loss-of-function *gdf6a* have a relatively higher number of melanocytes, potentially because of precocious differentiation. By contrast, in animals with forced expression of *gdf6a* or *gdf6b* in the melanocyte lineage, I noted a significant reduction in the number of differentiated melanocytes, potentially because of prolonged repression of *mitfa* and *sox9b* expression.

The role of BMP signaling during NC lineage segregation is potentially reiterated in NC-derived cancers. Tumors originating from the NC lineage adopt features of the NC (Maguire et al., 2015); however, the mechanisms involved in the establishment of these embryonic identities remain unclear. In this study, I demonstrated that the reawakening of NC identities in melanomas is regulated by BMP signaling and predicted that this ability of BMP signaling is due to its role in inhibiting differentiation of melanocyte lineage from the NC. Studies have indicated that BMP signaling promotes the differentiation of the NC into neurons and glia (Gajavelli et al., 2004; Goldstein et al., 2005; Saito et al., 2012; Schneider et al., 1999). Notably, in neuroblastomas and glioblastomas (tumors arising from neuronal and glial cells, respectively), BMP signaling promotes tumor differentiation and suppresses cancer initiation and growth (Du and Yip, 2010; Lee et al., 2008; Piccirillo et al., 2006). Therefore, I predicted that BMP signaling has contrasting roles in glioblastomas and neuroblastomas compared with those in melanomas and that this role depends on the activity of BMP signaling during differentiation of the NC into these specific lineages.

Clinical Relevance of This Study

Importance of GDF6 Expression in Patients with Melanomas

Melanoma therapeutics has considerably advanced in the last decade; however, many patients do not respond to current therapies. The current study provided a novel target for therapeutic targeting of melanomas. In two

independent patient cohorts, GDF6 expression was noted in a majority of melanomas (approximately 80%). Furthermore, GDF6 is critical for melanoma cell survival because inhibition of this pathway led to tumor cell death. Moreover, the prosurvival role of GDF6 is potentially independent of the underlying driver mutations. Taken together, these findings indicate that approaches targeting GDF6 and BMP pathway components may have therapeutic benefits.

Several approaches can be used for targeting this pathway in melanomas. Here, I performed a proof-of-principal study to demonstrate that targeting BMP signaling by using a small molecule inhibitor DMH1 could reduce tumor growth *in vivo.* However, in future, targeting GDF6 ligand, rather than the pleotropic BMP pathway, would be ideal. As previously mentioned, GDF6 expression in adult tissues is limited to the regions of bone repair. Therefore, GDF6-targeting strategies may have a lower toxic effect than anti-BMP targeting strategies would. Moreover, GDF6 is a secretory protein; this enables the use of non–cell-permeable strategies to target this factor.

The use of GDF6 targeting drugs may be therapeutically beneficial when used alone or in combination with BRAF and MAPK pathway inhibitors. First, the analysis of TCGA melanomas demonstrated that in melanomas, *GDF6* expression is independent of driver mutations, such as those is *BRAF* and *NRAS*. Second, the prosurvival role of GDF6 signaling is independent of *BRAF* or *NRAS* mutations, and GDF6 loss results in cell death in MeWo melanoma cells (BRAF and NRAS wild-type). Therefore, the use of anti-GDF6 strategies

may function independent of current targeted strategies. However, the use of GDF6-targeting strategies can also be used to further bolster the antitumor effects of BRAF and MAPK pathway inhibitors.

Importance of NC Identities in Patients with Melanomas

Although melanomas can adopt NC identities, the clinical significance of these identities remains unknown. The expression of several NC factors, such as *SOX10, FOXD3, TWIST*, and *SNAIL*, has been observed in patients with melanomas; however, no study has revealed the prognostic outcome of melanomas expressing these factors. I noted that the RNA expression of NC factors—which have been implicated in melanoma progression—cannot independently predict melanoma patient survival. Because changes in cellular identity involve a global gene expression shift, I predicted that NC identities could be best defined by a set of NC genes.

We have now used zebrafish melanomas to identify such an NC gene signature. Zebrafish melanomas initiate from melanocytic cells that have adopted NC identities (Kaufman et al., 2016). The analysis of zebrafish melanomas has also revealed robust expression of NC genes in all melanoma cells (White et al., 2011). In addition, I noted that genes differentially regulated in zebrafish melanomas compared with normal melanocytes are enriched for NC pathway genes. Taken together, these data indicate that zebrafish melanomas may resemble human melanomas that have adopted NC identities. I observed that the

NC gene signature identified using the zebrafish melanoma transcriptome data correlated with the expression of SOX10, a factor implicated in maintaining NC state in human melanomas (Kaufman et al., 2016; Shakhova et al., 2012). In addition, in the current study, patients with melanomas containing high NC gene signature levels had lower chances of survival. This study is the first report identifying a prognostic NC signature for melanomas.

The NC gene signature may have the potential to predict melanoma treatment strategies in future. Studies from the Zon lab have identified a DHODH inhibitor, leflunomide, which can target mechanisms common to the NC and melanomas (White et al., 2011). It inhibits translational elongation of c-MYC target genes in the NC and melanomas. Currently, the suitability of this drug for melanomas is being tested in clinical trials. Nevertheless, this and other drug targeting NC mechanisms in melanomas may be effective routes for melanoma therapy. Future studies should analyze whether the NC gene signature can be a tool for predicting the efficacy of these drugs in treating melanoma.

Caveats of this study

This study has shown that GDF6 acts as an oncogene via the BMP signaling pathway. However, some of the functional and mechanistic analyses presented in this study need further validation. Firstly, we present a model where GDF6-activated BMP signaling regulates both MITF and SOX9, thereby inhibiting melanoma cell differentiation and death, respectively. We see phoshp-

SMAD1/5/8 binding peaks upstream of the *MITF* gene, which is lost upon *GDF6* knockdown. Based on this we predict direct regulation of MITF by GDF6 and BMP signaling. However, experiments with melanoma cells whose phosphoSMAD1/5/8 binding sites upstream of MITF are deleted are required to directly test whether BMP pathway regulates MITF. Another possibility is that BMP signaling regulates MITF indirectly via SOX9, as SOX9 is known to regulate MITF during embryogenesis (Greenhill et al., 2011). Secondly, this study does not exclude the possibility that GDF6-activated BMP pathway also acts via non-canonical pathways to promote melanomas. BMP receptors are also known to activate phosphor p38 and JNK pathways (Pant et al., 2013; Wang et al., 2013b), both of which have known tumor-promoting roles in melanomagenesis. The role of GDF6 in melanoma cell survival is dependent on SMAD1 axis of BMP signaling, but the non-canonical arm of BMP signaling may be important for other tumor-promoting roles. Thirdly, our functional studies show Caspase 3 activation in melanoma cells with GDF6 knockdown. Caspase 3 activation is majorly used as a cell death marker, and in this study based on activation of Caspase 3 and other apoptotic assays like TUNEL staining and Annexin V positivity, we claim that GDF6 knockdown causes apoptotic death of melanoma cells. However, Caspase 3 also has other biological functions like regulation of differentiation of the hematopoietic lineage. Whether such functions are relevant to melanoma cells needs further testing. This would also indicate whether it is appropriate to use Caspase 3 as a cell death marker alone in this context. Finally, our data also

show that GDF6 is necessary for melanoma cell survival. Melanoma cells do not survive in vitro or in vivo in mouse xenografts upon GDF6 knockdown. Zebrafish melanoma with loss of *gdf6a* show increased apoptosis and reduced growth. Although these studies strongly suggest that GDF6 is necessary for melanoma cell growth and survival, direct testing using conditional GDF6 knockdown systems in established tumors would have been ideal.

Future Directions

This thesis has incited several fundamental questions in the fields of cancer biology, developmental biology, and cancer therapeutics, which will be answered through further research in my lab. Some of the important future directions are listed as follows:

1) *Developing Anti-GDF6 Targeting Strategies for Melanoma Therapy*

Here, I identified of a novel therapeutic target for melanoma, GDF6. In collaboration with MassBiologics, Boston, MA, USA, I developed monoclonal anti-GDF6 antibodies through hybridoma technology. Monoclonal antibodies are highly specific targeting molecules, suitable for therapeutic purposes. The goal of our collaboration was to develop antibodies that can specifically bind to GDF6 and block its binding to BMP receptor, eventually abrogating BMP signaling. Through this collaboration, several antibodies have already been developed. Currently, their ability to bind GDF6 is being analyzed *in vitro*. Subsequently, the

efficacy of these antibodies will be analyzed in preclinical cancer models. This pathway has not been identified in melanomas previously, and we show that expression of GDF6 and activity of BMP pathway in promoting melanoma cell survival is independent of other known mutations like BRAF and NRAS. Therefore, targeting of BMP signaling can have independent effects on melanoma cells as compared to BRAF and MEK pathway inhibitors, and therefore can be used for adjuvant therapy of melanomas.

2) *Role of BMP Signaling in Inducing NC Identities During Melanoma Initiation*

As mentioned previously, studies have indicated the importance of NC identities in melanoma initiation; however, the present study implicated BMP signaling in invoking NC identities in melanomas. A future direction is to test whether the induction of NC identities during melanoma initiation is regulated directly by BMP signaling. This can be studied by combining the BMP reporter zebrafish (*Tg(BRE:mCherry)*) with the NC reporter (*Tg(crestin:EGFP)*) and monitoring in real-time the BMP pathway and NC identities, with respect to each other during tumor initiation. This can further be combined with GDF6 and BMP pathway modulation strategies to directly analyze the effect of the BMP pathway on NC identity induction during melanoma initiation. It has been difficult to understand how tumors initiate, in part due to the difficulty of lineage tracing studies in adult organisms. Here, this study provides a novel opportunity as it provides a potential signaling pathway that may be important for tumor initiation. This will not only

give us a better understanding of tumor biology, but may also be important for disease diagnosis.

3) *Role of GDF6 and BMP Signaling During Melanocyte Development*

The current study uncovered a new role of GDF6 and BMP signaling in melanocyte development. Nevertheless, identifying the precise function of this pathway may not only increase the understanding of melanocyte development but also provide more insight into the role of the pathway in tumorigenesis. The questions that need to be addressed here included the following: (1) What process during melanocyte development is regulated by BMP signaling—fate specification, differentiation, proliferation, or a combination of these? (2) Whether BMP signaling acts by repressing *mitfa* and *sox9b* similar to that in melanomas? (3) In addition to gdf6, are there other BMP ligands contributing to the role of BMP signaling in melanocyte development?

BIBILOGRAPHY

ENCODE project Consortium (2012). An integrated encyclopedia of DNA elements in the human genome. Nature *489*, 57-74.

GTEx Consortium (2013). The Genotype-Tissue Expression (GTEx) project. Nature genetics *45*, 580-585.

TCGA Consortium (2015). Genomic Classification of Cutaneous Melanoma. Cell *161*, 1681-1696.

Akbani R, A.K., Aksoy BA, Albert M, Ally A, Amin SB, Arachchi H, Arora A, Auman JT, Ayala B, Baboud J, Balasundaram M, Balu S, Barnabas N, Bartlett J, Bartlett P, Bastian BC, Baylin SB, Behera M, Belyaev D, Benz C, Bernard B, Beroukhim R, Bir N, Black AD, Bodenheimer T, Boice L, Boland GM, Bono R, Bootwalla MS, Bosenberg M, Bowen J, Bowlby R, Bristow CA, Brockway-Lunardi L, Brooks D, Brzezinski J, Bshara W, Buda E, Burns WR, Butterfield YS, Button M, Calderone T, Cappellini GA, Carter C, Carter SL, Cherney L, Cherniack AD, Chevalier A, Chin L, Cho J, Cho RJ, Choi YL, Chu A, Chudamani S, Cibulskis K, Ciriello G, Clarke A, Coons S, Cope L, Crain D, Curley E, Danilova L, D'Atri S, Davidsen T, Davies MA, Delman KA, Demchok JA, Deng QA, Deribe YL, Dhalla N, Dhir R, DiCara D, Dinikin M, Dubina M, Ebrom JS, Egea S, Eley G, Engel J, Eschbacher JM, Fedosenko KV, Felau I, Fennell T, Ferguson ML, Fisher S, Flaherty KT, Frazer S, Frick J, Fulidou V, Gabriel SB, Gao J, Gardner J, Garraway LA, Gastier-Foster JM, Gaudioso C, Gehlenborg N, Genovese G,

Gerken M, Gershenwald JE, Getz G, Gomez-Fernandez C, Gribbin T, Grimsby J, Gross B, Guin R, Gutschner T, Hadjipanayis A, Halaban R, Hanf B, Haussler D, Haydu LE, Hayes DN, Hayward NK, Heiman DI, Herbert L, Herman JG, Hersey P, Hoadley KA, Hodis E, Holt RA, Hoon DS, Hoppough S, Hoyle AP, Huang FW, Huang M, Huang S, Hutter CM, Ibbs M, Iype L, Jacobsen A, Jakrot V, Janning A, Jeck WR, Jefferys SR, Jensen MA, Jones CD, Jones SJ, Ju Z, Kakavand H, Kang H, Kefford RF, Khuri FR, Kim J, Kirkwood JM, Klode J, Korkut A, Korski K, Krauthammer M, Kucherlapati R, Kwong LN, Kycler W, Ladanyi M, Lai PH, Laird PW, Lander E, Lawrence MS, Lazar AJ, Łaźniak R, Lee D, Lee JE, Lee J, Lee K, Lee S, Lee W, Leporowska E, Leraas KM, Li HI, Lichtenberg TM, Lichtenstein L, Lin P, Ling S, Liu J, Liu O, Liu W, Long GV, Lu Y, Ma S, Ma Y, Mackiewicz A, Mahadeshwar HS, Malke J, Mallery D, Manikhas GM, Mann GJ, Marra MA, Matejka B, Mayo M, Mehrabi S, Meng S, Meyerson M, Mieczkowski PA, Miller JP, Miller ML, Mills GB, Moiseenko F, Moore RA, Morris S, Morrison C, Morton D, Moschos S, Mose LE, Muller FL, Mungall AJ, Murawa D, Murawa P, Murray BA, Nezi L, Ng S, Nicholson D, Noble MS, Osunkoya A, Owonikoko TK, Ozenberger BA, Pagani E, Paklina OV, Pantazi A, Parfenov M, Parfitt J, Park PJ, Park WY, Parker JS, Passarelli F, Penny R, Perou CM, Pihl TD, Potapova O, Prieto VG, Protopopov A, Quinn MJ, Radenbaugh A, Rai K, Ramalingam SS, Raman AT, Ramirez NC, Ramirez R, Rao U, Rathmell WK, Ren X, Reynolds SM, Roach J, Robertson AG, Ross MI, Roszik J, Russo G, Saksena G, Saller C, Samuels Y, Sander C, Sander C, Sandusky G, Santoso N, Saul M, Saw RP,

Schadendorf D, Schein JE, Schultz N, Schumacher SE, Schwallier C, Scolyer RA, Seidman J, Sekhar PC, Sekhon HS, Senbabaoglu Y, Seth S, Shannon KF, Sharpe S, Sharpless NE, Shaw KR, Shelton C, Shelton T, Shen R, Sheth M, Shi Y, Shiau CJ, Shmulevich I, Sica GL, Simons JV, Sinha R, Sipahimalani P, Sofia HJ, Soloway MG, Song X, Sougnez C, Spillane AJ, Spychała A, Stretch JR, Stuart J, Suchorska WM, Sucker A, Sumer SO, Sun Y, Synott M, Tabak B, Tabler TR, Tam A, Tan D, Tang J, Tarnuzzer R, Tarvin K, Tatka H, Taylor BS, Teresiak M, Thiessen N, Thompson JF, Thorne L, Thorsson V, Trent JM, Triche TJ Jr, Tsai KY, Tsou P, Van Den Berg DJ, Van Allen EM, Veluvolu U, Verhaak RG, Voet D, Voronina O, Walter V, Walton JS, Wan Y, Wang Y, Wang Z, Waring S, Watson IR, Weinhold N, Weinstein JN, Weisenberger DJ, White P, Wilkerson MD, Wilmott JS, Wise L, Wiznerowicz M, Woodman SE, Wu CJ, Wu CC, Wu J, Wu Y, Xi R, Xu AW, Yang D, Yang L, Yang L, Zack TI, Zenklusen JC, Zhang H, Zhang J, Zhang W, Zhao X, Zhu J, Zhu K, Zimmer L, Zmuda E, Zou L. (2015). Genomic Classification of Cutaneous Melanoma. Cell *161*, 1681-1696.

Alarmo, E.L., Korhonen, T., Kuukasjarvi, T., Huhtala, H., Holli, K., and Kallioniemi, A. (2008). Bone morphogenetic protein 7 expression associates with bone metastasis in breast carcinomas. Annals of oncology : official journal of the European Society for Medical Oncology *19*, 308-314.

Altschul, S.F., Gish, W., Miller, W., Myers, E.W., and Lipman, D.J. (1990). Basic local alignment search tool. Journal of molecular biology *215*, 403-410.

Anders, S., Pyl, P.T., and Huber, W. (2015). HTSeq--a Python framework to work with high-throughput sequencing data. Bioinformatics (Oxford, England) *31*, 166-169.

Asai-Coakwell, M., French, C.R., Ye, M., Garcha, K., Bigot, K., Perera, A.G., Staehling-Hampton, K., Mema, S.C., Chanda, B., Mushegian, A.*, et al.* (2009). Incomplete penetrance and phenotypic variability characterize Gdf6-attributable oculo-skeletal phenotypes. Human molecular genetics *18*, 1110-1121.

Asai-Coakwell, M., March, L., Dai, X.H., Duval, M., Lopez, I., French, C.R., Famulski, J., De Baere, E., Francis, P.J., Sundaresan, P.*, et al.* (2013). Contribution of growth differentiation factor 6-dependent cell survival to early-onset retinal dystrophies. Human molecular genetics *22*, 1432-1442.

Atkins, M.B., and Larkin, J. (2016). Immunotherapy Combined or Sequenced With Targeted Therapy in the Treatment of Solid Tumors: Current Perspectives. Journal of the National Cancer Institute *108*, djv414.

Barrett, T., Wilhite, S.E., Ledoux, P., Evangelista, C., Kim, I.F., Tomashevsky, M., Marshall, K.A., Phillippy, K.H., Sherman, P.M., Holko, M.*, et al.* (2013). NCBI GEO: archive for functional genomics data sets--update. Nucleic acids research *41*, D991-995.

Basile, K.J., Abel, E.V., and Aplin, A.E. (2012). Adaptive upregulation of FOXD3 and resistance to PLX4032/4720-induced cell death in mutant B-RAF melanoma cells. Oncogene *31*, 2471-2479.

Berghmans, S., Murphey, R.D., Wienholds, E., Neuberg, D., Kutok, J.L., Fletcher, C.D., Morris, J.P., Liu, T.X., Schulte-Merker, S., Kanki, J.P.*, et al.* (2005). tp53 mutant zebrafish develop malignant peripheral nerve sheath tumors. Proceedings of the National Academy of Sciences of the United States of America *102*, 407-412.

Beroukhim, R., Mermel, C.H., Porter, D., Wei, G., Raychaudhuri, S., Donovan, J., Barretina, J., Boehm, J.S., Dobson, J., Urashima, M.*, et al.* (2010). The landscape of somatic copy-number alteration across human cancers. Nature *463*, 899-905.

Bhaskara, V.K., Mohanam, I., Rao, J.S., and Mohanam, S. (2012). Intermittent hypoxia regulates stem-like characteristics and differentiation of neuroblastoma cells. PloS one *7*, e30905.

Boiko, A.D., Razorenova, O.V., van de Rijn, M., Swetter, S.M., Johnson, D.L., Ly, D.P., Butler, P.D., Yang, G.P., Joshua, B., Kaplan, M.J.*, et al.* (2010). Human melanoma-initiating cells express neural crest nerve growth factor receptor CD271. Nature *466*, 133-137.

Bollag, G., Hirth, P., Tsai, J., Zhang, J., Ibrahim, P.N., Cho, H., Spevak, W., Zhang, C., Zhang, Y., Habets, G.*, et al.* (2010). Clinical efficacy of a RAF inhibitor needs broad target blockade in BRAF-mutant melanoma. Nature *467*, 596-599.

Braig, S., and Bosserhoff, A.K. (2013). Death inducer-obliterator 1 (Dido1) is a BMP target gene and promotes BMP-induced melanoma progression. Oncogene *32*, 837-848.

Bruneau, S., and Rosa, F.M. (1997). Dynamo, a new zebrafish DVR member of the TGF-beta superfamily is expressed in the posterior neural tube and is up-regulated by Sonic hedgehog. Mechanisms of development *61*, 199-212.

Buijs, J.T., Henriquez, N.V., van Overveld, P.G., van der Horst, G., Que, I., Schwaninger, R., Rentsch, C., Ten Dijke, P., Cleton-Jansen, A.M., Driouch, K.*, et al.* (2007). Bone morphogenetic protein 7 in the development and treatment of bone metastases from breast cancer. Cancer research *67*, 8742-8751.

Cai, J., Pardali, E., Sanchez-Duffhues, G., and ten Dijke, P. (2012). BMP signaling in vascular diseases. FEBS letters *586*, 1993-2002.

Carreira, S., Goodall, J., Denat, L., Rodriguez, M., Nuciforo, P., Hoek, K.S., Testori, A., Larue, L., and Goding, C.R. (2006). Mitf regulation of Dia1 controls melanoma proliferation and invasiveness. Genes & development *20*, 3426-3439.

Catchen, J.M., Braasch, I., and Postlethwait, J.H. (2011). Conserved synteny and the zebrafish genome. Methods in cell biology *104*, 259-285.

Ceol, C.J., Houvras, Y., Jane-Valbuena, J., Bilodeau, S., Orlando, D.A., Battisti, V., Fritsch, L., Lin, W.M., Hollmann, T.J., Ferre, F.*, et al.* (2011). The histone methyltransferase SETDB1 is recurrently amplified in melanoma and accelerates its onset. Nature *471*, 513-517.

Chapman, P.B., Hauschild, A., Robert, C., Haanen, J.B., Ascierto, P., Larkin, J., Dummer, R., Garbe, C., Testori, A., Maio, M.*, et al.* (2011). Improved survival with vemurafenib in melanoma with BRAF V600E mutation. The New England journal of medicine *364*, 2507-2516.

Cheung, M., and Briscoe, J. (2003). Neural crest development is regulated by the transcription factor Sox9. Development (Cambridge, England) *130*, 5681-5693.

Clendenning, D.E., and Mortlock, D.P. (2012). The BMP ligand Gdf6 prevents differentiation of coronal suture mesenchyme in early cranial development. PloS one *7*, e36789.

Collins, J.E., White, S., Searle, S.M., and Stemple, D.L. (2012). Incorporating RNA-seq data into the zebrafish Ensembl genebuild. Genome research *22*, 2067-2078.

Cunha, S.I., Pardali, E., Thorikay, M., Anderberg, C., Hawinkels, L., Goumans, M.J., Seehra, J., Heldin, C.H., ten Dijke, P., and Pietras, K. (2010). Genetic and pharmacological targeting of activin receptor-like kinase 1 impairs tumor growth and angiogenesis. The Journal of experimental medicine *207*, 85-100.

Daley, G.Q. (2008). Common themes of dedifferentiation in somatic cell reprogramming and cancer. Cold Spring Harbor symposia on quantitative biology *73*, 171-174.

Davies, H., Bignell, G.R., Cox, C., Stephens, P., Edkins, S., Clegg, S., Teague, J., Woffendin, H., Garnett, M.J., Bottomley, W.*, et al.* (2002). Mutations of the BRAF gene in human cancer. Nature *417*, 949-954.

Delot, E., Kataoka, H., Goutel, C., Yan, Y.L., Postlethwait, J., Wittbrodt, J., and Rosa, F.M. (1999). The BMP-related protein radar: a maintenance factor for dorsal neuroectoderm cells? Mechanisms of development *85*, 15-25.

Demetri, G.D., von Mehren, M., Blanke, C.D., Van den Abbeele, A.D., Eisenberg, B., Roberts, P.J., Heinrich, M.C., Tuveson, D.A., Singer, S., Janicek, M.*, et al.* (2002). Efficacy and safety of imatinib mesylate in advanced gastrointestinal stromal tumors. The New England journal of medicine *347*, 472-480.

Deng H, M.R., Ravikumar TS, Dong H, Yang W, Yang WL (2007). Bone morphogenetic protein-4 is overexpressed in colonic adenocarcinomas and promotes migration and invasion of HCT116 cells. Exp Cell Res *2007 Mar 10; 313(5):1033-44. Epub 2007 Jan 10*.

Dobin, A., Davis, C.A., Schlesinger, F., Drenkow, J., Zaleski, C., Jha, S., Batut, P., Chaisson, M., and Gingeras, T.R. (2013). STAR: ultrafast universal RNA-seq aligner. Bioinformatics (Oxford, England) *29*, 15-21.

Du, Y., and Yip, H. (2010). Effects of bone morphogenetic protein 2 on Id expression and neuroblastoma cell differentiation. Differentiation; research in biological diversity *79*, 84-92.

Eccles, M.R., He, S., Ahn, A., Slobbe, L.J., Jeffs, A.R., Yoon, H.S., and Baguley, B.C. (2013). MITF and PAX3 Play Distinct Roles in Melanoma Cell Migration; Outline of a "Genetic Switch" Theory Involving MITF and PAX3 in Proliferative and Invasive Phenotypes of Melanoma. Frontiers in oncology *3*, 229.

Eggermont, A.M., Chiarion-Sileni, V., Grob, J.J., Dummer, R., Wolchok, J.D., Schmidt, H., Hamid, O., Robert, C., Ascierto, P.A., Richards, J.M.*, et al.* (2016). Prolonged Survival in Stage III Melanoma with Ipilimumab Adjuvant Therapy. The New England journal of medicine *375*, 1845-1855.

Feng, J., Liu, T., Qin, B., Zhang, Y., and Liu, X.S. (2012). Identifying ChIP-seq enrichment using MACS. Nature protocols *7*, 1728-1740.

Forbes, S.A., Beare, D., Boutselakis, H., Bamford, S., Bindal, N., Tate, J., Cole, C.G., Ward, S., Dawson, E., Ponting, L.*, et al.* (2017). COSMIC: somatic cancer genetics at high-resolution. Nucleic acids research *45*, D777-D783.

Fuse, N., Yasumoto, K., Suzuki, H., Takahashi, K., and Shibahara, S. (1996). Identification of a melanocyte-type promoter of the microphthalmia-associated transcription factor gene. Biochemical and biophysical research communications *219*, 702-707.

Gajavelli, S., Wood, P.M., Pennica, D., Whittemore, S.R., and Tsoulfas, P. (2004). BMP signaling initiates a neural crest differentiation program in embryonic rat CNS stem cells. Experimental neurology *188*, 205-223.

Gazin, C., Wajapeyee, N., Gobeil, S., Virbasius, C.M., and Green, M.R. (2007). An elaborate pathway required for Ras-mediated epigenetic silencing. Nature *449*, 1073-1077.

Goding, C.R. (2011). Commentary. A picture of Mitf in melanoma immortality. Oncogene *30*, 2304-2306.

Goldstein, A.M., Brewer, K.C., Doyle, A.M., Nagy, N., and Roberts, D.J. (2005). BMP signaling is necessary for neural crest cell migration and ganglion formation in the enteric nervous system. Mechanisms of development *122*, 821-833.

Gosse, N.J., and Baier, H. (2009). An essential role for Radar (Gdf6a) in inducing dorsal fate in the zebrafish retina. Proceedings of the National Academy of Sciences of the United States of America *106*, 2236-2241.

Greenhill, E.R., Rocco, A., Vibert, L., Nikaido, M., and Kelsh, R.N. (2011). An iterative genetic and dynamical modelling approach identifies novel features of the gene regulatory network underlying melanocyte development. PLoS genetics *7*, e1002265.

Grijelmo C, R.C., Svrcek M, Bruyneel E, Hendrix A, de Wever O, Gespach C (2007). Proinvasive activity of BMP-7 through SMAD4/src-independent and ERK/Rac/JNK-dependent signaling pathways in colon cancer cells. Cell Signal.

Gupta, P.B., Kuperwasser, C., Brunet, J.P., Ramaswamy, S., Kuo, W.L., Gray, J.W., Naber, S.P., and Weinberg, R.A. (2005). The melanocyte differentiation program predisposes to metastasis after neoplastic transformation. Nature genetics *37*, 1047-1054.

Hanel, M.L., and Hensey, C. (2006). Eye and neural defects associated with loss of GDF6. BMC developmental biology *6*, 43.

Hao, J., Ho, J.N., Lewis, J.A., Karim, K.A., Daniels, R.N., Gentry, P.R., Hopkins, C.R., Lindsley, C.W., and Hong, C.C. (2010). In vivo structure-activity relationship study of dorsomorphin analogues identifies selective VEGF and BMP inhibitors. ACS chemical biology *5*, 245-253.

Hao, J., Lee, R., Chang, A., Fan, J., Labib, C., Parsa, C., Orlando, R., Andresen, B., and Huang, Y. (2014). DMH1, a small molecule inhibitor of BMP type i receptors, suppresses growth and invasion of lung cancer. PloS one *9*, e90748.

Hardwick, J.C., Van Den Brink, G.R., Bleuming, S.A., Ballester, I., Van Den Brande, J.M., Keller, J.J., Offerhaus, G.J., Van Deventer, S.J., and Peppelenbosch, M.P. (2004). Bone morphogenetic protein 2 is expressed by, and acts upon, mature epithelial cells in the colon. Gastroenterology *126*, 111-121.

Heinz, S., Benner, C., Spann, N., Bertolino, E., Lin, Y.C., Laslo, P., Cheng, J.X., Murre, C., Singh, H., and Glass, C.K. (2010). Simple combinations of lineage-determining transcription factors prime cis-regulatory elements required for macrophage and B cell identities. Molecular cell *38*, 576-589.

Helms, M.W., Packeisen, J., August, C., Schittek, B., Boecker, W., Brandt, B.H., and Buerger, H. (2005). First evidence supporting a potential role for the BMP/SMAD pathway in the progression of oestrogen receptor-positive breast cancer. The Journal of pathology *206*, 366-376.

Hendrix, M.J., Seftor, E.A., Seftor, R.E., Kasemeier-Kulesa, J., Kulesa, P.M., and Postovit, L.M. (2007). Reprogramming metastatic tumour cells with embryonic microenvironments. Nature reviews Cancer *7*, 246-255.

Hodis, E., Watson, I.R., Kryukov, G.V., Arold, S.T., Imielinski, M., Theurillat, J.P., Nickerson, E., Auclair, D., Li, L., Place, C.*, et al.* (2012). A landscape of driver mutations in melanoma. Cell *150*, 251-263.

Hoek, K.S., and Goding, C.R. (2010). Cancer stem cells versus phenotype-switching in melanoma. Pigment cell & melanoma research *23*, 746-759.

Hohenauer, T., Berking, C., Schmidt, A., Haferkamp, S., Senft, D., Kammerbauer, C., Fraschka, S., Graf, S.A., Irmler, M., Beckers, J.*, et al.* (2013). The neural crest transcription factor Brn3a is expressed in melanoma and required for cell cycle progression and survival. EMBO molecular medicine *5*, 919-934.

Hover, L.D., Young, C.D., Bhola, N.E., Wilson, A.J., Khabele, D., Hong, C.C., Moses, H.L., and Owens, P. (2015). Small molecule inhibitor of the bone morphogenetic protein pathway DMH1 reduces ovarian cancer cell growth. Cancer letters *368*, 79-87.

Howe, K., Clark, M.D., Torroja, C.F., Torrance, J., Berthelot, C., Muffato, M., Collins, J.E., Humphray, S., McLaren, K., Matthews, L.*, et al.* (2013). The zebrafish reference genome sequence and its relationship to the human genome. Nature *496*, 498-503.

Hsu, M.Y., Rovinsky, S.A., Lai, C.Y., Qasem, S., Liu, X., How, J., Engelhardt, J.F., and Murphy, G.F. (2008). Aggressive melanoma cells escape from BMP7-mediated autocrine growth inhibition through coordinated Noggin upregulation. Laboratory investigation; a journal of technical methods and pathology *88*, 842-855.

Hu-Lowe, D.D., Chen, E., Zhang, L., Watson, K.D., Mancuso, P., Lappin, P., Wickman, G., Chen, J.H., Wang, J., Jiang, X.*, et al.* (2011). Targeting activin

receptor-like kinase 1 inhibits angiogenesis and tumorigenesis through a mechanism of action complementary to anti-VEGF therapies. Cancer research *71*, 1362-1373.

Ischenko, I., Zhi, J., Moll, U.M., Nemajerova, A., and Petrenko, O. (2013). Direct reprogramming by oncogenic Ras and Myc. Proceedings of the National Academy of Sciences of the United States of America *110*, 3937-3942.

Jin, E.J., Erickson, C.A., Takada, S., and Burrus, L.W. (2001). Wnt and BMP signaling govern lineage segregation of melanocytes in the avian embryo. Developmental biology *233*, 22-37.

Kajita, M., McClinic, K.N., and Wade, P.A. (2004). Aberrant expression of the transcription factors snail and slug alters the response to genotoxic stress. Molecular and cellular biology *24*, 7559-7566.

Kantarjian, H., Sawyers, C., Hochhaus, A., Guilhot, F., Schiffer, C., Gambacorti-Passerini, C., Niederwieser, D., Resta, D., Capdeville, R., Zoellner, U.*, et al.* (2002). Hematologic and cytogenetic responses to imatinib mesylate in chronic myelogenous leukemia. The New England journal of medicine *346*, 645-652.

Katsuno, Y., Hanyu, A., Kanda, H., Ishikawa, Y., Akiyama, F., Iwase, T., Ogata, E., Ehata, S., Miyazono, K., and Imamura, T. (2008). Bone morphogenetic protein signaling enhances invasion and bone metastasis of breast cancer cells through Smad pathway. Oncogene *27*, 6322-6333.

Kaufman, C.K., Mosimann, C., Fan, Z.P., Yang, S., Thomas, A.J., Ablain, J., Tan, J.L., Fogley, R.D., van Rooijen, E., Hagedorn, E.J.*, et al.* (2016). A zebrafish

melanoma model reveals emergence of neural crest identity during melanoma initiation. Science (New York, NY) *351*, aad2197.

Kim, D., Pertea, G., Trapnell, C., Pimentel, H., Kelley, R., and Salzberg, S.L. (2013). TopHat2: accurate alignment of transcriptomes in the presence of insertions, deletions and gene fusions. Genome biology *14*, R36.

Kodach, L.L., Wiercinska, E., de Miranda, N.F., Bleuming, S.A., Musler, A.R., Peppelenbosch, M.P., Dekker, E., van den Brink, G.R., van Noesel, C.J., Morreau, H.*, et al.* (2008). The bone morphogenetic protein pathway is inactivated in the majority of sporadic colorectal cancers. Gastroenterology *134*, 1332-1341.

Kraehn, G.M., Utikal, J., Udart, M., Greulich, K.M., Bezold, G., Kaskel, P., Leiter, U., and Peter, R.U. (2001). Extra c-myc oncogene copies in high risk cutaneous malignant melanoma and melanoma metastases. British journal of cancer *84*, 72-79.

Krzywinski, M., Schein, J., Birol, I., Connors, J., Gascoyne, R., Horsman, D., Jones, S.J., and Marra, M.A. (2009). Circos: an information aesthetic for comparative genomics. Genome research *19*, 1639-1645.

Kuphal, S., and Bosserhoff, A.K. (2006). Influence of the cytoplasmic domain of E-cadherin on endogenous N-cadherin expression in malignant melanoma. Oncogene *25*, 248-259.

Lam, S.H., and Gong, Z. (2006). Modeling liver cancer using zebrafish: a comparative oncogenomics approach. Cell cycle (Georgetown, Tex) *5*, 573-577.

Langmead, B., and Salzberg, S.L. (2012). Fast gapped-read alignment with Bowtie 2. Nature methods *9*, 357-359.

Langmead, B., Trapnell, C., Pop, M., and Salzberg, S.L. (2009). Ultrafast and memory-efficient alignment of short DNA sequences to the human genome. Genome biology *10*, R25.

Larkin, J., Ascierto, P.A., Dreno, B., Atkinson, V., Liszkay, G., Maio, M., Mandala, M., Demidov, L., Stroyakovskiy, D., Thomas, L.*, et al.* (2014). Combined vemurafenib and cobimetinib in BRAF-mutated melanoma. The New England journal of medicine *371*, 1867-1876.

Leach, D.R., Krummel, M.F., and Allison, J.P. (1996). Enhancement of antitumor immunity by CTLA-4 blockade. Science (New York, NY) *271*, 1734-1736.

Lee, J., Son, M.J., Woolard, K., Donin, N.M., Li, A., Cheng, C.H., Kotliarova, S., Kotliarov, Y., Walling, J., Ahn, S.*, et al.* (2008). Epigenetic-mediated dysfunction of the bone morphogenetic protein pathway inhibits differentiation of glioblastoma-initiating cells. Cancer cell *13*, 69-80.

Li, H., Handsaker, B., Wysoker, A., Fennell, T., Ruan, J., Homer, N., Marth, G., Abecasis, G., and Durbin, R. (2009). The Sequence Alignment/Map format and SAMtools. Bioinformatics (Oxford, England) *25*, 2078-2079.

Lin, W.M., Baker, A.C., Beroukhim, R., Winckler, W., Feng, W., Marmion, J.M., Laine, E., Greulich, H., Tseng, H., Gates, C.*, et al.* (2008). Modeling genomic diversity and tumor dependency in malignant melanoma. Cancer research *68*, 664-673.

Lister, J.A., Robertson, C.P., Lepage, T., Johnson, S.L., and Raible, D.W. (1999). nacre encodes a zebrafish microphthalmia-related protein that regulates neural-crest-derived pigment cell fate. Development (Cambridge, England) *126*, 3757-3767.

Love, M.I., Huber, W., and Anders, S. (2014). Moderated estimation of fold change and dispersion for RNA-seq data with DESeq2. Genome biology *15*, 550.

Lynch, T.J., Bell, D.W., Sordella, R., Gurubhagavatula, S., Okimoto, R.A., Brannigan, B.W., Harris, P.L., Haserlat, S.M., Supko, J.G., Haluska, F.G.*, et al.* (2004). Activating mutations in the epidermal growth factor receptor underlying responsiveness of non-small-cell lung cancer to gefitinib. The New England journal of medicine *350*, 2129-2139.

Mack, S.C., Hubert, C.G., Miller, T.E., Taylor, M.D., and Rich, J.N. (2016). An epigenetic gateway to brain tumor cell identity. Nature neuroscience *19*, 10-19.

Maguire, L.H., Thomas, A.R., and Goldstein, A.M. (2015). Tumors of the neural crest: Common themes in development and cancer. Developmental dynamics : an official publication of the American Association of Anatomists *244*, 311-322.

Massague, J., Seoane, J., and Wotton, D. (2005). Smad transcription factors. Genes & development *19*, 2783-2810.

Miyazaki, H., Watabe, T., Kitamura, T., and Miyazono, K. (2004). BMP signals inhibit proliferation and in vivo tumor growth of androgen-insensitive prostate carcinoma cells. Oncogene *23*, 9326-9335.

Na, Y.R., Seok, S.H., Kim, D.J., Han, J.H., Kim, T.H., Jung, H., Lee, B.H., and Park, J.H. (2009). Bone morphogenetic protein 7 induces mesenchymal-to-epithelial transition in melanoma cells, leading to inhibition of metastasis. Cancer science *100*, 2218-2225.

Paez, J.G., Janne, P.A., Lee, J.C., Tracy, S., Greulich, H., Gabriel, S., Herman, P., Kaye, F.J., Lindeman, N., Boggon, T.J.*, et al.* (2004). EGFR mutations in lung cancer: correlation with clinical response to gefitinib therapy. Science (New York, NY) *304*, 1497-1500.

Pant, S.D., March, L.D., Famulski, J.K., French, C.R., Lehmann, O.J., and Waskiewicz, A.J. (2013). Molecular mechanisms regulating ocular apoptosis in zebrafish gdf6a mutants. Investigative ophthalmology & visual science *54*, 5871-5879.

Patton, E.E., Widlund, H.R., Kutok, J.L., Kopani, K.R., Amatruda, J.F., Murphey, R.D., Berghmans, S., Mayhall, E.A., Traver, D., Fletcher, C.D.*, et al.* (2005). BRAF mutations are sufficient to promote nevi formation and cooperate with p53 in the genesis of melanoma. Current biology : CB *15*, 249-254.

Piccirillo, S.G., Reynolds, B.A., Zanetti, N., Lamorte, G., Binda, E., Broggi, G., Brem, H., Olivi, A., Dimeco, F., and Vescovi, A.L. (2006). Bone morphogenetic proteins inhibit the tumorigenic potential of human brain tumour-initiating cells. Nature *444*, 761-765.

Pirker, C., Holzmann, K., Spiegl-Kreinecker, S., Elbling, L., Thallinger, C., Pehamberger, H., Micksche, M., and Berger, W. (2003). Chromosomal

imbalances in primary and metastatic melanomas: over-representation of essential telomerase genes. Melanoma research *13*, 483-492.

Postlethwait, J., Amores, A., Force, A., and Yan, Y.L. (1999). The zebrafish genome. Methods in cell biology *60*, 149-163.

Reichert, S., Randall, R.A., and Hill, C.S. (2013). A BMP regulatory network controls ectodermal cell fate decisions at the neural plate border. Development (Cambridge, England) *140*, 4435-4444.

Richard, G., Dalle, S., Monet, M.A., Ligier, M., Boespflug, A., Pommier, R.M., de la Fouchardiere, A., Perier-Muzet, M., Depaepe, L., Barnault, R.*, et al.* (2016). ZEB1-mediated melanoma cell plasticity enhances resistance to MAPK inhibitors. EMBO molecular medicine *8*, 1143-1161.

Rissi, M., Wittbrodt, J., Delot, E., Naegeli, M., and Rosa, F.M. (1995). Zebrafish Radar: a new member of the TGF-beta superfamily defines dorsal regions of the neural plate and the embryonic retina. Mechanisms of development *49*, 223-234.

Ritchie, M.E., Phipson, B., Wu, D., Hu, Y., Law, C.W., Shi, W., and Smyth, G.K. (2015). limma powers differential expression analyses for RNA-sequencing and microarray studies. Nucleic acids research *43*, e47.

Robert, C., Karaszewska, B., Schachter, J., Rutkowski, P., Mackiewicz, A., Stroiakovski, D., Lichinitser, M., Dummer, R., Grange, F., Mortier, L.*, et al.* (2015a). Improved overall survival in melanoma with combined dabrafenib and trametinib. The New England journal of medicine *372*, 30-39.

Robert, C., Long, G.V., Brady, B., Dutriaux, C., Maio, M., Mortier, L., Hassel, J.C., Rutkowski, P., McNeil, C., Kalinka-Warzocha, E.*, et al.* (2015b). Nivolumab in previously untreated melanoma without BRAF mutation. The New England journal of medicine *372*, 320-330.

Rothhammer, T., Bataille, F., Spruss, T., Eissner, G., and Bosserhoff, A.K. (2007). Functional implication of BMP4 expression on angiogenesis in malignant melanoma. Oncogene *26*, 4158-4170.

Rothhammer, T., Poser, I., Soncin, F., Bataille, F., Moser, M., and Bosserhoff, A.K. (2005). Bone morphogenic proteins are overexpressed in malignant melanoma and promote cell invasion and migration. Cancer research *65*, 448-456.

Roy, N., and Hebrok, M. (2015). Regulation of Cellular Identity in Cancer. Developmental cell *35*, 674-684.

S, A. (2010). FastQC: a quality control tool for high throughput sequence data.

Saito, D., Takase, Y., Murai, H., and Takahashi, Y. (2012). The dorsal aorta initiates a molecular cascade that instructs sympatho-adrenal specification. Science (New York, NY) *336*, 1578-1581.

Sanchez-Garcia, F., Akavia, U.D., Mozes, E., and Pe'er, D. (2010). JISTIC: identification of significant targets in cancer. BMC bioinformatics *11*, 189.

Sartori, R., Schirwis, E., Blaauw, B., Bortolanza, S., Zhao, J., Enzo, E., Stantzou, A., Mouisel, E., Toniolo, L., Ferry, A.*, et al.* (2013). BMP signaling controls muscle mass. Nature genetics *45*, 1309-1318.

Sauka-Spengler, T., and Bronner-Fraser, M. (2008). A gene regulatory network orchestrates neural crest formation. Nature reviews Molecular cell biology *9*, 557-568.

Schneider, C., Wicht, H., Enderich, J., Wegner, M., and Rohrer, H. (1999). Bone morphogenetic proteins are required in vivo for the generation of sympathetic neurons. Neuron *24*, 861-870.

Schwitalla, S., Fingerle, A.A., Cammareri, P., Nebelsiek, T., Goktuna, S.I., Ziegler, P.K., Canli, O., Heijmans, J., Huels, D.J., Moreaux, G.*, et al.* (2013). Intestinal tumorigenesis initiated by dedifferentiation and acquisition of stem-cell-like properties. Cell *152*, 25-38.

Settle, S.H., Jr., Rountree, R.B., Sinha, A., Thacker, A., Higgins, K., and Kingsley, D.M. (2003). Multiple joint and skeletal patterning defects caused by single and double mutations in the mouse Gdf6 and Gdf5 genes. Developmental biology *254*, 116-130.

Shakhova, O. (2014). Neural crest stem cells in melanoma development. Current opinion in oncology *26*, 215-221.

Shakhova, O., Cheng, P., Mishra, P.J., Zingg, D., Schaefer, S.M., Debbache, J., Hausel, J., Matter, C., Guo, T., Davis, S.*, et al.* (2015). Antagonistic cross-regulation between Sox9 and Sox10 controls an anti-tumorigenic program in melanoma. PLoS genetics *11*, e1004877.

Shakhova, O., Zingg, D., Schaefer, S.M., Hari, L., Civenni, G., Blunschi, J., Claudinot, S., Okoniewski, M., Beermann, F., Mihic-Probst, D.*, et al.* (2012).

Sox10 promotes the formation and maintenance of giant congenital naevi and melanoma. Nature cell biology *14*, 882-890.

Shirai, Y.T., Ehata, S., Yashiro, M., Yanagihara, K., Hirakawa, K., and Miyazono, K. (2011). Bone morphogenetic protein-2 and -4 play tumor suppressive roles in human diffuse-type gastric carcinoma. The American journal of pathology *179*, 2920-2930.

Su, F., Viros, A., Milagre, C., Trunzer, K., Bollag, G., Spleiss, O., Reis-Filho, J.S., Kong, X., Koya, R.C., Flaherty, K.T.*, et al.* (2012). RAS mutations in cutaneous squamous-cell carcinomas in patients treated with BRAF inhibitors. The New England journal of medicine *366*, 207-215.

Tarragona, M., Pavlovic, M., Arnal-Estape, A., Urosevic, J., Morales, M., Guiu, M., Planet, E., Gonzalez-Suarez, E., and Gomis, R.R. (2012). Identification of NOG as a specific breast cancer bone metastasis-supporting gene. The Journal of biological chemistry *287*, 21346-21355.

Thorvaldsdottir, H., Robinson, J.T., and Mesirov, J.P. (2013). Integrative Genomics Viewer (IGV): high-performance genomics data visualization and exploration. Briefings in bioinformatics *14*, 178-192.

Tian, A., Benchabane, H., Wang, Z., and Ahmed, Y. (2016). Regulation of Stem Cell Proliferation and Cell Fate Specification by Wingless/Wnt Signaling Gradients Enriched at Adult Intestinal Compartment Boundaries. PLoS genetics *12*, e1005822.

Trapnell, C., Roberts, A., Goff, L., Pertea, G., Kim, D., Kelley, D.R., Pimentel, H., Salzberg, S.L., Rinn, J.L., and Pachter, L. (2012). Differential gene and transcript expression analysis of RNA-seq experiments with TopHat and Cufflinks. Nature protocols *7*, 562-578.

Tsuji, K., Bandyopadhyay, A., Harfe, B.D., Cox, K., Kakar, S., Gerstenfeld, L., Einhorn, T., Tabin, C.J., and Rosen, V. (2006). BMP2 activity, although dispensable for bone formation, is required for the initiation of fracture healing. Nature genetics *38*, 1424-1429.

Tsukamoto, S., Mizuta, T., Fujimoto, M., Ohte, S., Osawa, K., Miyamoto, A., Yoneyama, K., Murata, E., Machiya, A., Jimi, E.*, et al.* (2014). Smad9 is a new type of transcriptional regulator in bone morphogenetic protein signaling. Scientific reports *4*, 7596.

Wang, J., Duncan, D., Shi, Z., and Zhang, B. (2013a). WEB-based GEne SeT AnaLysis Toolkit (WebGestalt): update 2013. Nucleic acids research *41*, W77-83.

Wang, S.S., Huang, H.Y., Chen, S.Z., Li, X., Zhang, W.T., and Tang, Q.Q. (2013b). Gdf6 induces commitment of pluripotent mesenchymal C3H10T1/2 cells to the adipocyte lineage. The FEBS journal *280*, 2644-2651.

Weber, J.S., Kahler, K.C., and Hauschild, A. (2012). Management of immune-related adverse events and kinetics of response with ipilimumab. Journal of clinical oncology : official journal of the American Society of Clinical Oncology *30*, 2691-2697.

Weinstein, I.B. (2002). Cancer. Addiction to oncogenes--the Achilles heal of cancer. Science (New York, NY) *297*, 63-64.

White, R.M., Cech, J., Ratanasirintrawoot, S., Lin, C.Y., Rahl, P.B., Burke, C.J., Langdon, E., Tomlinson, M.L., Mosher, J., Kaufman, C.*, et al.* (2011). DHODH modulates transcriptional elongation in the neural crest and melanoma. Nature *471*, 518-522.

Wilks, C., Cline, M.S., Weiler, E., Diehkans, M., Craft, B., Martin, C., Murphy, D., Pierce, H., Black, J., Nelson, D.*, et al.* (2014). The Cancer Genomics Hub (CGHub): overcoming cancer through the power of torrential data. Database : the journal of biological databases and curation *2014*.

Wong, S.H., Goode, D.L., Iwasaki, M., Wei, M.C., Kuo, H.P., Zhu, L., Schneidawind, D., Duque-Afonso, J., Weng, Z., and Cleary, M.L. (2015). The H3K4-Methyl Epigenome Regulates Leukemia Stem Cell Oncogenic Potential. Cancer cell *28*, 198-209.

Wu, Q., Kirschmeier, P., Hockenberry, T., Yang, T.Y., Brassard, D.L., Wang, L., McClanahan, T., Black, S., Rizzi, G., Musco, M.L.*, et al.* (2002). Transcriptional regulation during p21WAF1/CIP1-induced apoptosis in human ovarian cancer cells. The Journal of biological chemistry *277*, 36329-36337.

Xu, Z., Huo, X., Tang, C., Ye, H., Nandakumar, V., Lou, F., Zhang, D., Jiang, S., Sun, H., Dong, H.*, et al.* (2014). Frequent KIT mutations in human gastrointestinal stromal tumors. Scientific reports *4*, 5907.

Yen, J., White, R.M., Wedge, D.C., Van Loo, P., de Ridder, J., Capper, A., Richardson, J., Jones, D., Raine, K., Watson, I.R.*, et al.* (2013). The genetic heterogeneity and mutational burden of engineered melanomas in zebrafish models. Genome biology *14*, R113.

Zhang, G., Hoersch, S., Amsterdam, A., Whittaker, C.A., Beert, E., Catchen, J.M., Farrington, S., Postlethwait, J.H., Legius, E., Hopkins, N.*, et al.* (2013). Comparative oncogenomic analysis of copy number alterations in human and zebrafish tumors enables cancer driver discovery. PLoS genetics *9*, e1003734.

Zhang, G., Hoersch, S., Amsterdam, A., Whittaker, C.A., Lees, J.A., and Hopkins, N. (2010). Highly aneuploid zebrafish malignant peripheral nerve sheath tumors have genetic alterations similar to human cancers. Proceedings of the National Academy of Sciences of the United States of America *107*, 16940-16945.

Zhang, L., Sun, H., Zhao, F., Lu, P., Ge, C., Li, H., Hou, H., Yan, M., Chen, T., Jiang, G.*, et al.* (2012). BMP4 administration induces differentiation of CD133+ hepatic cancer stem cells, blocking their contributions to hepatocellular carcinoma. Cancer research *72*, 4276-4285.

Zhu, L.J., Gazin, C., Lawson, N.D., Pages, H., Lin, S.M., Lapointe, D.S., and Green, M.R. (2010). ChIPpeakAnno: a Bioconductor package to annotate ChIP-seq and ChIP-chip data. BMC bioinformatics *11*, 237.